2022

Study of Electric Vehicle Smart Charging and Energy Management for Vehicle-Grid Integration Systems

Zhouquan Wu
Michigan Technological University, wzhouqua@mtu.edu

STUDY OF ELECTRIC VEHICLE SMART CHARGING AND ENERGY MANAGEMENT FOR VEHICLE-GRID INTEGRATION SYSTEMS

By

Zhouquan Wu

A DISSERTATION

Submitted in partial fulfillment of the requirements for the degree of

DOCTOR OF PHILOSOPHY

In Electrical Engineering

MICHIGAN TECHNOLOGICAL UNIVERSITY

2022

This dissertation has been approved in partial fulfillment of the requirements for the Degree of DOCTOR OF PHILOSOPHY in Electrical Engineering.

Department of Electrical and Computer Engineering

Dissertation Advisor:	*Dr. Bo Chen*
Committee Member:	*Dr. Lan Zhang*
Committee Member:	*Dr. Zhaohui Wang*
Committee Member:	*Dr. Ye Sun*
Department Chair:	*Dr. Jin W. Choi*

Contents

List of Figures

List of Tables

Author Contribution Statement

Included in Chapter 2 is a conference technical paper. Included in Chapter 3 is a journal article. Included in Chapter 4 is a journal article under review. Included in Chapter 5 is a conference technical paper and selected to appear in journal. They are republished in their entirety as chapters in this dissertation. I have written these papers as the lead contributor. For the conference paper presented in Chapter 2, co-author Chong Cao contributes to debug simulation models. For the article presented in Chapter 5, co-authors Naga Nithin Manne and Jason Harper provide ideas and coding for rule-based control as included in section 5.3.3. Co-author Daniel Dobrzynski contributes to test the developed platform with real facilities. As the co-author of all articles, my advisor Dr. Bo Chen has provided critical advice and guidance.

Acknowledgements

Firstly, I would like to express my sincere gratitude to my advisor Dr. Bo Chen for the continuous support of my Ph.D. study and related research, for her patience, motivation, and immense knowledge. Her guidance helped me in all the time of research and writing of this dissertation. I am thankful for the extraordinary experiences she arranged for me and for providing opportunities for me to grow professionally. I could not have imagined having a better advisor my Ph.D. study.

Besides my advisor, I would like to thank the rest of my committee: Dr. Lan Zhang, Dr. Zhaohui Wang, and Dr. Ye Sun for their insightful comments and encouragement, but also for the hard question which incented me to widen my research from various perspectives.

My sincere thanks also go my previous colleagues at Argonne National Laboratory: Keith Hardy, Jason D. Harper, Daniel S. Dobrzynski, Naga Nithin Manne, and Bryan W Nystrom. They provided me an opportunity to join their team, and who gave access to the laboratory and research facilities. This project experience is the most precious treasure in my life.

I thank my fellow labmates in MTU for the stimulating discussions, for the sleepless nights we were working together, and for all the fun we have had in the last five years. I would like to give my sincere gratitude to my lab colleagues: Chong Cao, Xin Wang, Luting Wang, Pradeep Krishna Bhat, Joe Oncken, Yugandhara Yuvraj Patil, Mahalakshmi Madhoolika Jammalamadaka, and my friends: Jiongxun Zhang, Meng Tang, Le Zhao, Xuebin Yang, Xiucheng Zhu, Zhihao Zhao, Mingyang Li.

Last but not the least, I am grateful for my parents whose constant love and support keep me motivated and confident. My accomplishments and success are because they believed in me. I owe my deepest gratitude to Emma, who is my love. I am forever thankful for the unconditional love and support throughout the entire dissertation process and every day.

List of Abbreviations

AC – Alternating Current

ADMM – Alternative Direction Method of Multipliers

DC – Direct Current

DCFC – DC Fast Charging

DSO – Distribution System Operator

ESS – Energy Storage Systems

EV – Electric Vehicle

EVA – Electric Vehicle Aggregator

EVCS – EV Charge Scheduler

EVSE – Electric Vehicle Supply Equipment

HIL – Hard-ware-in-the-Loop

MC – Monte Carlo

M2M – Machine to machine

MQTT – Message Queuing Telemetry Transport

OCPP – Open Charge Point Protocol

PV – Photovoltaic

SOC – State of Charge

TE – Transactive Energy

TEM – Transactive Energy management

VGI – Vehicle-Grid Integration

XFC – Extreme Fast Charging

Abstract

The emerging need of building an efficient Electric Vehicle (EV) charging infrastructure requires the investigation of all aspects of Vehicle-Grid Integration (VGI). This dissertation studies the optimal EV charging control and energy management of VGI system to address the economic benefits of EV charging customers and operation stability of distribution power grids. First of all, a centralized EV charging control method is developed under the transactive energy environment to minimize the EV charging cost and avoid the distribution power grid overloading. The quadratic programming is used to obtain optimized charging control actions. Case studies with hundreds of EVs are conducted and analyzed. Secondly, to explore a more effective and securer VGI system, an advanced distributed algorithm is developed for solving the large-scale EV charging scheduling problem, including the perspectives at an individual EV level, the distribution node level, and the distribution network level. A clearing electricity price is attained by a negotiation method among the distribution system operator and the EV aggregators (EVAs). This mechanism provides incentive for EV charging customers to improve network operation performance. Thus, EVAs and EVs can make their charging scheduling autonomously with the clearing price signals. Thirdly, to realistically estimate the charging power demand of extreme fast charging (XFC) stations, a Monte Carlo (MC) simulation tool is developed based on the EV arrival time and state of charge (SOC) distributions obtained from vehicle travel survey dataset. To reduce the investment and operation costs of XFC stations and avoid overloading the grid due to XFC events, an optimal configuration method is presented for the multiple XFC stations in a distribution

network to determine the optimal energy capacity of energy storage system (ESS), ESS rated power, and the size of photovoltaic (PV) panels, which are integrated with XFC stations. The MC simulation tool is valuable since little XFC charging dataset is available at the current stage and the optimal configuration method can reduce the investment and operation costs of XFC stations while meeting the charging demand and the operational constraints of the distribution network, XFC, ESS, and PV panels. Finally, a cloud-based simulation and testing platform for the development and Hardware-in-the-Loop (HIL) testing of VGI technologies is presented. This test platform considers the impact of EV charging on the grid, optimal EV charging control at scale, and communication interoperability. The modular open systems design approach of the platform allows the integration of EV charging control algorithms and hardware charging systems for performance evaluation and interoperability testing.

1 Introduction

1.1 Background

1.1.1 Motivation

The growing adoption rate of electric vehicles greatly reduces the greenhouse gas emissions and fuel consumption in the transportation sector. Most national governments and automakers are phasing out gasoline vehicle sales by 2040, or by no later than 2035 in a leading market. At the 2021 United Nations Climate Change Conference, over 30 national governments, including Austria, Canada, Demark, Finland, Ireland, Netherlands, United Kingdom and so on, have agreed to shift entirely to "all new sales of zero-emission cars and vans globally by 2040" [1]. As shown in Figure 1.1, the global EV sales have increased from several thousand in 2010 to over 3 million in 2020. The world's EV stock have surpassed 10 million in 2020 [2]. With government incentives and technology advancements continuous, automakers estimate that annual EV sales will be reach to 22 million by 2025 and about 100 million EVs will be on the road worldwide by 2035 [2]. Thus, transportation electrification is the main research area for the past and future decades.

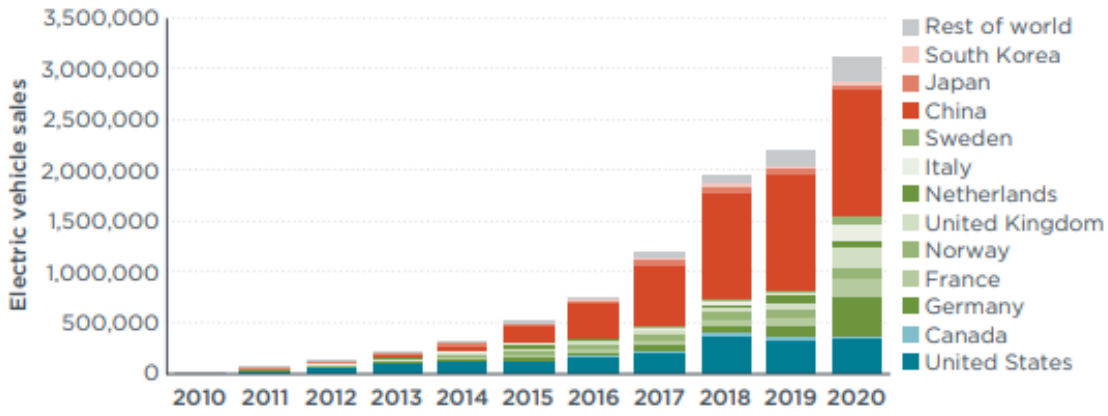

Figure 1.1. Global EV Sales, 2010-2020 [2].

Meanwhile, the high penetrations of EVs will lead to over millions of batteries will be charged by electric power system. The impact of EVs integration to the grid is the key challenge that needs to be resolved. Massive integration of EVs into the distribution network will cause negative impacts, including power system components overloading, power loss increasing, voltage and frequency unbalancing, and causing instability in the power system [3-7]. In [3], a worst case scenarios of EV penetration in Toronto was studied. Results showed that 35 EVs charge together during the peak load will cause transformer overloading. In [4], it showed that power system needs to generate and transmit additional load demand for EVs. The extra loads can cause components overloading and transformer aging. In [5], it indicated that large-scale EV charging can cause a voltage drop and deviation. In [6], the authors observed that 60% penetration of EVs caused 40% higher power loss at the off-peak hours. Furthermore, a large amount of EV charging power in short duration will cause instability in the power system. The power system will take longer time to return to the steady state [7].

Therefore, to connect EVs to current power grids and ensure the distribution power system stability, efficient EV charging control and energy management strategies need to be explored to reduce or eliminate the negative impacts for the distribution grid. By using scheduled charging, better EV energy management can be achieved to provide grid services, such as load balancing, voltage and frequency regulation, and power quality improvement. Moreover, EVs can operate as energy storage to reduce the power fluctuations from renewable energy resources, such as PV panels. Smart EV charging and energy management can provide economic benefits for both distribution grid and EV customers as well as reduce emissions.

1.1.2 Types of EV Chargers

The charging levels are classified in terms of the power level the chargers can provide. In the United States, SAE J1772 and CHAdeMO are two currently competing standards. J1772 is the main standard for Level 1 and Level 2 charging and CHAdeMO only used for DC Fast Charging (DCFC) [8]. Recently, XFC has been introduced to compete with the short refueling period of internal combustion vehicles [9]. The comparison of charging levels, time, and location is summarized in Table 1.1 [8, 9]. AC Level 2 is widely adopted for current electric vehicle supply equipment (EVSE) at work and home places due to its relative low installation and operation cost. XFC will be the future trend because the short charging time, which is close to pumping gas for the traditional internal combustion engine vehicles. Thus, AC Level 2 and XFC are studied in this dissertation.

Table 1.1. Comparison of Charging Levels, Time, and Location

Type of Charging	**Power Levels**	**Charging Time (for 200 Miles)**	**Where to Charge**
AC Level 1	• 110/120 V AC electric circuit • 12 to 16 A • 1.4 to 1.9 kW	• Up to 36 hours • 0.082 miles/minute	At home or workplace
AC Level 2	• 208/240 V AC electric circuit • 15 to 80 A • 3.1 to 19.2 kW	• Up to 7 hours • 0.42 miles/minute	At home, workplace, or public charging stations
DC Fast Charging (DCFC)	• There-phase 440/480 V AC circuit converted to DC to EV • Up to 500 A • 50 to 350 kW	• Up to 1 hour • 2.92 miles/minute	Public or commercial charging stations
Extreme Fast Charging (XFC)	• 800 V DC electric circuit • 350 kW or more	• 7.5 minutes • 23.3 miles/minute	Public or commercial charging stations

1.1.3 Concept of Transactive Energy

With load growth through electrification of transportation and an increasing use of renewable energy resources, existing power distribution networks is moving toward an intelligent and smart power grid. Besides the features of traditional power systems, such as reliability, flexibility, efficiency, sustainability, etc., transactive energy (TE) concept offers a new economic process to improve the grid operation efficiency through market-based transactive exchange [10]. The concept was first introduced by U.S. Department of Energy's Gridwise Architecture Council and defined as: "a system of economic and control mechanisms that allows the dynamic balance of supply and demand across the entire electrical infrastructure using value as a key operational parameter" [10]. To develop a VGI system which will maximize the economic benefits of both system operators and end-user EV customers, TE concept is explored in this dissertation.

1.2 Literature Review

1.2.1 EV Smart Charging Control and Energy Management

In the aspect of power distribution network, EV charging control can be classified as uncoordinated and coordinated EV charging. For the uncoordinated charging, EV owners request the power system to charge vehicle batteries immediately until the vehicles are disconnected or fully charged. Local distribution circuit components will be stressful due to large EV charging load. Uncoordinated EV charging potentially causes series problems to the power grid system. To mitigate the negative impacts, coordinated or smart EV charging can be used allowing the distribution network and EV customers to schedule charging time to achieve economic benefits and technical advantages [11]. The optimization is implemented for coordinated or smart EV charging and energy

management to reduce overloading, eliminate voltage and frequency violation, avoid massive power losses, and decrease operation cost. In the smart EV charging, an EV aggregator (EVA) is commonly applied to manage amount of EVs in a specific area. EVA operates as an agent to ensure charging requirements of EV customers as well as support the technical operation of entire power distribution network. The control and optimization methods for coordinated or smart EV charging and energy management in this dissertation can be categorized as two strategies: the centralized charging control and distributed charging control.

In the centralized EV charging control, a center controller is responsible for managing the EV charging demand as well as the distribution grid operation improvement. The architecture of centralized EV charging control is shown in Figure 1.2. EVAs acquire the charging demands from the EVs and process and forward the information to the center controller. Then, the center controller will provide a global solution considering all EVs' charging requirements and grid conditions. A linear optimization method is introduce in [12] to manage large-scale EV charging and discharging. The issues of distribution network overload, voltage violation, and transformer aging can be fixed. In [13], a heuristic genetic algorithm of online centralized charging is proposed to limit transformer loading and bus voltage profiles. In [14], the optimal power flow (OPF) technique is performed to manage EV charging process. Results indicate that the proposed algorithm can avoid overloading, shift most charging to valley hours, and reduce power loss and generation costs. In [15], a centralized model predictive control method is developed to suppress the system frequency fluctuation. Although the centralized control can reach a global optimal solution of EV charging and

grid operation, it has the limitation to apply to large-scale EV charging because it requires huge computing power and communications bandwidth with the increased number of EVs.

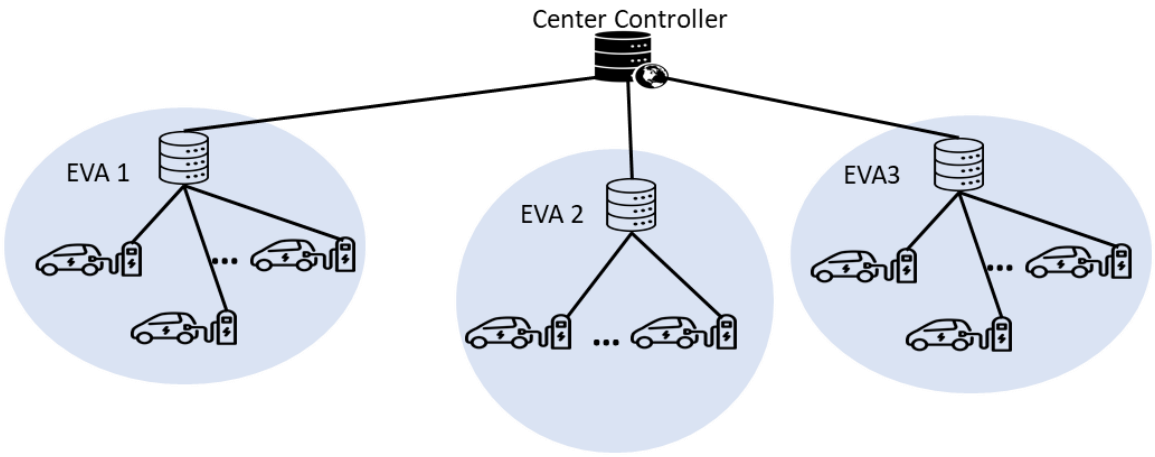

Figure 1.2. Centralized Control Architecture.

The distributed EV charging control is not dependent on a central controller. As shown in Figure 1.3, local controllers operate at EVA level can make control decisions based on the negation with other agents. EVA can independently improve charging benefit for its aggerated EVs as well as considers the grid control signals. Therefore, the communication load is much lower than the centralized control. In [16], a distributed game approach is introduced for EV charging management. Individual EVAs respond pricing signals to minimize its aggregated EVs' charging cost as well as consider distribution network constraints. In [17], a distributed control algorithm based on the alternating direction method of multipliers (ADMM) is proposed to recover voltage in a VGI distribution grid. The integration of distributed optimal power flow and EV charging is presented in [18]. The power loss is reduced significantly. The distributed EV charging methods with consensus algorithm are developed in [19, 20]. With limited

communication, smart EV charging can reduce charging power loss and provide grid frequency regulation. A real-time agent-based control system to manage the EV battery charging is presented in [21]. It operates like a distributed coordination process and is capable of preventing the transformer congestion. Although distributed control cannot guarantee to reach the exact global optimal solution for the overall system as centralized control, comparison in [14, 22-27] verified that the EV charging load can satisfy the grid requirements by practicing electricity price mechanism and EV user responsible behavior.

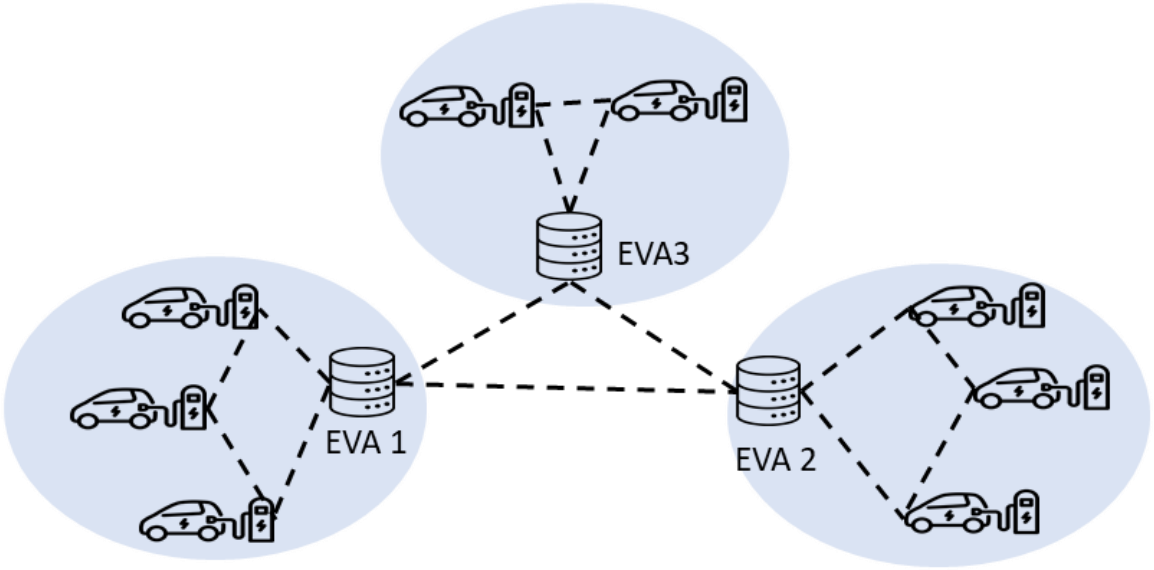

Figure 1.3. Distributed Control Architecture.

1.2.2 Fast Charging with Renewable Energy Sources

Since XFC has the potential to provide a short charging duration as the refueling process of traditional vehicles, the charging process is not necessary being controlled and shifted to off-peak periods. Instead, XFC stations are always equipped with renewable energy resources, such as photovoltaic (PV) and energy storage systems (ESS), to reduce the significant impacts on the distribution grid. The configurations of XFC stations are shown in Figure 1.4 [28]. For the AC-connected system, control strategy is complex, but

the protection is straightforward. Differently, the DC-connected system requires complex protection but simple control strategy [28-31]. The optimal sizing of PV and ESS and the energy management of ESS lead the effectiveness of the integration of XFC stations and power distribution networks.

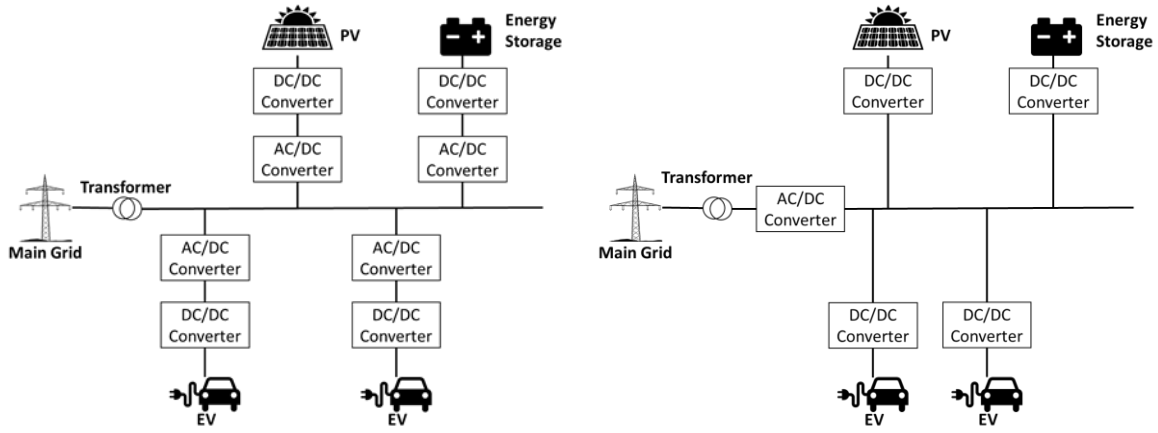

(a) (b)

Figure 1.4. Configurations for XFC Stations. (a) AC-connected System. (b) DC-connected System [28].

A real implementation of single EV fast charging station coupled with ESS is described in [32]. Results show the good performance of peak load shaving and nearly zero-impact on the distribution grid. A hybrid DC charge stations supplied by PV is introduced in [33]. In [34], a fast charging station is composed of a PV and a ESS with a decentralized control. The charging station is able to work as a stand-alone system and provide grid support. In [35], a decentralized voltage drop control of fast DC microgrid is proposed to maintain bus voltage, dispatch load power, and maintain SOC balancing of EV and ESS. In [36], a dynamic charging strategy of ESS is developed for fast charging stations to minimize peak demand on the grid side. Various optimization models for

sizing PV and ESS of fast charging stations have been proposed in [37-40]. All methods address the economic benefits of single or multiple fast charging stations.

From recent research, few work studied the operation and energy management of XFCs in the distribution networks. The operation of XFCs in a distribution network for large-scale EV charging need to be investigated.

1.2.3 TE Design for VGI System

For modern VGI system, TE concept enables EV customers actively participate in and contribute to the enhancement of the distribution system reliability, security, and efficiency. There are several publications related to EV auction mechanism instead of traditional demand response. In [41-45], optimal bidding approaches are proposed to support the EVA participating in the electricity market. In [46], an iterative auction design is introduced for EV charging station scheduling. In [47], each EV is designed to submit a multidimensional bid to support grid energy allocation. In [48], the auction mechanism is used for EV charging management to reduce PV curtailment in distribution networks. The bidding strategies for fast charging stations with battery ESS is introduced in [49]. Several studies focus on the local markets design for energy trading of renewable energy resources containing EVs. In [50-53], virtual markets are developed in microgrid level to integrate buildings and distrusted energy resources including EVs. In [54], a transactive market model is designed in distribution system operator(DSO)to manage the distribution network operation and participate in wholesale market. A case study of TE trading in distribution network is introduced in [55]. In [56], an optimal scheduling and trading framework is proposed for multi-microgrids integrated with an urban

transportation networks. The EV charging prices is analyzed with the traffic flow. In [57], a Stackelberg game for energy trading with dynamic pricing is proposed for EVs in the smart city. In [58], an optimal energy management algorithm based on the mixed-integer-linear programming method for EVs is designed with online energy trading. In [59], a TE trading framework is proposed to balancing the economic efficiency and distribution system operation. Therefore, implementing TE concept in modern VGI system is proper to be investigated in this dissertation.

1.3 Research Objectives and Contributions

The research objectives of this dissertation are to provide solutions for effectively integrating large-scale EV charging with power distribution networks, as well as improve the cost-effectiveness, reliability, and grid security. The smart EV charging control and energy management in the distribution networks are explored to mitigate the negative impacts of EV charging and provide grid services.

The main contributions of this dissertation are:

- A centralized EV charging control algorithm is developed to coordinate large-scale EV charging with TE concept. An EV bidding strategy is designed to minimize charging cost as well as consider charging requirements. With the day-ahead electricity price, all controllable EVs setup their bids for the remaining charging period optimally. A competitive market clears the price and the available energy to aggregators based on the bids, grid constraints, and the day-ahead electricity price. When congestion happens, economic energy dispatch is performed to minimize the grid power loss and the difference of bidding cost and

actual cost. This control design reduces heavy communication and computational load for the VGI central controller.

- A distributed EV charging scheduling with transactive energy management is developed. Besides the improved bidding strategies, EVAs and DSO operate as multi-agent and negotiate with each other to clear the electricity price based on ADMM. DSO ensures the system operation with OPF technique and EVA minimize its charging cost. Particularly, an EV charging price clearing mechanism is developed for the negotiation process. EVA and DSO can make their own decisions. This mechanism provides economic benefits of EV charging and ensures the stability of the distribution network. This work addresses a realistic EV charging scheduling problem for modern VGI systems. The research on applying TE to distribution network operation and large-scale EV charging energy management is still at early stage.
- A Monte Carlo (MC) simulation tool is developed based on the EV arrival time and SOC distributions obtained from vehicle travel survey dataset to realistically estimate the charging power demand of XFC stations. The MC simulation algorithm considers various impact factors, such as EV scale, EV model type, the percentage of each type in the total simulated EVs, EV charging curves for different EV model types, XFC station port availability, and maximum waiting time. An optimal configuration method is also developed for the multiple XFC stations in a distribution network to determine the optimal energy capacity of ESS, ESS rated power, and the size of PV panels, which are integrated with XFC stations. Unlike most existing literature on the sizing of a single XFC station at

the microgrid level, this method studies the optimal configuration of multiple XFC stations at the distribution network level. It can reduce both investment and operation costs while meeting the charging demand and the operational constraints of the distribution network, XFC, ESS, and PV panels.

- A cloud-based simulation and testing platform is presented for the development and Hard-ware-in-the-Loop (HIL) testing of VGI technologies. To fill the gap between spatially distributed EV charging stations and communication interoperability, the platform is developed to consists of multiple subsystems: real-time power system simulators, such as OPAL-RT and RTDS, Smart EV Charge Scheduler (EVCS) System, and a real Smart Energy Plaza (SEP) with various types of charging stations, solar panels, and energy storage systems. The subsystems can communicate with each other via message queuing telemetry transport communication (MQTT) protocol. The platform also considered standardized communication protocols: Open Charge Point Protocol (OCPP) 2.0 for charging station networks and ISO 15118 between EVs and charging stations. The modular open systems design approach of the platform allows the integration of EV charging control algorithms and hardware charging systems for performance evaluation and interoperability testing.

1.4 Outline of the Dissertation

The content of this dissertation is organized as below:

- Chapter 2 presents a TE-based centralized control algorithm for large-scale EV charging coordination. The bidding strategy is designed to consider charging

requirement and minimize the charging cost. A case study shows that the EV charging cost and the overloading of the distribution network can be reduced significantly.

- Chapter 3 presents an ADMM-based distributed EV charging scheduling strategy with transactive energy management. The negotiation process among DSO and EVAs is designed to clear the charging electricity price with OPF technique. The simulation results show that the presented algorithm can balance distribution network operation stability and EV charging cost efficiency.
- Chapter 4 introduces the optimal configuration of XFC stations integrated with ESS and PV panels in distribution networks. A MC simulation tool has been developed to estimate the charging demand of XFC stations with the consideration of various aspects, including EV scale, types of EV models, the percentage of different EV models in the total simulated EVs, EV charging curves for different EV models, XFC station port availability, and the maximum waiting time.
- Chapter 5 demonstrates a cloud-based simulation and testing platform for large-scale EV charging management and EV charging control. A real-world implementation shows that the communication links of the platform work properly, and the EV charging control algorithms can respond to transmission level grid service request with minimal impact on local operations.
- Chapter 6 provides the conclusion of the dissertation and discusses the possible future work on EV charging and energy management on VGI systems.

2 Centralized EV Charging Control based on Transactive Energy Concept [1] [60]

This chapter presents a TE-based control approach for planning the charging activities of EVs. In the presented framework, individual EV owners propose charging bids to minimize the charging cost. The proposed bids depend on the charging urgency and the day-ahead electricity price forecast. Considering the scalability of the system, aggregators at the node-level are designed to collect the bids for a group of EVs within a node and submit a combined bid for the node to the market in a distribution network. The market clears the electricity price based on the bids, grid constraints, and the day-ahead electricity price. When the received power from the market is less than that of the total EV power demand, power dispatch is required to effectively allocate the available power to individual distribution nodes and EVs.

2.1 General Framework

The system in consideration is shown in Figure 2.1, which consists of a competitive market at distribution network level, aggregators at node-level, and a large number of EVs. The competitive market negotiates electricity price and energy amount with controllable EVs through aggregators. Each node-level aggregator serves as an interface between the market and a group of EVs. The dynamic balance of supply and EV charging demand is achieved by following five steps.

[1] © [2019] IEEE. Reprinted, with permission, from [Zhouquan Wu, Chong Cao, Bo Chen, Transactive Energy Based Approach for Large-Scale Plug-in Electric Vehicle Charging Control, 2019 IEEE PES Asia-Pacific Power and Energy Engineering Conference (APPEEC), 12/2019] See Appendix 0 for documentation of permission to reuse this material

1) Each controllable EV proposes a charging scheduling for the remaining parking time based on day-ahead electricity price and its charging requirement, including charging time, current SOC, and target SOC.
2) A node aggregator gathers EV demand bids for a node. The aggregator forms an overall bidding strategy for the node based on EV bids and feeder limits, and then, submits the node bidding strategy to the market.
3) The market clears the electricity price at which the objectives can be achieved. The clearing price and the amount of energy are sent to aggregators.
4) Base on the market clearing and bidding information, an optimal power allocation for each node is performed if the bidding demands cannot be met.
5) Similarly, each aggregator dispatches electric power to individual EVs.

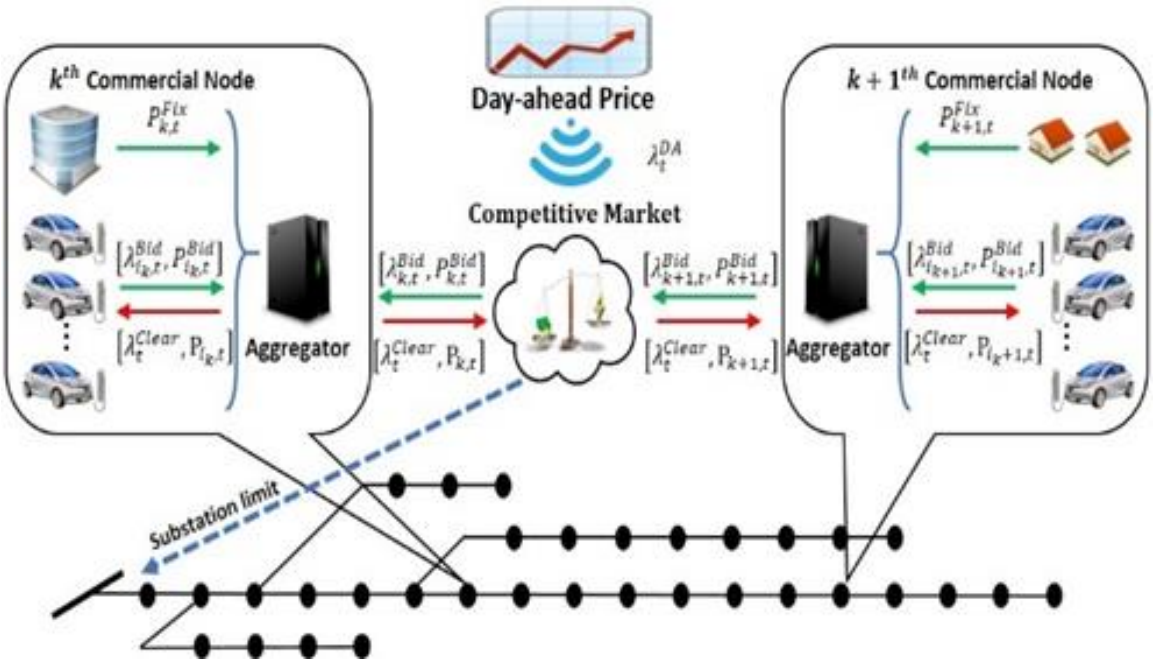

Figure 2.1. System Diagram of TE-Based EV Charging Control in a Distribution Network.

2.2 Mathematical Modeling

2.2.1 EV Bidding Price Function

The bidding price for each controllable EV is defined as a function of bidding power demand, charging urgency, and day-ahead price. Considering the i^{th} EV under node k, the charging urgency $\mu_{i_k,t}$ at time t is defined in (2.1),

$$\mu_{i_k,t} = \begin{cases} \frac{P_{i_k,t}^{avg}}{P_{i_k}^{\max}} & \text{if } P_{i_k,t}^{avg} < P_{i_k}^{\max} \\ 1 & \text{else} \end{cases} \tag{2.1}$$

where $P_{i_k,t}^{avg}$ is the required average charging power and $P_{i_k,t}^{max}$ is the rated charging power.

The required average charging power is calculated by (2.2),

$$P_{i_k,t}^{avg} = \frac{(SOC_{i_k}^{tar} - SOC_{i_k,t_c})C_{b,i_k}}{(T_{i_k} - t_c)\eta_{i_k}} \tag{2.2}$$

where $SOC_{i_k}^{tar}$ and T_{i_k} are the target SOC and the departure time of EV i_k; the $SOC_{i_k,t}$ and t_c are current SOC and time; and the parameters η_{i_k} and C_{b,i_k} represent the charging efficiency and battery capacity. When $\mu_{i_k,t}$ equals to one, the maximum charging power is needed for the remaining charging period.

The bidding price $\lambda_{i_k,t}^{Bid}$ is defined as below:

$$\lambda_{i_k,t}^{Bid} = \lambda_t^{DA} + \frac{\lambda_t^{Cap} - \lambda_t^{DA}}{P_{i_k}^{\max}} \mu_{i_k,t} P_{i_k,t}^{Bid} \tag{2.3}$$

where λ_t^{DA} is the day-ahead electricity price at time t; and λ_t^{Cap} is the highest bidding price. The bidding price depends on the bidding power and charging urgency two factors. As shown in Figure 2.2, EV with higher charging urgency and power demand will offer higher bidding price to compete with others.

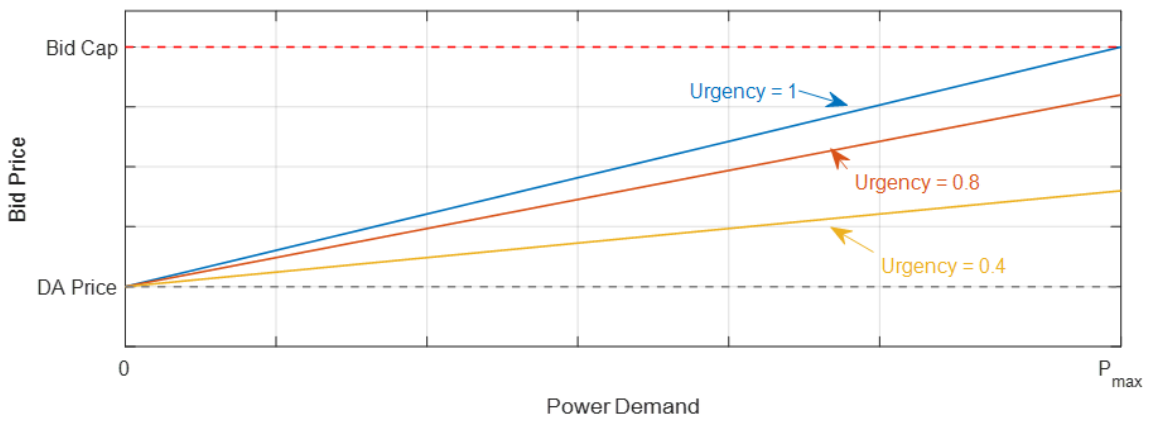

Figure 2.2. Bidding Price Curve of EVs.

2.2.2 EV Bidding Strategy

Controllable EVs receive the day-ahead electricity price forecast and perform the optimal bidding planning with its charging requirement. The optimal bidding planning minimizes the bidding cost subject to the charging energy requirements. The planning only covers the time duration from the current time t_c to the departure time T_{i_k}. The charging cost prior to the current time is not considered. Therefore, the bidding planning of an EV based on day-ahead price is formulated as below.

$$\min_{P^{Bid}_{i_k,t}} \sum_{t\in[t_c,T_{i_k})} \lambda^{Bid}_{i_k,t} P^{Bid}_{i_k,t} \tag{2.4}$$

$$s.t. \quad SOC_{i_k,T_{i_k}} = SOC^{tar}_{i_k} \tag{2.5}$$

$$SOC_{i_k,T_{i_k}} = SOC_{i_k,t_c} + \frac{\sum_{t\in[t_c,T_{i_k})} P^{Bid}_{i_k,t}\eta_{i_k}}{C_{b,i_k}} \tag{2.6}$$

$$P^{Bid}_{i_k,t} \in \begin{cases} (0, P^{\max}_{i_k}] & \text{if } a_{i_k,t}=1 \\ 0 & \text{if } a_{i_k,t}=0 \end{cases}, \ \forall i_k \in \{\mathbf{I_k}\} \tag{2.7}$$

Constraint (2.5) considers the target SOC requirement. The target SOC is calculated by equation (2.6). Constraint (2.7) limits the EV bidding demand under the maximum charging power. The symbol, $\boldsymbol{I_k}$, represents a vector of controllable EVs at node k. The

parameter $a_{i_k,t}$ indicates the charging status: charging or idle. The minimal charging power is assumed to be zero and the maximum value of charging power, $P_{i_k}^{max}$ depends on the type of EV charger. The individual EV bidding strategies are generated by solving above optimization problem with quadratic programming.

2.2.3 Node Aggregator

A node-level aggregator bridges the communication between EVs and the market in TE-based EV charging control systems. The aggregator serves two purposes in this chapter: prepares a bidding strategy for a node and dispatches power to individual EVs. There are two categories of loads in a node: fixed loads, such as building loads and uncontrolled EV charging loads, and flexible EV charging loads.

The node-level bidding strategy is defined in (2.8) and (2.9), where $P_{k,t}^{Bid}$ is the node k bidding power and $\lambda_{k,t}^{Bid}$ is the bidding price. $P_{k,t}^{Cap}$ is the node k power limit and $P_{k,t}^{Fix}$ denotes the fixed power demand of the node k. When $P_{k,t}^{Bid}$ is larger than the power capability of the feeder, the bidding power is limited to protect overloading.

$$P_{k,t}^{Bid} = \min\left(\left(\sum_{i_k \in \mathbf{I_k}} P_{i_k,t}^{Bid}\right), (P_k^{Cap} - P_{k,t}^{Fix})\right) \tag{2.8}$$

$$\lambda_{k,t}^{Bid} = \sum_{i_k \in \mathbf{I_k}} (\lambda_{i_k,t}^{Bid} \frac{P_{i_k,t}^{Bid}}{\sum_{i_k \in \mathbf{I_k}} P_{i_k,t}^{Bid}}) \tag{2.9}$$

The energy management algorithm of the aggregator is introduced in the Economic Power Dispatch section.

2.2.4 Market Clearing

The market unit plays an important role in a transactive energy system. Several computing methods for the market have been discussed in the literatures [61-63]. This chapter employs a non-iteration-based clearing mechanism. This method sorts all bids by price in descending order. Given the substation capacity and the day-ahead electricity price at current time step, the market clears the price in following ways. If the total power demand is less than the substation available capacity, which means that no congestion happens, the clearing price is set as the day-ahead electricity price. Otherwise, as Figure 2.3 shown, the clear price will be increased to cap the demand under the substation capacity. This method was validated in AEP gridSMART demonstration project [63].

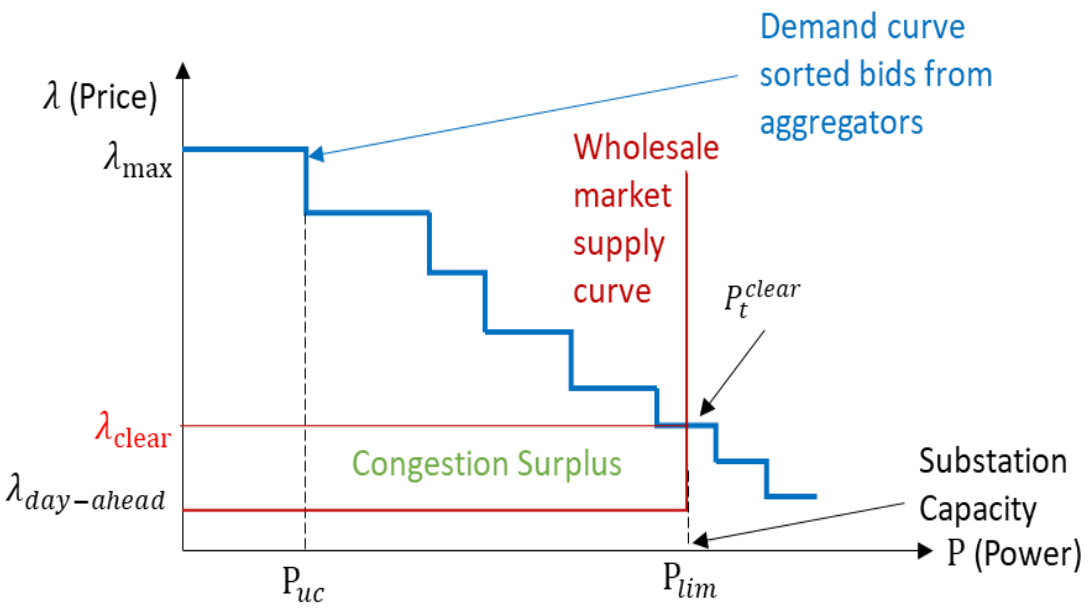

Figure 2.3. Graphical Illustration of Market Clearing – Congested Case [63].

2.2.5 Economic Power Dispatch

When the received power from the market, P_t^{Clear}, is less than that of the total EV power demand, power dispatch is required to effectively allocate the available power to

individual distribution nodes and EVs. At the node-level, the objective is to minimize the grid power loss.

The line current $I_{k_l,t}$ is updated in each time step by equation (2.10). The notation k_l indicates the line before node k and k_{l+1} represents the line after node k. $I_{k_b,t}$ represents the line current of a branch at node k. The variables $I_{k,t}$, $V_{k,t}$, $P_{k,t}$, and $Q_{k,t}$ are the current, voltage, real power, and reactive power of node k, respectively. The line current can be update from any end nodes of branches.

$$\begin{aligned} I_{k_l,t} &= I_{k,t} + I_{k_{l+1},t} + I_{k_b,t} \\ &= \left(\frac{P_{k,t} + jQ_{k,t}}{V_{k,t}} \right)^* + I_{k_{l+1},t} + I_{k_b,t} \end{aligned} \tag{2.10}$$

$I_{k_{l+1},t} = 0,$ if k is an end node

$I_{k_b,t} = 0,$ if k is a node without branch

The optimization problem can be formulated as:

$$\min_{I_{l,t}} \sum_{k_l \in \mathbf{K_L}} \mathrm{R}_{k_l} \left| I_{k_l,t} \right|^2 \tag{2.11}$$

$$s.t. \quad \sum_{k \in \mathbf{K}} P_{k,t} = P_t^{clear} \tag{2.12}$$

$$P_{k,t} \in [0, P_{k,t}^{Bid}], \ \forall k \in \{\mathbf{K}\} \tag{2.13}$$

R_{k_l} and $I_{k_l,t}$ are the resistance and the current of line k_l. $\boldsymbol{K_L}$ is the vector of lines in a distribution network under consideration. The line current $I_{k_l,t}$ is updated in each time step by equation (2.10). The notation k_l indicates the line before node k and k_{l+1} represents the line after node k. $I_{k_b,t}$ represents the line current of a branch at node k. The variables $I_{k,t}$, $V_{k,t}$, $P_{k,t}$, and $Q_{k,t}$ are the current, voltage, real power, and reactive power of node k, respectively. The line current can be update from any end nodes of branches.

The total node power equals to the available power P_t^{Clear} as defined in (2.12). $\boldsymbol{K}$ is the vector of nodes. The constraint (2.13) limits node powers under the individual node bidding power $P_{k,t}^{Bid}$. With the quadratic objective function (2.11), this optimization can be solved by the sequential method in a centralized manner. Based on the $P_{k,t}^{Fix}$ load of each node, a flat voltage profile is computed based on backward-forward sweep methods, and then, the optimal power allocation profile is determined through the quadratic optimization. After that, the node voltages are updated. The process continues until the differences of node voltages are smaller than a predefined tolerance value.

At the EV-level within a node, the objective is to minimize the difference of the total charging cost of the node with the bidding cost. The optimization problem is formulated as:

$$\min_{P_{i_k,t}} \sum_{i_k \in \mathbf{I_k}} (\lambda_t^{Clear} P_{i_k,t} \Delta t - \lambda_{i_k,t}^{Bid} P_{i_k,t}^{Bid} \Delta t)^2 \tag{2.14}$$

$$s.t. \quad \sum_{i_k \in \mathbf{I_k}} P_{i_k,t} = P_{k,t} \tag{2.15}$$

$$P_{i_k,t} \in [0, P_{i_k,t}^{Bid}], \ \forall i_k \in \{\mathbf{I_k}\} \tag{2.16}$$

where $P_{i_k,t}$ denotes the allocated power for i^{th} EV at node k, and λ_t^{Clear} indicates the market clearing price. Constraint (2.15) caps the total charging power of controllable EVs to the available power $P_{k,t}$ at the node. Constraint (2.16) specifies the charging power of controllable EVs varying from zero to the bidding power. The actual charging power for each controllable EV in the node is allocated by solving this optimization problem with quadratic programming.

2.3 Case Study

2.3.1 System Setup

The presented TE-based control approach is tested on a 33-bus distribution test feeder [64] with commercial area and residential area. Table 2.1 lists the load distribution of the grid. The commercial area consists of 22 nodes, which contains offices, restaurants, malls, supermarkets, retails, school, warehouses, parking lots and hotels. For the residential area, houses and apartments are located at 10 nodes. All the building loads are obtained from [65] for the area of Chicago O'Hare International Airport in Illinois, USA. It is assumed that there are total of 381 EVs in the distribution network, including Chevrolet Volt 2019 and Nissan Leaf 2019. The average charging efficiency of all EVs is assumed to be 80%. The EV arrival/departure time and initial/target SOC are randomly generated based on[12, 66]. The EV charging under residential nodes are during the evening or night and must be complete by 7:00 a.m. on the second day. The commercial EV charging customers prefer to stay 2 to 6 hours during daytime. The day-ahead electricity price shown in Figure 2.4 is based on the average day-ahead price forecast in August 2016 obtained from [67]. The price cap λ_t^{Cap} is 2¢/kWh higher than the day-ahead electricity price.

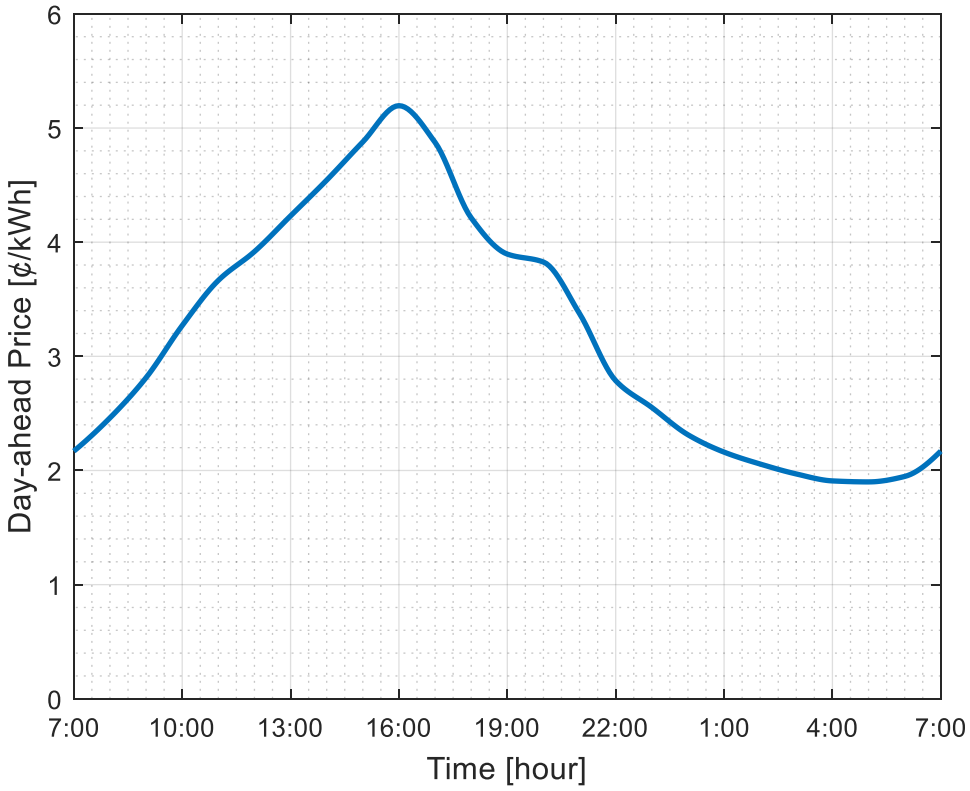

Figure 2.4. Day-ahead Electricity Price.

Table 2.1. List of Loads in the Distribution Network

Residential				**Commercial**			
10 Nodes		183 EVs		22 Nodes		198 EVs	
Categories	Node	No of EVs	Node Limit	Categories	Node	No of EVs	Node Limit
20 Houses	11	20	75	Warehouse	1,28	10,0,	100,100
19 Houses	12	19	75	Strip Mall	2	0	100
Apartment	13	24	100	Retail	3	0	100
23 Houses	14	23	100	Full-Service Restaurant	4, 8, 9, 26	8, 0, 5, 6	75, 75, 75, 75
16 Houses	15	16	75	Quick Service Restaurant	5, 10, 22, 25	4, 0, 0, 0	50, 50, 50, 50
19 Houses	16	19	75	Hotel	6	10	150
22 Houses	17	22	100	Office (M)	7, 29	35, 0	250,250
Apartment	18	20	100	Office (S)	20, 32	10, 0	100,50
Apartment	19	0	100	School	21	0	50
27 Houses	27	20	75	Supermarket	23, 24	20, 20	400,400
				Parking Lot	30, 31	30, 40	100,200

2.3.2 Simulation Results

With 5-minute step time, this use case simulates a 24-hour period for the system under three scenarios, including the uncontrolled charging, 50% and 100% of participation rates. For uncontrolled EVs, the charge starts at the arrival time with

maximum charge power. When the SOC reaches to the target, the charging will be stopped. Any uncontrolled EV is considered as fixed load.

The impact of the load profile with different EV participation rates is shown in Figure 2.5. During the period of 17:00 to 21:00, the total load for uncontrolled charging scenario exceeds the 2400 kW substation capacity. With the increase of EV participation rate, the charging power shifts to late night gradually and the power profile is no longer to reach substation capacity. Particularly, for 100% participation scenario, the peak load is close to base load but has the highest load value during late night when the day-ahead electricity price is lower. From the simulation results, uncontrolled charging is more likely to cause overloading during peak load time, but the TE-based method can reduce distribution network congestion and shift the charging load to the off-peak period.

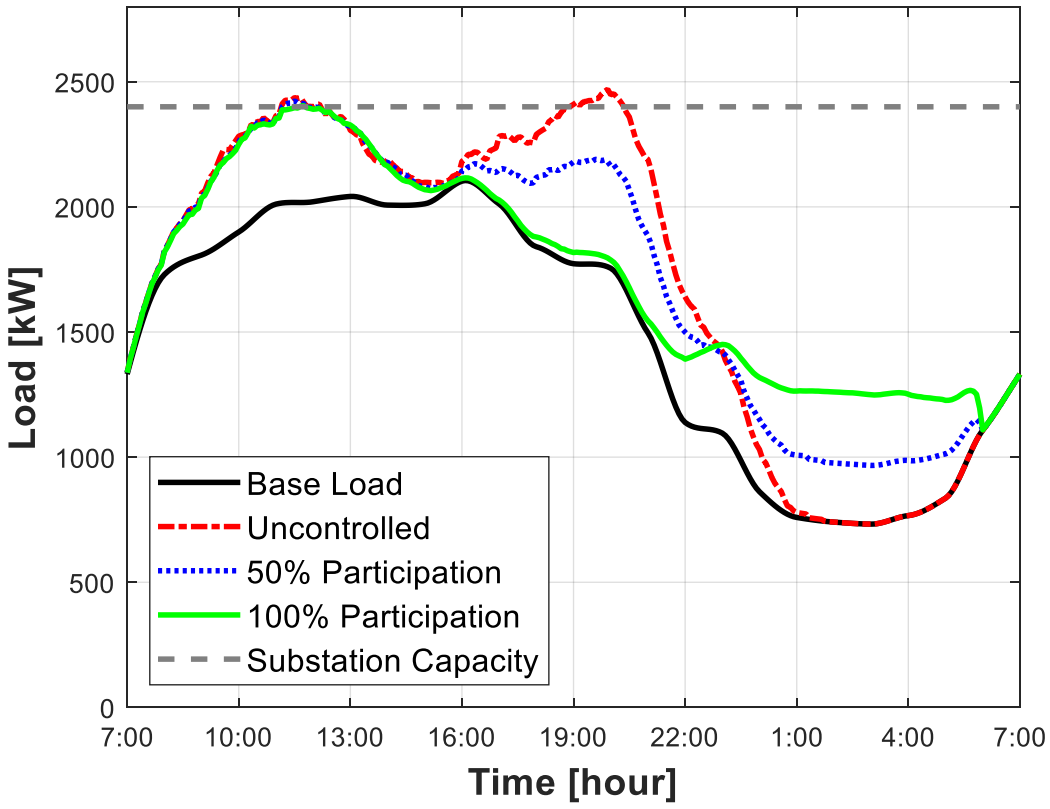

Figure 2.5. Load Profile of the Distribution Network

The presented method can also well manage the node-level congestion. Figure 2.6 shows the aggregated load of the commercial node 7. All the EVs choose maximum charging power as soon as they arrive. However, once the aggregated load reaches the feeder limit after 9:00am, the aggregator will cut the total feeder charging power.

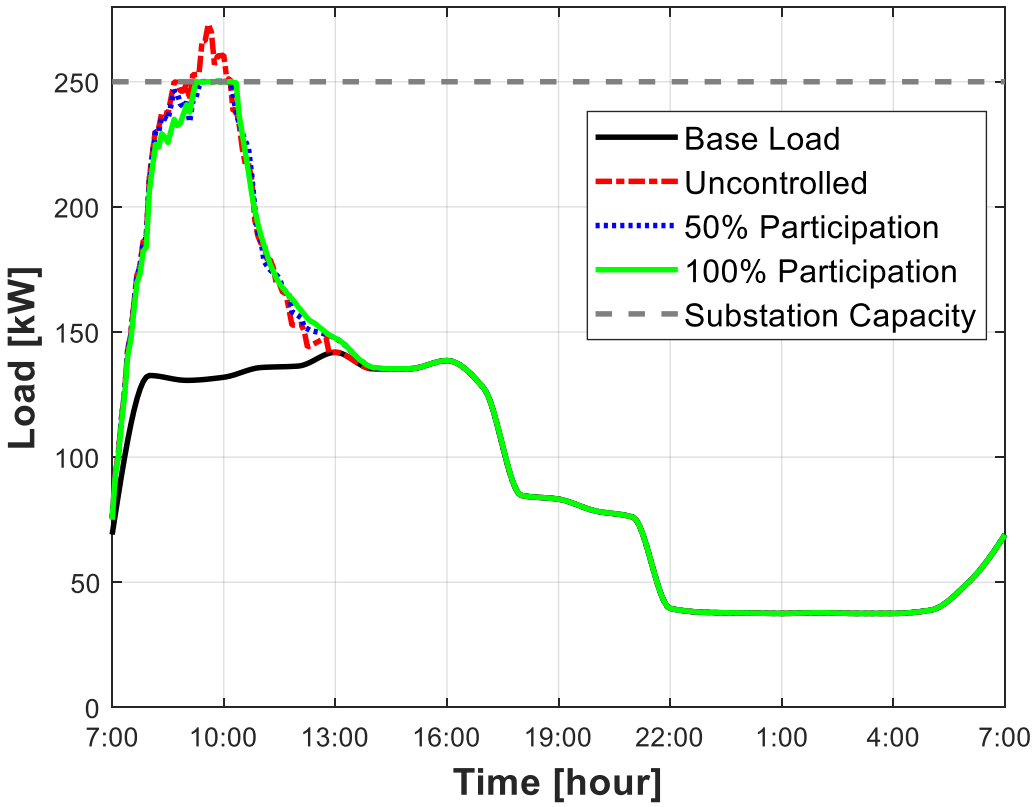

Figure 2.6. Load Profile of the Commercial Node 7

Figure 2.7 shows the aggregated load of residential node 15. Either uncontrolled scenario or 50% participation scenario will cause the feeder congestion. In the 100% participation scenario, all the EV customers are able to select low price time period to charge their vehicles.

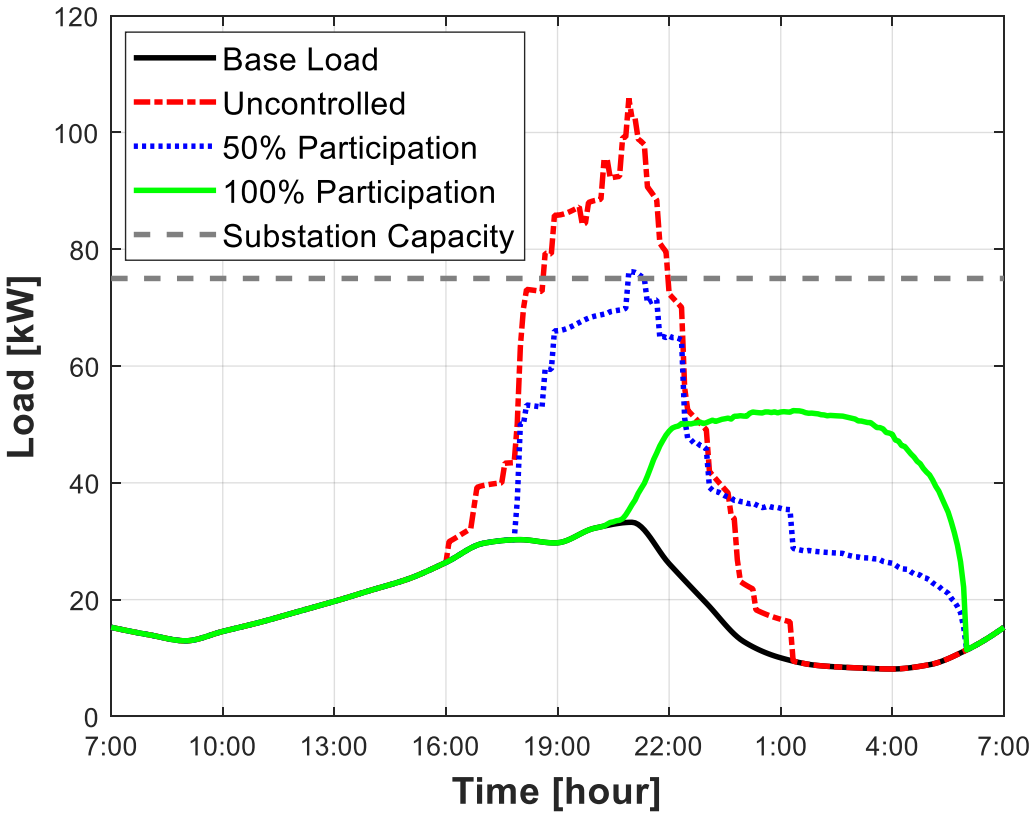

Figure 2.7. Load Profile of the Residential Node 15

Table 2.2 compares the charging cost in different scenarios. It is observed that 100% participation scenario has the lowest charging cost. The charging cost increases when the participation rate decreases. Considering the commercial node 7, the cost is only reduced a little bit. That is because EVs under these nodes have less opportunity to avoid peak price. However, EV customers under the residential nodes 15 can reduce the charging cost significantly due to lower price and loads during nighttime.

Table 2.2. Comparison of Charging Cost (price does not consider various service fees)

Scenario		Uncontrolled	50% Participation	100% Participation
Charging Cost [¢]	Overall	20724	18373	15427
	Node 7	1222	1219	1214
	Node 15	1056	874	658

Figure 2.8 shows the individual charging cost of all EVs. The actual charging cost is perfectly tracking with the bidding cost. Meanwhile, the actual charging costs of individual EVs are reduced effectively. It must be noticed that uncontrolled charging scenario applies the day-ahead electricity price as the actual charging price and does not consider the grid congestion. This will cause a few EVs have higher actual charging cost during peak price duration.

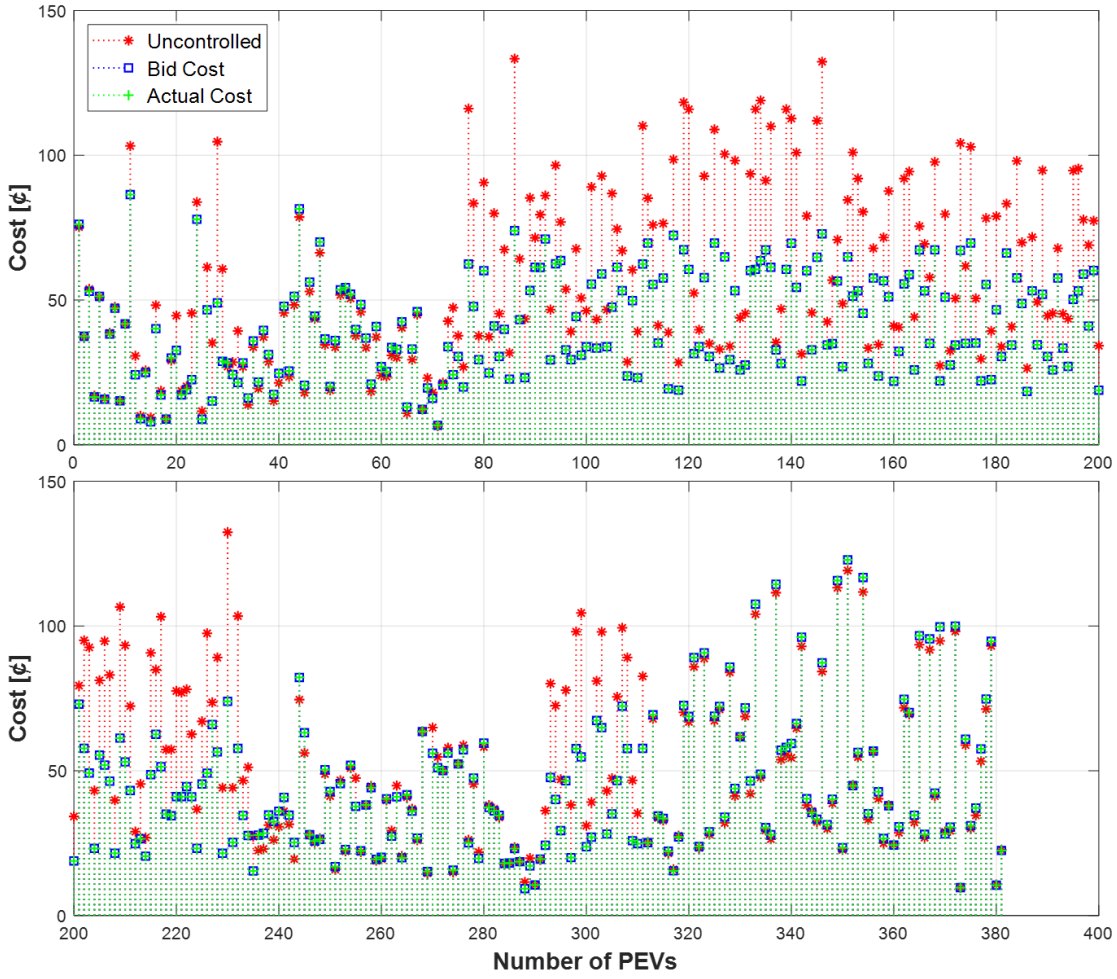

Figure 2.8. Individual EV Charging Cost

2.4 Chapter Conclusion

This chapter presents a TE-based control strategy to optimize the EV charging. With the day-ahead electricity price forecast, all controllable EVs setup their bids for the remaining charging period optimally. Moreover, given the bids, grid constraints, and the day-ahead electricity price, a competitive market clears the price and the available energy to aggregators. When congestion happens, economic energy dispatch is performed to minimize the grid power loss and the difference of bidding cost and actual cost. The simulation results show that the charging cost of controllable EVs can be reduced

especially at night. The charging load is also shifted to off-peak period to avoid distribution network congestion.

However, the optimization problems are solved in a centralized manner. The proposed strategy is only suitable to control EV charging rate for current timestep instead of schedule the whole EV charging process. The distribute EV charging scheduling need to be explored to apply to modern power system.

3 Distributed EV Charging Scheduling with Transactive Energy Management [2] [68]

A distributed EV charging scheduling strategy with transactive energy management (TEM) is presented in this chapter to deal with technical issues in distribution network operation and discuss the economic benefits of EV charging. At an individual EV level, EV owners propose bids to actively participate in the distribution system operation. At the node level, an electric vehicle aggregator optimally allocates the available charging power to meet EV charging requirements and cost benefits. At the distribution network level, a distribution system operator integrates an electricity price market clearing mechanism with the optimal power flow technique to ensure the reliability of the distribution network. Moreover, a distributed algorithm is discussed for solving the EV charging problem with transactive energy management. The clearing electricity price is achieved through a negotiation process be-tween the DSO and EVAs using the alternating direction method of multipliers.

3.1 Overview of EV Charging Scheduling Management

Consider a radial distribution network with J buses, a DSO is designed at the slack bus to ensure grid stability and address the economic benefits. In addition, several EVAs are located at each node except the slack bus. Each EVA responds to a group of EVs based on their physical locations. As shown in Figure 3.1, the system includes multi-criterion optimizations among the DSO, EVAs, and individual EVs.

[2]

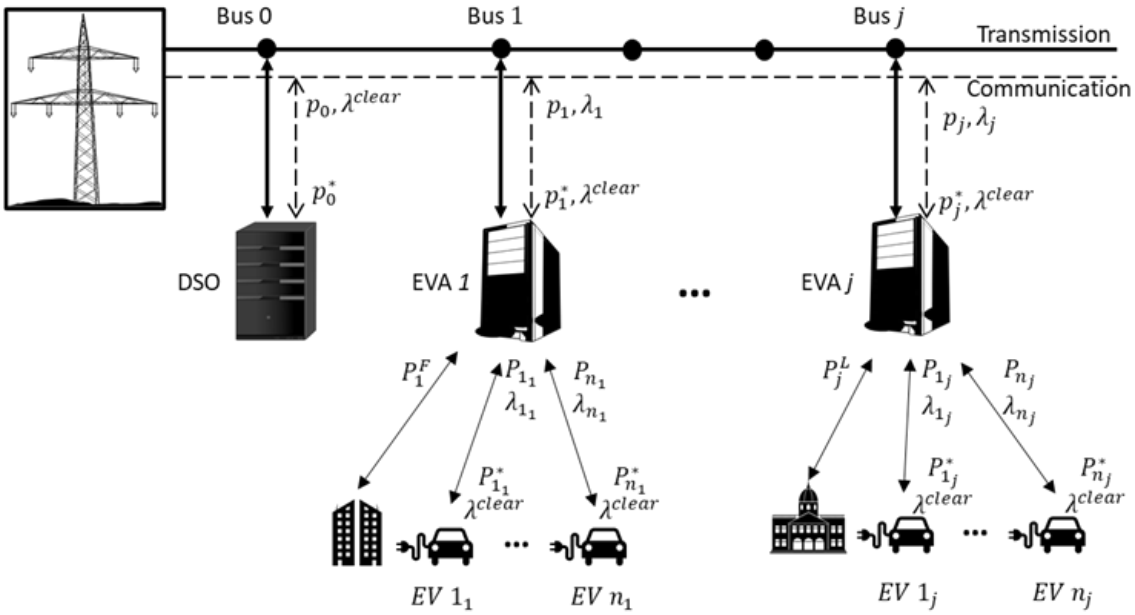

Figure 3.1. The System diagram of TE-based EV Charging

To coordinate the operation of the integrated EVs, EVAs, and DSO, a TE-based EV charging mechanism is designed to achieve a reliable and cost-efficient electricity system. In contrast to the traditional demand response control, EV customers can choose to buy and prioritize the charging cost. As shown in Figure 3.2, EV charging scheduling management comprises three stages. In Stage 1, an optimal EV bidding strategy of individual EV and node-level aggregation is designed. Individual EV owners will propose their optimal bidding strategy based on day-ahead electricity price forecasts and charging requirements. Then, a node-level EVA will collect all bidding information within the node and form a bidding price for the node. With this strategy, EVs can directly participate in the distribution-level market clearing mechanism in Stage 2. In Stage 2, the DSO will clear the electricity bidding and find the clearing electricity price, and EVA will adjust its feasible power demand. Meanwhile, the OPF technique will be addressed in this stage to ensure the smooth operation of the grid. In Stage 3, the node-

level EVA will optimally determine the charging rate for individual EVs within the node by considering EV owners' bidding demands in Stage 1, the clearing electricity prices, and the available power in the node.

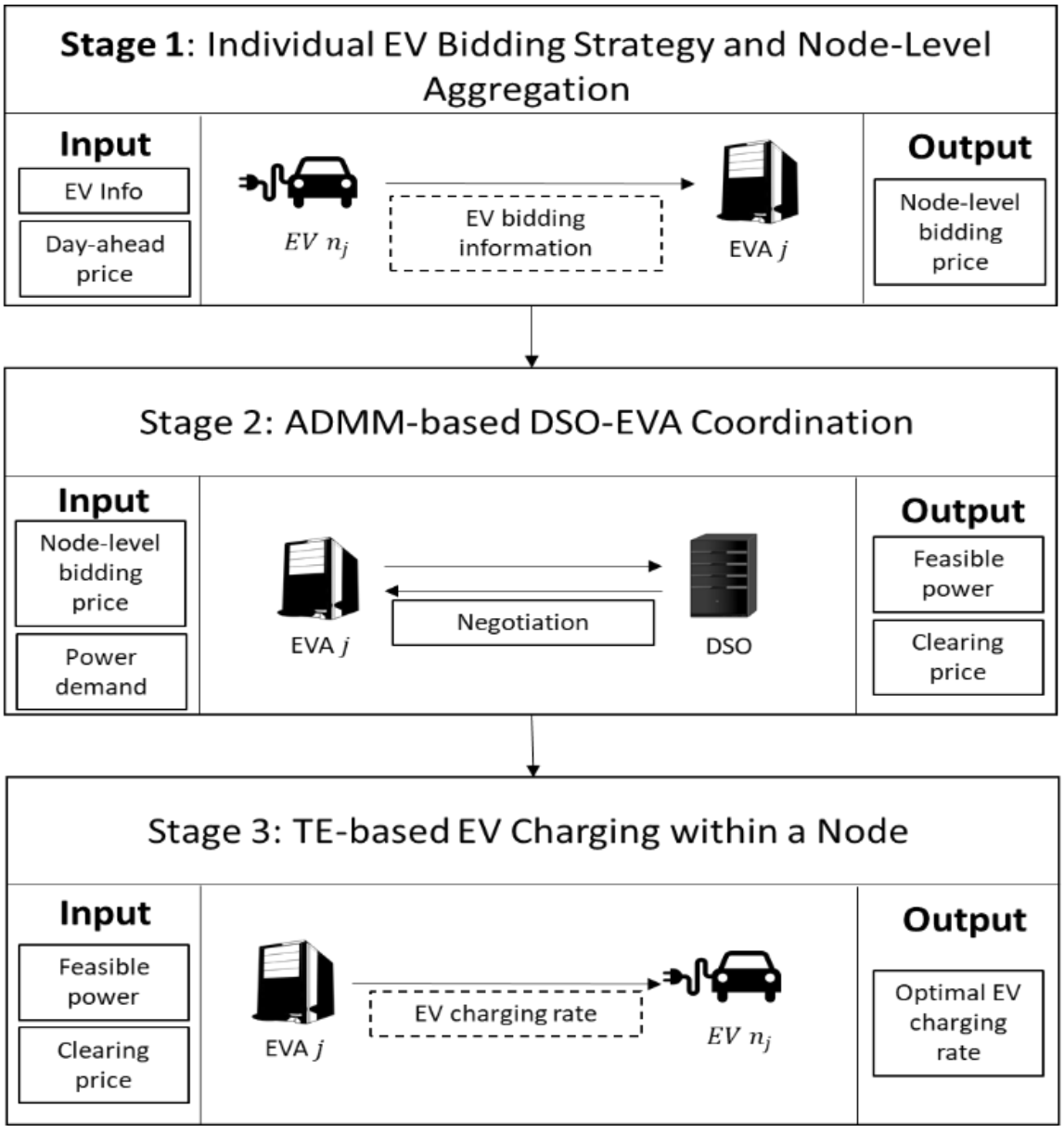

Figure 3.2. Three-stage EV Charging Scheduling Management.

3.2 EV Charging and Distribution Network Model

3.2.1 EV Charing Model

An individual EV seeks to optimize its charging power scheduling for a time period of T as defined by a vector of $\boldsymbol{P_{n_j}} = \left[P_{n_j}(1), \dots, P_{n_j}(t), P_{n_j}(t+1), \dots, P_{n_j}(T)\right]$, where $n_j \in \{1_j, \dots, N_j\}$ represents the location of n^{th} EV supplied by EVA j. The EV charging process is modeled as a discrete-time linear system as:

$$SoC_{n_j}(t+1) = SoC_{n_j}(t) + \frac{\eta_{n_j} P_{n_j}(t) \Delta t}{E^C_{n_j}} \tag{3.1}$$

where $P_{n_j}(t)$ is the charging power at time step t, $E^C_{n_j}$ indicates the battery capacity, η_{n_j} is the charging efficiency, and Δt represents the time step duration. The energy requirement, maximal and minimal charger power rating of individual EVs are defined as a series of constraints. It is assumed that the charging duration and energy requirement are known as soon as EVs connect to the charging stations. The constraints of individual EV charging schedules are:

$$\begin{cases} P^{\min}_{n_j} \le P_{n_j}(t) \le P^{\max}_{n_j} & \text{if active} \\ P_{n_j}(t) = 0 & \text{if inactive} \end{cases} \tag{3.2}$$

$$SoC_{n_j}(t + d_{n_j}) = SoC^T_{n_j} \tag{3.3}$$

Vehicle-to-grid power flow is not considered in this paper. Therefore, the values $P^{max}_{n_j}$ and $P^{min}_{n_j}$ indicate the maximal and minimal EV charging rate for the time horizon. The parameter d_{n_j} denotes the number of time steps remaining until departure and $SoC^T_{n_j}$ is the target SoC by the next departure.

3.2.2 Distribution Network Model

Given a radial distribution network represented by graph $G = (J, E), J = \{0, \dots, J\}$ represents the set of feeder nodes and E denotes the set of lines between the buses in the network, e.g., $(i, j) \in E$ indicates the line that from bus i to bus j. Let bus 0 represent the substation bus that connects to the utility as an external power source. The branch flow model in a radial distribution network is shown in Figure 3.3.

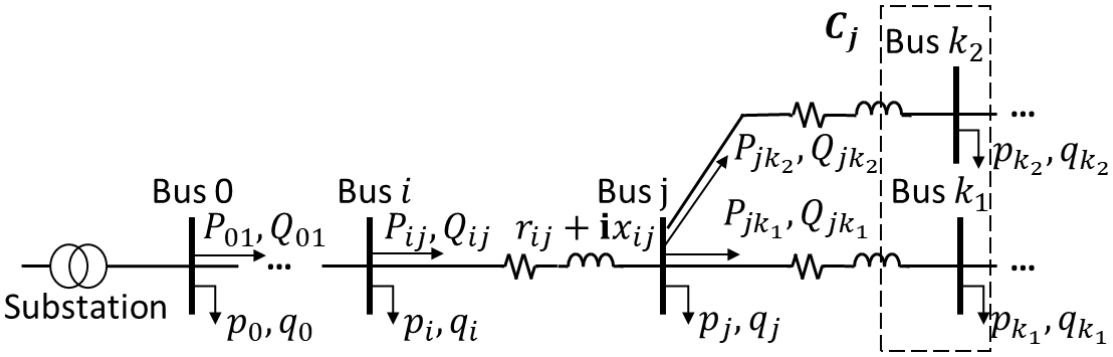

Figure 3.3. The Branch Flow Model in A Radial Distribution Network.

For each node $j \in J$, let p_j and q_j be the active and reactive injection power, and V_j denote the complex voltage on this bus. For each link $(i, j) \in E$, r_{ij} and x_{ij} are the resistance and reactance of this line; I_{ij} represents the complex current; P_{ij} and Q_{ij} denote the sending-end complex power from bus i to j. Except for the substation bus (indexed as 0), each node j has a unique parent node i and a set of child nodes C_j. Let $l_{ij} = |I_{ij}|^2$ denote the squared line current magnitude of the line (i, j) and $v_j = |V_j|^2$ be the squared voltage magnitude of node j. The power balance and flow equations of the distribution network can be formulated as [69]:

$$
\begin{aligned}
p_j(t) &= P_{ij}(t) - r_{ij} l_{ij}(t) - \sum_{k \in C_j} P_{jk}(t), \quad \forall j \in J \\
q_j(t) &= Q_{ij}(t) - x_{ij} l_{ij}(t) - \sum_{k \in C_j} Q_{jk}(t), \quad \forall j \in J
\end{aligned} \tag{3.4}
$$

$$
v_j(t) = v_i(t) - 2(r_{ij} P_{ij}(t) + x_{ij} Q_{ij}(t)) + (r_{ij}^2 + x_{ij}^2) l_{ij}(t), \quad \forall (i, j) \in E
$$

$$
l_{ij}(t) = \frac{P_{ij}(t)^2 + Q_{ij}(t)^2}{v_i(t)}, \quad \forall (i, j) \in E \tag{3.5}
$$

However, the quadratic equalities in (3.5) will cause non-convex optimization, which is difficult to solve and does not guarantee convergence. Thus, a second-order cone relaxation [70] is applied as the inequality constraints:

$$
l_{ij}(t) \geq \frac{P_{ij}(t)^2 + Q_{ij}(t)^2}{v_i(t)}, \quad \forall (i, j) \in E \tag{3.6}
$$

The OPF problem will be transformed to a convex one for radial networks. Meanwhile, to satisfy this relaxation, the voltage of buses should be very close to the nominal value and the power input to the bus should be under a certain limit. The additional constraints to ensure the prescribed region are:

$$
v_j^{\min} \leq v_j(t) \leq v_j^{\max}, \quad \forall j \in J \tag{3.7}
$$

$$
0 \leq l_{ij}(t) \leq l_{ij}^{\max}, \quad \forall (i, j) \in E \tag{3.8}
$$

(3.7) prevents voltage violation, and (3.8) limits the current of each line ij respectively. The values v_j^{min} and v_j^{max} are the minimum and maximum of voltage magnitude, and l_{ij}^{max} is considered as the maximum of the current magnitude.

3.3 Problem Formulation of Distributed EV Charging Scheduling with Transactive Energy Management

3.3.1 Individual EV Bidding Strategy and Node-Level Aggregation

The framework for individual EV bidding strategy and node-level aggregation is shown in Figure 3.4. Firstly, according to the charging request, demand, and duration, individual EVs will find the optimal bidding strategy and forward it to the EVA. Then, to coordinate with others, the EVA needs to form the final bidding price and netload demand.

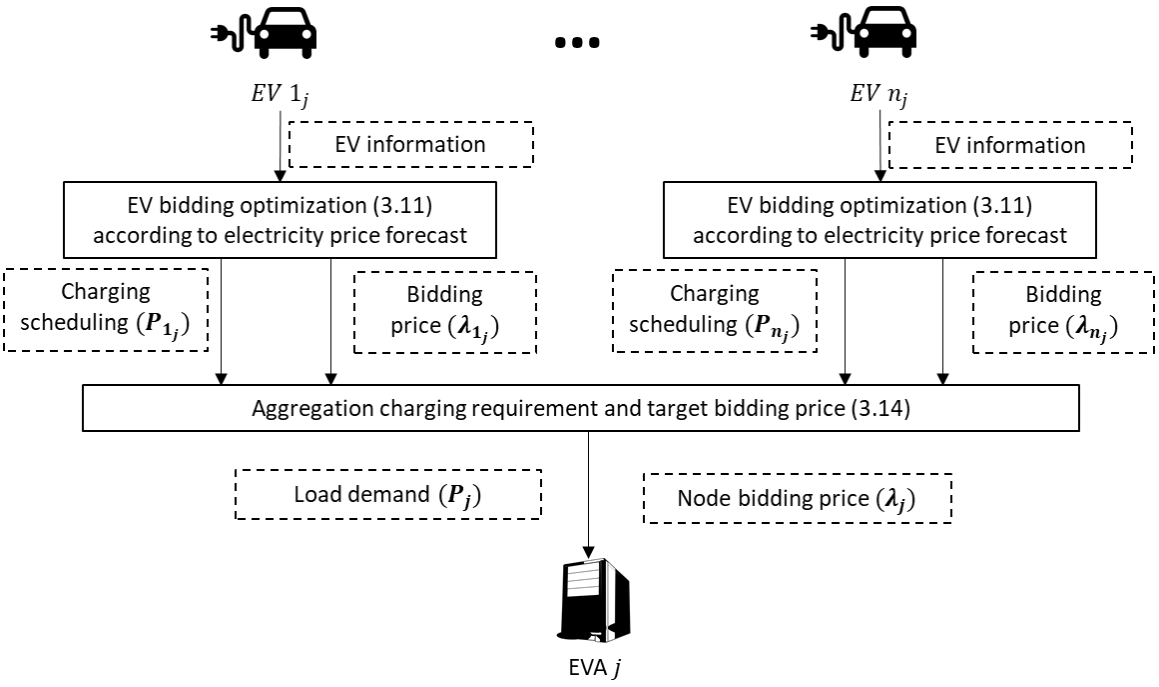

Figure 3.4. EV Bidding and Nnode-level Aggregation.

Individual EV owners need to propose a bidding price to compete with others. To be fair, a blind auction mechanism is considered in the bidding process. The bidding price is defined by a vector $\boldsymbol{\lambda}_{n_j} = \left[\lambda_{n_j}(1), \dots, \lambda_{n_j}(t), \lambda_{n_j}(t+1), \dots, \lambda_{n_j}(T)\right]$. At each time step,

the bidding price reflects both the current charging power demand and the remaining charging flexibility. For example, an EV owner whose vehicle has a longer charging duration and a lower energy requirement is not inclined to offer a high price to obtain more charging power. Thus, the preferred charging electricity price $\lambda_{n_j}(t)$ is formulated as:

$$\lambda_{n_j}(t) = \lambda^{DA}(t) + \frac{\lambda^{Cap}(t)}{P_{n_j}^{\max} - P_{n_j}^{\min}} \mu_{n_j}(t)(P_{n_j}(t) - P_{n_j}^{\min}) \tag{3.9}$$

$$\mu_{n_j}(t) = \min\left[\frac{\left(SoC_{n_j}^{T}(t) - SoC_{n_j}(t)\right)E_{n_j}^{C}}{\eta_{n_j} P_{n_j}^{\max} d_{n_j} \Delta t}, 1\right] \tag{3.10}$$

At time step t, the day-ahead electricity price λ^{DA} and the feasible increase range of the preferred charging electricity price λ^{Cap} are assumed to be forecasted by the utility. The charging urgency μ_{n_j} is defined in (3.10) to reflect the flexibility of the remaining charging duration $d_{n_j} \times \Delta t$.

Once the pricing principle was defined, individual EV owners will propose their bidding schedule without negotiation with others. Each EV customer pursues a target charging cost. The optimization formulation is given below:

$$\begin{aligned} &\min \quad \boldsymbol{\lambda}_{n_j} \cdot \mathbf{P}_{n_j}^{T} \cdot \Delta t \\ &\text{s.t.} \quad (3.1)\text{-}(3.3) \\ &\qquad \mathbf{P}_{\mathbf{n_j}}, \forall n_j \in N_j \end{aligned} \tag{3.11}$$

$$C_{n_j} = \boldsymbol{\lambda}_{n_j}^{*} \cdot \mathbf{P}_{n_j}^{*T} \cdot \Delta t \tag{3.12}$$

where C_{n_j} indicates the target optimal cost during the bidding process, while $\boldsymbol{P}_{\boldsymbol{n_j}}^{*}$ and $\boldsymbol{\lambda}_{\boldsymbol{n_j}}^{*}$ are the optimal power demand and bidding price solved by problem (3.11). These only

depend on the day-ahead electricity price forecast and individual EV charging requirements. The results can be solved with quadratic programming and selected as the target of initial charging cost in stage 3.

The EVA serves as the bridge between individual EVs and the DSO. In stage 1, the EVA aggregates power demand and finds bidding prices for all the EVs in the node. The aggregated bidding price will inform the DSO for market clearing via the communication shown in Figure 1. For individual EVA $j \in \{1, \dots, J\}$, where N denotes the number of EVAs in the distribution network, the aggregated power demand can be formulated by:

$$\mathbf{p_j} = \mathbf{P_j^F} + \sum_{n \in \mathbf{N_j}} \mathbf{P_{n_j}} \tag{3.13}$$

Let $\boldsymbol{p_j} = [p_j(1), \dots, p_j(T)]$ be the aggregated active power demand by EVA for bus j, and $\boldsymbol{P_j^F}$ is the vector of aggregated uncontrollable load demand. The aggregated bidding price for EVA j at time step t is:

$$\lambda_j(t) = \sum_{n \in \mathbf{N_j}} \left(\lambda_{n_j}(t) \frac{P_{n_j}(t)}{\sum_{n \in \mathbf{N_j}} P_{n_j}(t)} \right) \tag{3.14}$$

where the bidding price is denoted by λ_j. It is designed as the expected value of individual EV owners' bidding prices in proportion to the amount of power demand.

3.3.2 ADMM-based DSO-EVA Coordination

Figure 3.5 shows the negotiation process between the DSO and EVAs to determine the optimal clearing prices $\boldsymbol{\lambda}^*$ for the distribution network and optimal feasible netload $\boldsymbol{p_j^*}$ for each EVA.

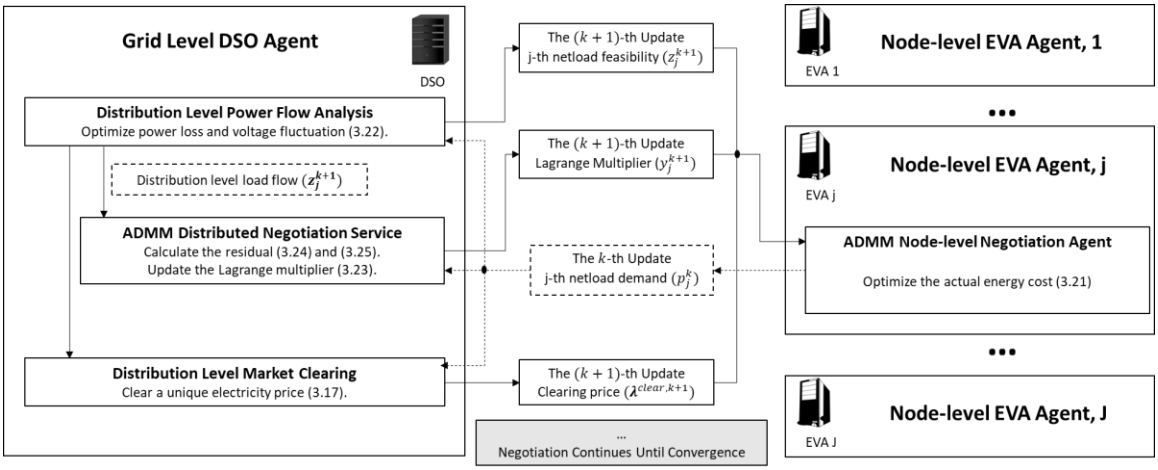

Figure 3.5. The Framework of ADMM-based DSO-EVA Coordination.

The EVA adjusts its power demand according to the clearing price and re-negotiates with the DSO. EVAs aim to reduce the charging cost in terms of group EVs, so the objective function can be formatted as:

$$f_j\left(\mathbf{p_j}\right) = \boldsymbol{\lambda}^{clear} \cdot \mathbf{p}_j^{\,T} \cdot \Delta t \tag{3.15}$$

where $\boldsymbol{\lambda^{clear}}$ indicates the vector of clearing electricity price proposed by the DSO during the negotiation.

The DSO is located at the substation bus 0 as shown in Figure 3.1. It purchases electricity from the utility and ensures the reliability of the distribution network using OPF techniques. The objective function of DSO is designed to reduce the cost due to energy loss as shown below.

$$g\left(\mathbf{p_j}\right) = \boldsymbol{\lambda}^{DA} \cdot \sum\nolimits_{ij \in E} \left(\mathbf{l_{ij}}^{T} \cdot \mathbf{r_{ij}}\right) \cdot \Delta t \tag{3.16}$$

where $\boldsymbol{l_{ij}} = \left\{l_{ij}(1), \ldots, l_{ij}(t), l_{ij}(t+1), \ldots, l_{ij}(T)\right\}$ indicates a vector of the square of line current magnitude for a time period of $T \times \Delta t$. The DSO also provides the functions of a competitive market for this distribution network. It collects bidding price information

from EVAs and clears a unique electricity price to coordinate the power schedules for EVAs. During negotiation, the clearing electricity price at time step t is given by:

$$\lambda^{clear}(t) = \frac{\sum_{j\neq 0: j\in \mathbf{N}} \left(\lambda_j(t) p_j(t)\right)}{p_0(t)} \tag{3.17}$$

where $\boldsymbol{p_0}$ and $\boldsymbol{q_0}$ represent the vector of active and reactive power purchase from the utility.

In this radial distribution system with a DSO and multi-EVAs, the goal of the DSO is to minimize energy loss, while EVAs prefer to reduce the actual charging cost. The optimal DSO-EVA coordination problem can be formulated as:

$$\begin{aligned} \min \quad & g\left(\mathbf{p_j}\right) + \sum_{j=1}^{J} f_j\left(\mathbf{p_j}\right) \\ \text{over} \quad & \mathbf{p_j} \qquad \forall j \in J \\ \text{s.t.} \quad & (3.4),(3.6),(3.7),(3.8) \\ & \mathbf{p}_j^{\min} \le \mathbf{p}_j \le \mathbf{p}_j^{\max} \end{aligned} \tag{3.18}$$

where $\boldsymbol{p_j^{min}}$ and $\boldsymbol{p_j^{max}}$ represent the minimum and maximum load for each EVA.

Although the optimization problems (3.18) can be solved by a centralized method, it is not computationally efficient and will cause privacy issues since all the information needs to be transmitted and processed by the DSO. The decision variables for the DSO are strongly coupled with each EVA's decision variable. By introducing an auxiliary variable $\boldsymbol{z_j}$, the ADMM method [71] can be used to solve the problem in a distributed manner. The problem (3.18) can be re-defined as:

$$\begin{aligned} \min \quad & g\left(\mathbf{z_j}\right)+\sum_{j=1}^{J} f_j\left(\mathbf{p_j}\right) \\ \text{s.t.} \quad & \mathbf{p}_j=\mathbf{z}_j \qquad \forall j \in J \\ & (3.4),(3.6),(3.7),(3.8) \text{ for DSO} \\ & \mathbf{p}_j^{\min} \le \mathbf{p}_j \le \mathbf{p}_j^{\max} \text{ for EVA} \end{aligned} \tag{3.19}$$

where the auxiliary variable $\boldsymbol{z_j = p_j}$ proposed by the DSO is to link the injection power $\boldsymbol{p_j}$ of each node. The augmented Lagrange function is defined as:

$$L_{\rho}(\mathbf{p_j}, \mathbf{z_j}, \mathrm{y}) = \sum_{j=1}^{J} f_j\left(\mathbf{p_j}\right)+\mathrm{g}\left(\mathbf{z_j}\right)+\sum_{j=0}^{J}\left(\mathbf{y}_j{}^{T}\left(\mathbf{p_j}-\mathbf{z_j}\right)+\frac{\rho}{2}\left\|\mathbf{p_j}-\mathbf{z_j}\right\|_2^2\right) \tag{3.20}$$

where $\boldsymbol{y_j}$ is a vector of Lagrange multiplier and $\rho > 0$ denotes the penalty parameter. Therefore, the optimization problem (3.19) can be solved concurrently by each EVA and DSO. At iteration k, each EVA solves the problem:

$$\begin{aligned} & \mathbf{p}_j^{k+1}=\operatorname{argmin}\left(\mathrm{f}_j\left(\mathbf{p}_j\right)+\mathbf{y}_j^{kT}\mathbf{p}_j+\frac{\rho}{2}\left\|\mathbf{p}_j-\mathbf{z}_j^k\right\|_2^2\right) \\ & \text{s.t.} \qquad \mathbf{p}_j^{\min} \le \mathbf{p}_j \le \mathbf{p}_j^{\max} \end{aligned} \tag{3.21}$$

The DSO solves the problem (3.22) to address the OPF. Meanwhile, it is also responsible for updating the auxiliary vector $\boldsymbol{z_j}$ through the problem (3.23) to coordinate with EVAs.

$$\mathbf{z}_j^{k+1}=\operatorname{argmin}\left(g\left(\mathbf{z}_j\right)+\sum_{j=1}^{J}\left(-\mathbf{y}_j^{kT}\mathbf{z}_j+\frac{\rho}{2}\left\|\mathbf{p}_j^{k+1}-\mathbf{z}_j\right\|_2^2\right)\right) \tag{3.22}$$

s.t. (3.4),(3.6),(3.7),(3.8)

$$\mathbf{y}_j^{k+1}=\mathbf{y}_j^k+\rho\left(\mathbf{p}_j^{k+1}-\mathbf{z}_j^{k+1}\right) \tag{3.23}$$

The ADMM iteration satisfies the residual, objective, and dual variable convergence. Given by the residuals of primal feasibility r and dual feasibility s, the stopping criteria is defined as:

$$\left\|r^k\right\|_2^2=\sum_{j=1}^{J}\left\|\mathbf{p}_j^k-\mathbf{z}_j^k\right\|_2^2 \le \varepsilon^{pri} \tag{3.24}$$

$$\left\|s^k\right\|_2^2=\rho\left\|\mathbf{z}_j^k-\mathbf{z}_j^{k\text{-}1}\right\|_2^2 \le \varepsilon^{dual} \tag{3.25}$$

where ε^{pri} and ε^{dual} are feasibility tolerances for the primal and dual residuals.

3.4 TE-based EV Charging within a Node

After the DSO-EVA negotiation process, each EVA will receive the optimal feasible power $\boldsymbol{p}_j^*$ and clearing prices $\boldsymbol{\lambda}^*$ from stage 2. Figure 3.6 shows the process of optimal EV charging management within a node.

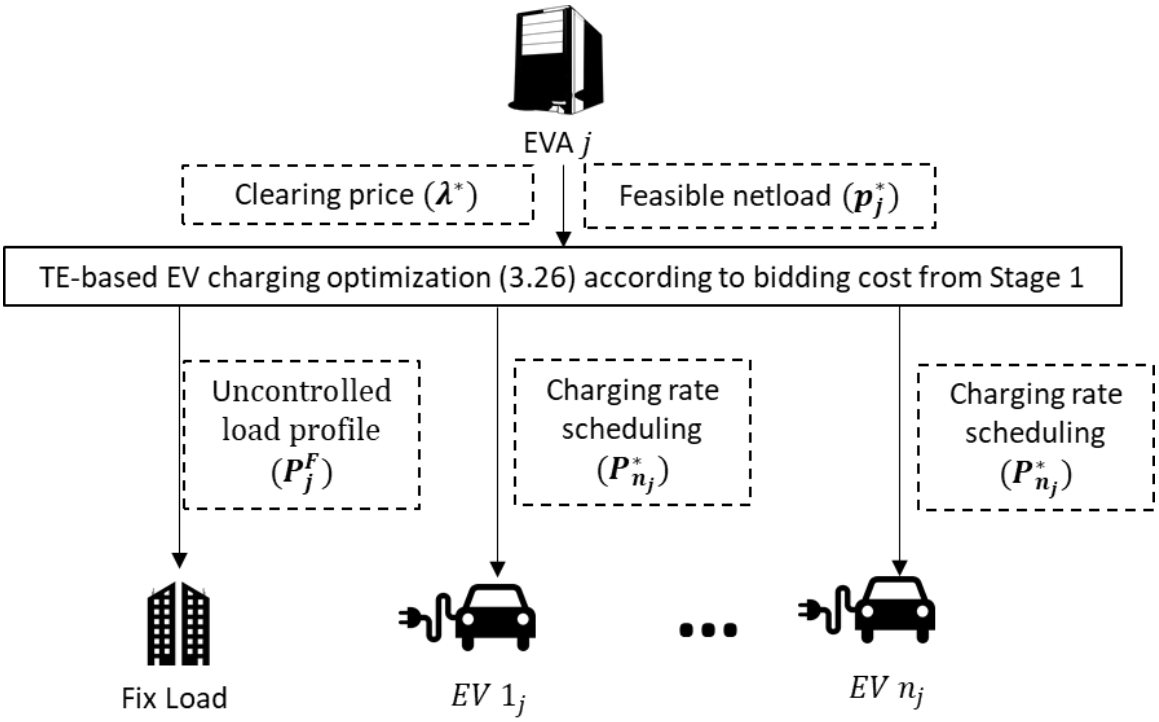

Figure 3.6. EV Charging Optimization within A Node

Individual EVs want to track the target charging cost C_{n_j} in stage 1 because it is the optimal solution without considering any distribution network congestion. Therefore, the EVA needs to generate a sequence of actual EV charging rates for each EV under the node to meet this objective. In this paper, the objective function of EV charging for a group of EVs under the EVA j is defined as:

$$\begin{aligned} \min \quad & \sum_{n=1}^{N_j} \left(\boldsymbol{\lambda}^* \cdot \mathbf{P}_{\mathbf{n_j}}{}^T \cdot \Delta t - C_{n_j} \right)^2 \\ \text{over} \quad & \mathbf{P}_{n_j}, \forall n_j \in N_j \\ \text{s.t.} \quad & \text{(3.1)-(3.3)} \end{aligned} \tag{3.1}$$

The optimal solutions of individual EV charging rate schedule $\boldsymbol{p}_{\boldsymbol{n_j}}^*$ can be solved by the quadratic programming method and the EVA will send this information to all EV charging stations in the region.

3.5 Use Case Study

To validate the presented TE-based EV charging scheduling management algorithm, a modified 33-bus system [64] is selected to simulate a medium-voltage distribution network. The distribution nodes are classified into residential nodes and commercial nodes based on their load patterns. Different building load profiles are obtained from [65] and modeled into each node. The nominal voltage of the 33-bus distribution system is 12.88 kV and the topology is shown in Figure 3.7. In addition to building loads, a total of 230 EV charging loads are modeled in 14 nodes. The battery capacity $E_{n_j}^C$ is 40 kWh, the minimal charge rate $P_{n_j}^{min}$ is 1.44 kW, and the maximum charge rate $P_{n_j}^{max}$ is 6.6 kW. The EV arrival/departure time and initial/target SOC are generated based on [72]. Most EVs charging at commercial areas will continue for two to four hours during the daytime. EVs charging at residential areas will start in the evening or at late night and will end by 6:30 a.m. Without considering the service fee, the day-ahead electricity prices are obtained from [67] as shown in Figure 3.8 and the feasible increasing range λ^{Cap} is set as ¢2/kWh. The length of the entire horizon is 24 h (7:00 a.m. – 7:00 a.m.) and the duration of each time step is 15 min.

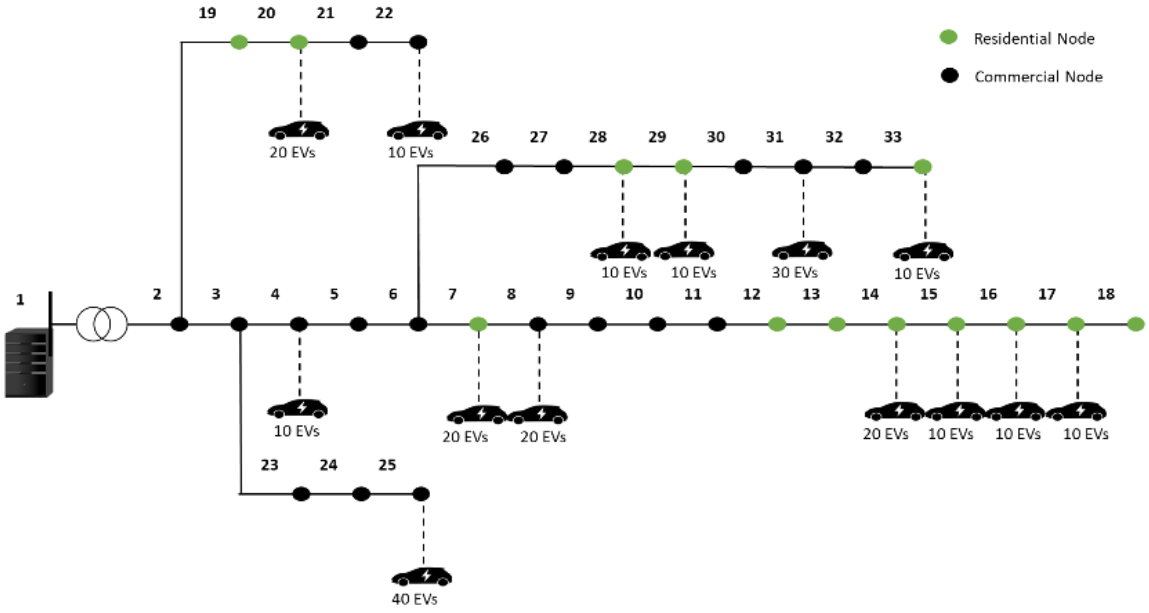

Figure 3.7. 33-bus Distribution System with EV Charging Loads.

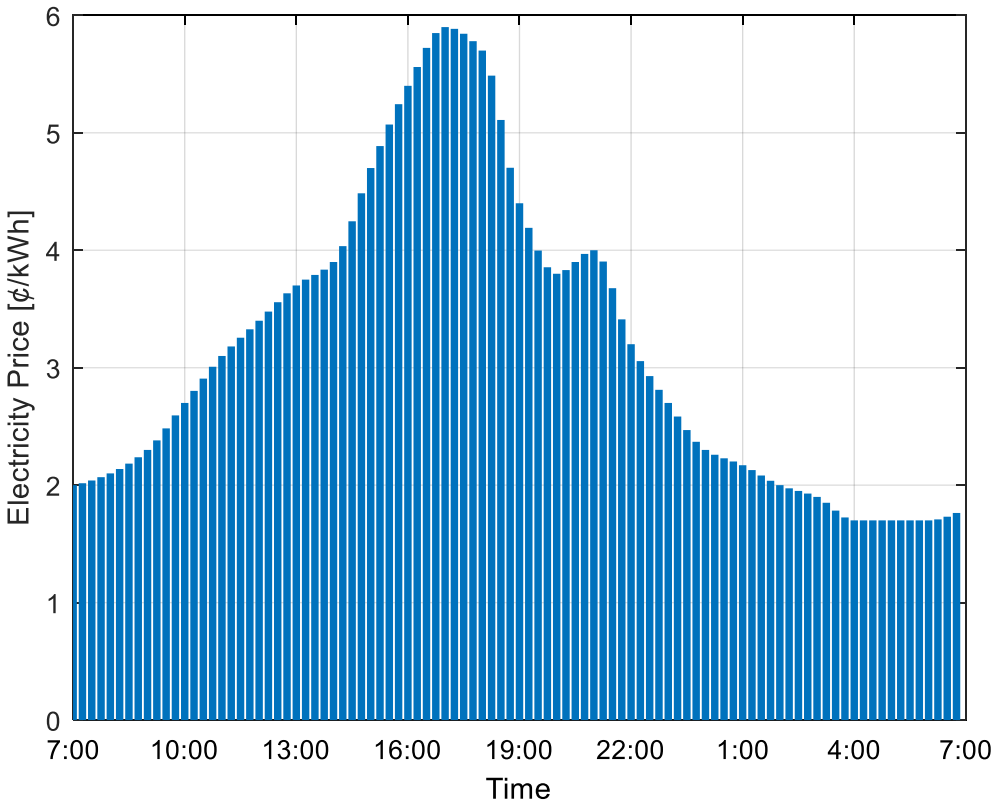

Figure 3.8. Day-ahead Electricity Price.

From the perspective of the distribution network, Figure 3.9 shows the load profiles of the 33-bus system with and without TEM. Without TEM, the overall load will exceed the substation capacity in the morning and evening when a large number of EVs are connected. However, the charging loads are shifted smoothly when TEM is introduced so that the load profile is always under the substation capacity. From Figure 3.9, it is obvious that residential EV charging loads in the peak period (17:00–20:00) are moved to the off-peak period (24:00–6:00). Figure 3.10 shows the voltage profile of the 33-bus system with TEM. No voltage violation is observed because the coordination of the DSO and EVAs ensures the stability of the distribution network. These results show that TE-based EV charging management can avoid load congestion and improve grid performance.

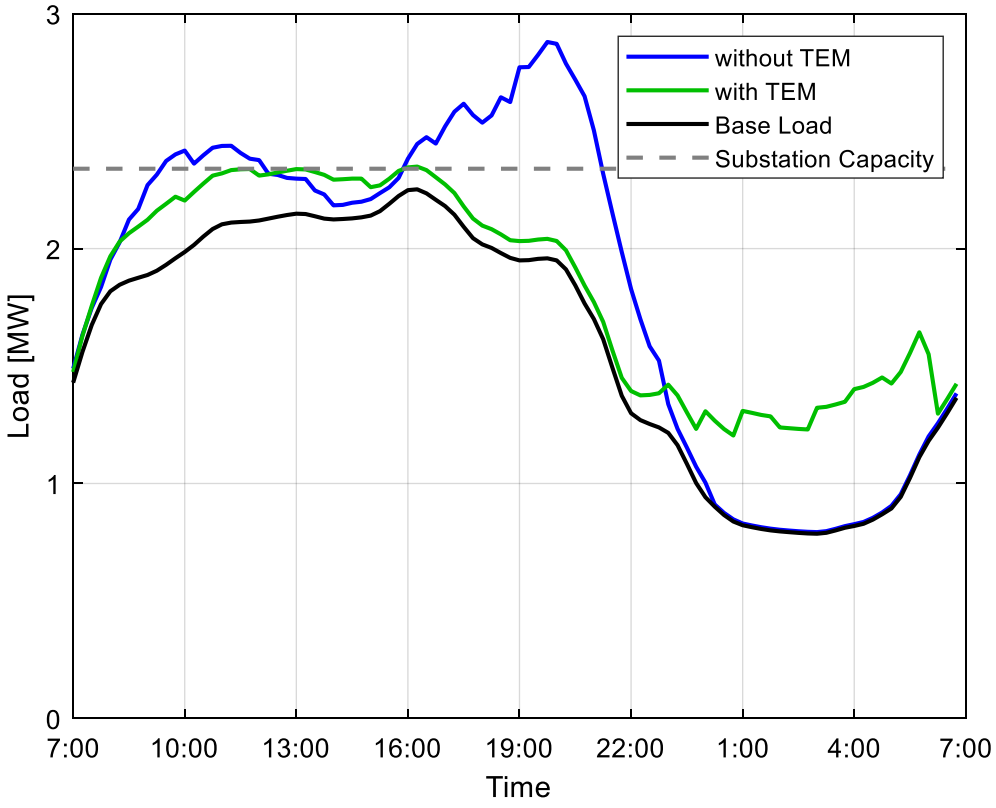

Figure 3.9. Load Profiles of 33-bus System with and without TEM.

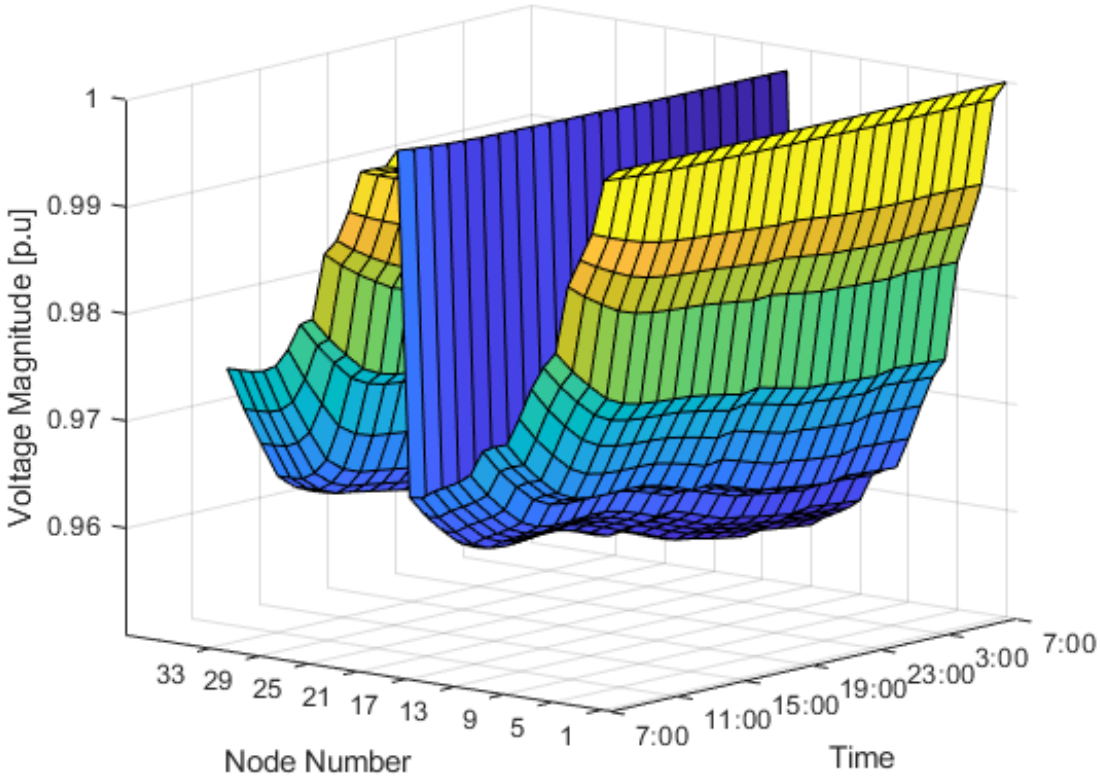

Figure 3.10. Voltage Magnitudes of 33-bus System with TEM.

From the perspective of nodes with EV charging loads, two representative nodes are selected to demonstrate the results. In particular, Node 4 is a commercial node with 10 EV charging loads, and Node 17 represents a residential node with 10 EV charging loads. Figure 3.11 and Figure 3.12 show the load profile and EV charging results of commercial Node 4. With TEM, part of the EV charging load is shifted to avoid exceeding the upper power bound of the node. At the same time, all EV charging requirements are met within their charging durations. Figure 3.13 and Figure 3.14 show the load profile and EV charging results of residential Node 17. After applying TEM, almost all EV charging loads are shifted from the peak period to an off-peak period. Residential EV charging has more flexibility to address its charging schedule as well as

provide grid service. Meanwhile, all EVs' charging requirements are satisfied. Therefore, TE-based EV charging management is feasible for individual nodes and EVs.

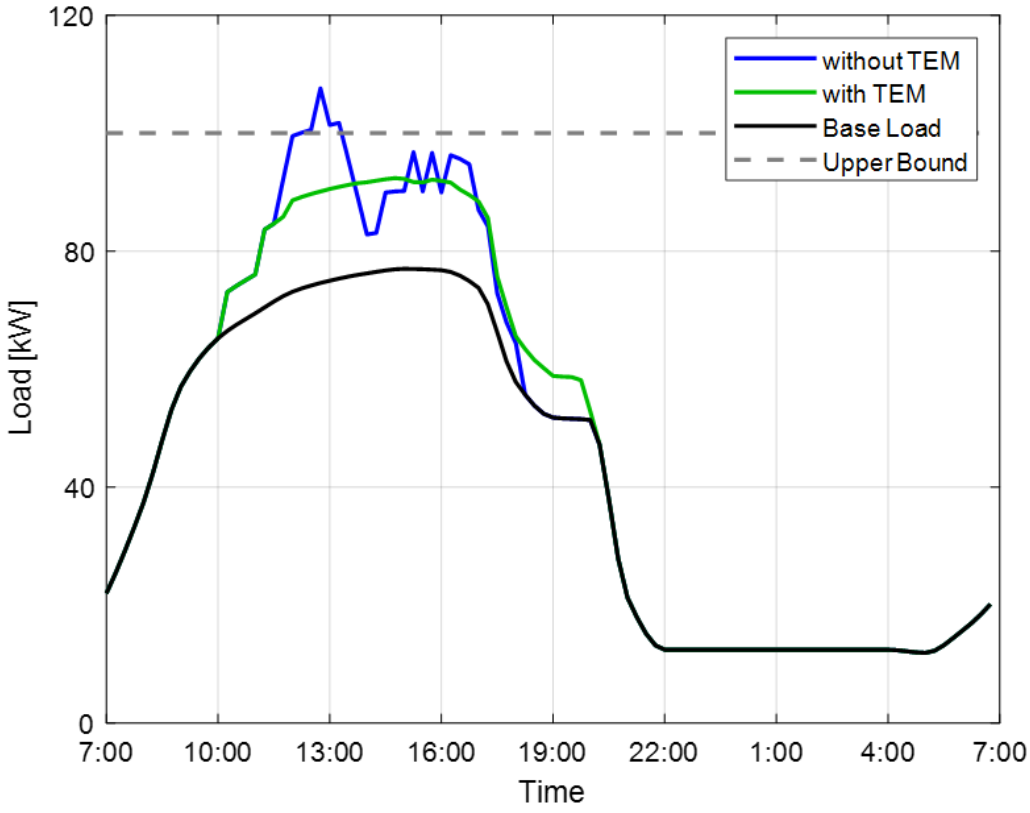

Figure 3.11. Load Profile of Node 4

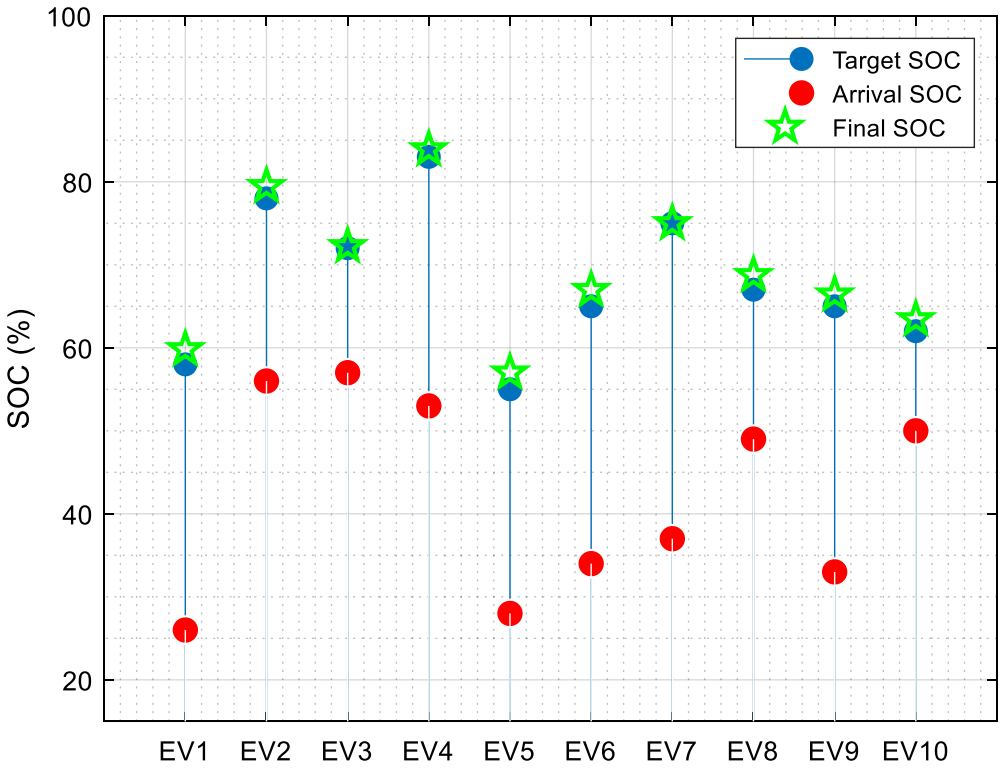

Figure 3.12. EV Charging Results of Node 4

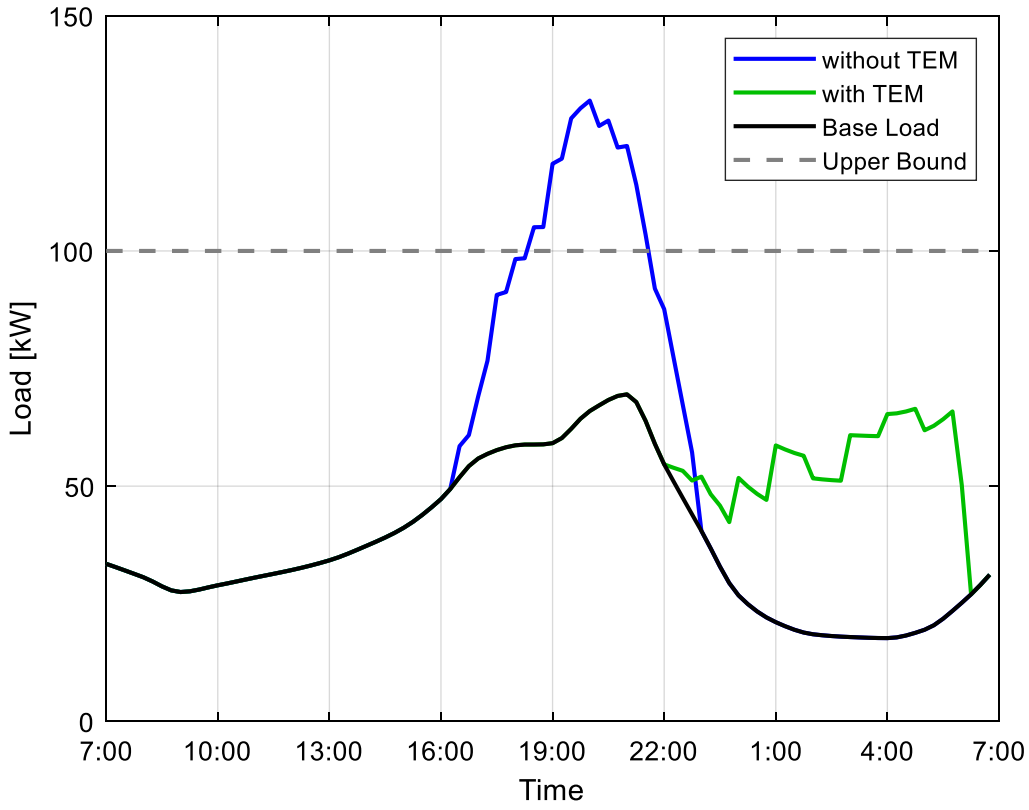

Figure 3.13. Load Profile of Node 17

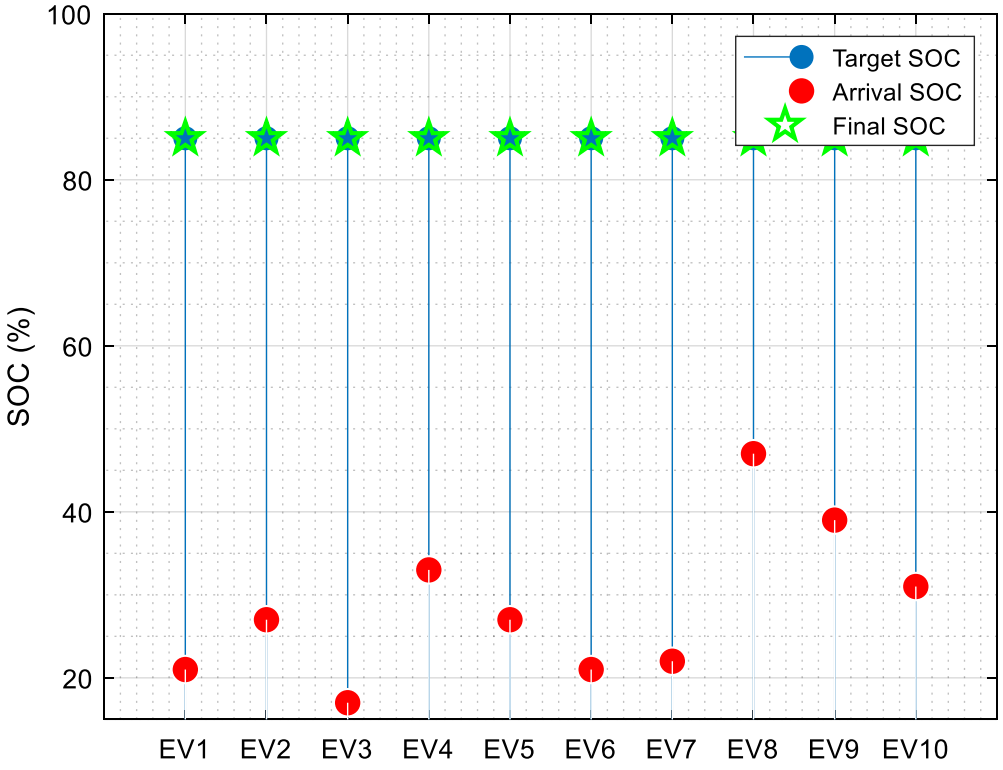

Figure 3.14. EV Charging Results of Node 17

Besides ensuring grid stability, TEM also considers customers' charging costs. Figure 3.15 shows the final EV charging price of EV charging with and without TEM. With TEM, to encourage EV owners to shift their charging demand to support grid operation, such as via voltage regulation and congestion management, the DSO will reduce the EV charging-electricity price in the market clearing mechanism. This incentive mechanism offers better economic benefits for any EVs participating in the TEM program. Table 3.1 lists the groups of EV charging costs with and without TEM. The results show that TEM can reduce about 39.55% cost for 230 EVs through a clearing price. Typically, at residential nodes, EVs can save more than 50% of their charging cost because of overnight charging periods. The charging of residential EVs presents more

flexibility to be scheduled according to clearing prices and grid peak/off-peak periods. At commercial nodes, although EVs have less flexibility to respond to clearing prices, TEM can still result in about 10–20% cost saving for connected EVs. As a result, TE-based EV charging management can also offer economic benefits for distribution networks, nodes, and individual EVs.

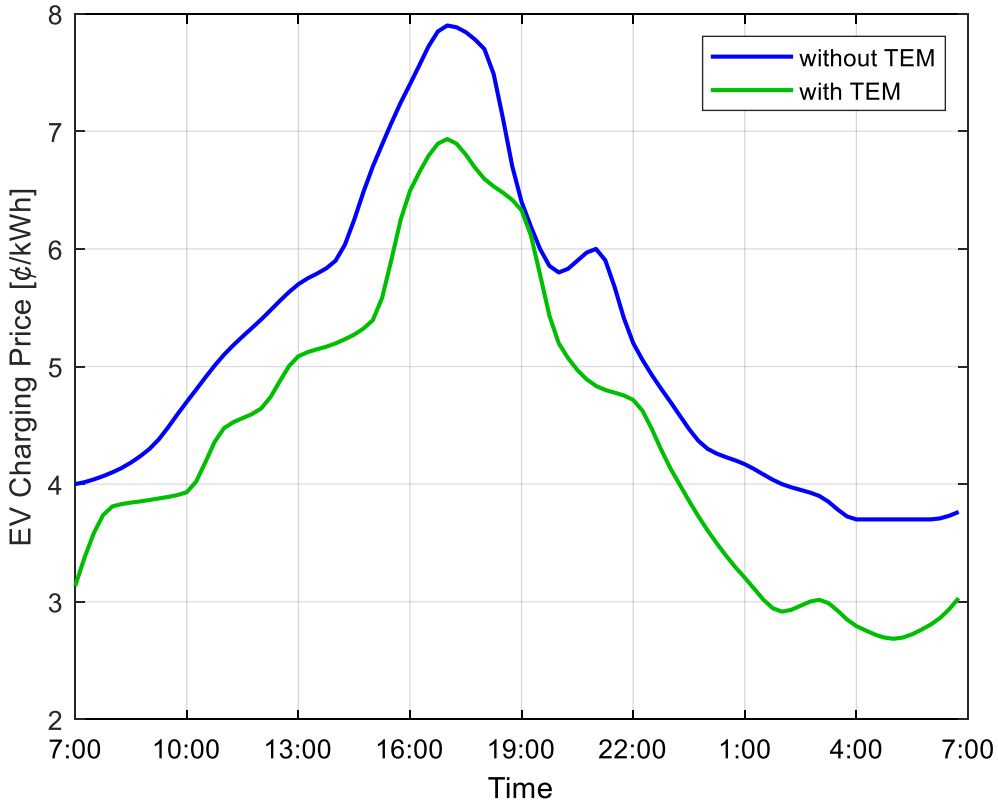

Figure 3.15. EV Charging Price with and without TEM.

Table 3.1. EV Charging cost of the 33-bus system with and without TEM.

Node Type	**Node Number**	**Number of EV**	**Cost with TEM [¢]**	**Cost without TEM [¢]**	**Cost Reduction [%]**
Commercial	4	10	685.54	778.54	11.95
	8	20	1732.07	1566.27	9.57
	22	10	445.9	568.7	21.59
	25	40	1990	2320.68	14.25
	31	30	2200.31	2432.68	9.55
Residential	7	20	1404.41	3049.55	53.95
	14	20	2846.94	1366.07	52.02
	15	10	1551.46	7045.9	54.59
	16	10	629.12	1405.74	55.25
	17	10	736.43	1589.63	53.67
	20	20	1518.65	2959.82	48.69
	28	10	647.3	1361.66	52.46
	29	10	695.28	1425.7	51.23
	33	10	721.79	1583.88	54.43
Overall		230	17805.2	29454.82	39.55

The presented method is simulated using MATLAB on a laptop with an Intel Core i7 of 2.8 GHz. The optimization problems are formulated using YALMIP [73] with CPLEX as the solver. Figure 3.16 shows the convergence process for solving the ADMM-based DSO-EVA coordination problem with the parameter values of $\rho = 1$ and $\varepsilon^{pri} = \varepsilon^{dual} = 0.01$. The norms of primal residual and dual residual converge to 0.01 within 244 iterations. The optimization problem has a large number of variables and constraints due to large-scale EVs and EVAs. Additional methods, such as the dynamic step size modification method introduced in [74], will be explored in the future to improve computational efficiency.

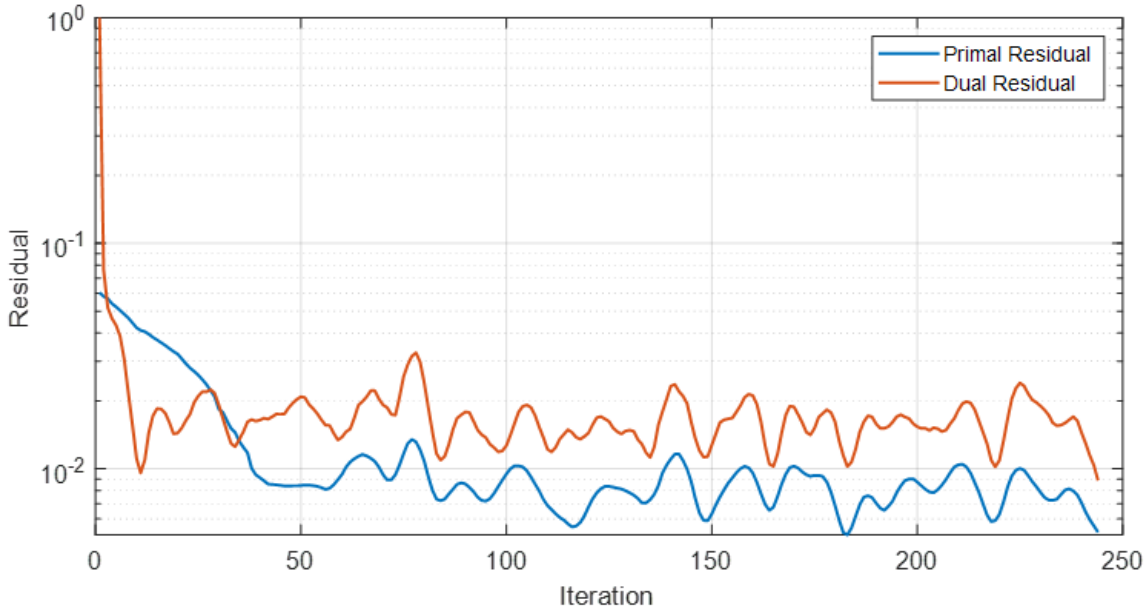

Figure 3.16. Iteration Process of ADMM-based DSO-EVA Coordination.

3.6 Chapter Conclusion

In this chapter, a distributed EV charging schedule with transactive energy management is presented. In the first stage, EVs will propose individual bidding strategies to reflect their charging requirements and cost benefits while the EVAs will generate node-level bidding strategies based on the individual EV bidding information in the node. At the second stage, DSO and EVAs will negotiate to find a balance between the distribution system operation stability and EV charging economic benefits. The DSO ensures network operation with the OPF technique and the EVAs minimize charging costs. In particular, an EV charging price clearing mechanism is developed, which is used in the coordination process. This mechanism provides the incentive for EV charging customers to improve network operation performance. Thus, EVAs and EVs can make their charging scheduling autonomously with clearing price signals.

However, the use case presented in this chapter only considers level-2 AC EV charging. DC fast charging and extreme fast charging with battery energy storage systems are not considered. These chargers will cause additional complexity in the distribution grid and will be a focus of the next chapter.

4 Optimal Configuration of Extreme Fast Charging Stations Integrated with Energy Storage System and Photovoltaic Panels in Distribution Networks

In this chapter, the analysis of XFC behaviors and the design of XFC stations with renewable energy resources for distribution networks is addressed. To realistically estimate the charging power demand of XFC stations, a Monte Carlo (MC) simulation tool is developed based on the EV arrival time and SOC distributions obtained from vehicle travel survey dataset. The MC simulation algorithm considers various impact factors, such as EV scale, EV model type, the percentage of each type in the total simulated EVs, EV charging curves for different EV model types, XFC station port availability, and maximum waiting time. To reduce the investment and operation costs of XFC stations and avoid overloading the grid due to XFC events, an optimal configuration method is presented for the multiple XFC stations in a distribution network to determine the optimal energy capacity of energy storage system (ESS), ESS rated power, and the size of photovoltaic (PV) panels, which are integrated with XFC stations. The optimal power flow technique is applied to this optimization so that the optimal solutions meet not only the charging demand but also the operational constraints of the distribution network, XFC, ESS, and PV panels.

4.1 EV Charging Demand Estimation

The EV charging demand at XFC stations is the key impact factor to determine the optimal ESS energy capacity, ESS rated power, and the PV size integrated with XFC stations. Due to the lack of real-world XFC station charging demand data, Monte Carlo simulation is employed to estimate the XFC station charging load. Figure 4.1 shows the

inputs, outputs, and estimation logic of the Monte Carlo simulation. The MC simulation parameters and the descriptions of these parameters are summarized in Table 4.1. The simulation inputs include EV scale, the number of station ports, battery characteristics, maximum waiting time, and EV arrival time and SOC distributions. The probability distributions of EV arrival time and SOC are obtained from a travel survey database. The outputs of the MC simulation are the load profiles and daily usage of each XFC station. A first come, first serve queuing method is adopted in the load estimation logic. When an EV arrives at a XFC station, the driver will wait in the queue if there is no charging port available. When a port becomes available, the first vehicle in the queue will start to be charged. A vehicle will leave without charging if the waiting time reaches the maximum waiting time.

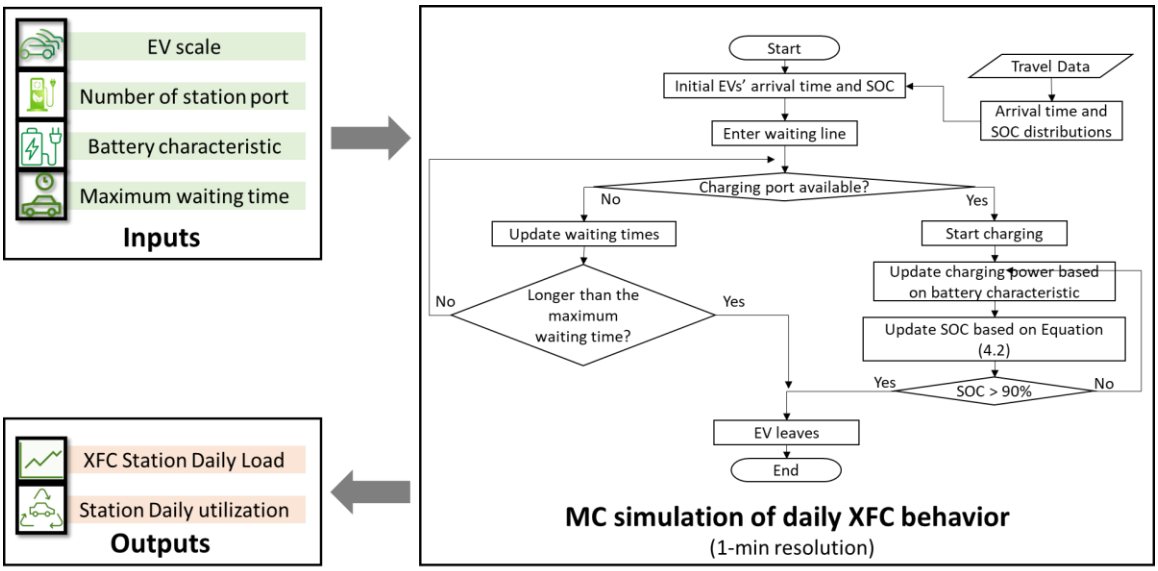

Figure 4.1. Charging Demand Estimation using Monte Carlo Simulation

Table 4.1. Parameters of EV Charging Demand Estimation

Input Parameters	
EV scale	Define the number of EVs visiting the XFC station daily.
Number of station ports	Define the number of charging ports of the XFC station
EV battery characteristics	Define the battery size, percentage in the total simulated EVs (Table 4.2), and charging curves (Figure 4.4) of different EV models.
Maximum waiting time	Define the maximum allowable waiting time of each EV at the XFC station. EVs will leave if the waiting time reaches the maximum waiting time.
Probability Distributions	
Arrival SOC at XFC station	The probability distribution of SOC when EVs need to be charged.
Arrival time at XFC station	The probability distribution of time when EVs visit the XFC station.

4.1.1 Probability Distribution of EV Arrival Time at XFC Stations

The probability distribution of EV arrival time at XFC stations is obtained based on the probability distributions of home departure time, the daily mileage, and the hourly probability of daily trips. To obtain a realistic probability distribution of EV arrival time, the probability distributions of home departure time, the daily mileage, and the hourly probability of daily trips [75] derived from an open database National Household Travel Survey (NHTS) [76] are used. The survey data provide information on driving patterns for 309,164 vehicles. The first peak of departure time from home to work is around 7:00 – 9:00 am, and most EVs travel within the range of 5 to 40 miles daily. Paper [75] analyzed the travel survey data thoroughly and presented the probability distributions of

home departure time and the daily mileage. It also provides the hourly probability distribution of daily trips for a weekday and a weekend. These probability distributions were used in this study, to generate the probability distribution of EV arrival time at XFC stations.

A total of 100,000 EVs are simulated to generate the probability distribution of EV arrival time at XFC stations. It is assumed that half of these vehicles leave home with 90% SOC, and the rest are 40% SOC. It is also assumed that the arrival SOC at XFC stations follows a normal distribution. Figure 4.2 shows an example of arrival SOC distribution with 25% mean and 3.4% standard deviation. In the simulation, the random values of home departure time, the daily mileage, and the threshold of SOC to charge the vehicle are generated for each EV from the probability distributions of home departure time, the daily mileage, and arrival SOC. The battery SOC of EVs at each time step (one hour) is updated by:

$$SOC_{EV}(t+1) = SOC_{EV}(t) - \frac{m(t)d}{d_{\max}} \times 100 \tag{4.1}$$

where $m(t)$ is the hourly probability of daily trip at time t, d denotes the daily mileage, and d_{max} is the maximum mileage range of EV battery. When an EV's SOC becomes below its threshold SOC, the vehicle needs to be charged and the current time is recorded. The collection of this time for all 100,000 EVs forms the probability distribution of EV arrival time at XFC stations as shown in Figure 4.3. Two peaks, which are the morning peak from 7:00 am to 9:00 am and the evening peak from 5:00 pm to 8:00 pm, are observed during the commuter periods.

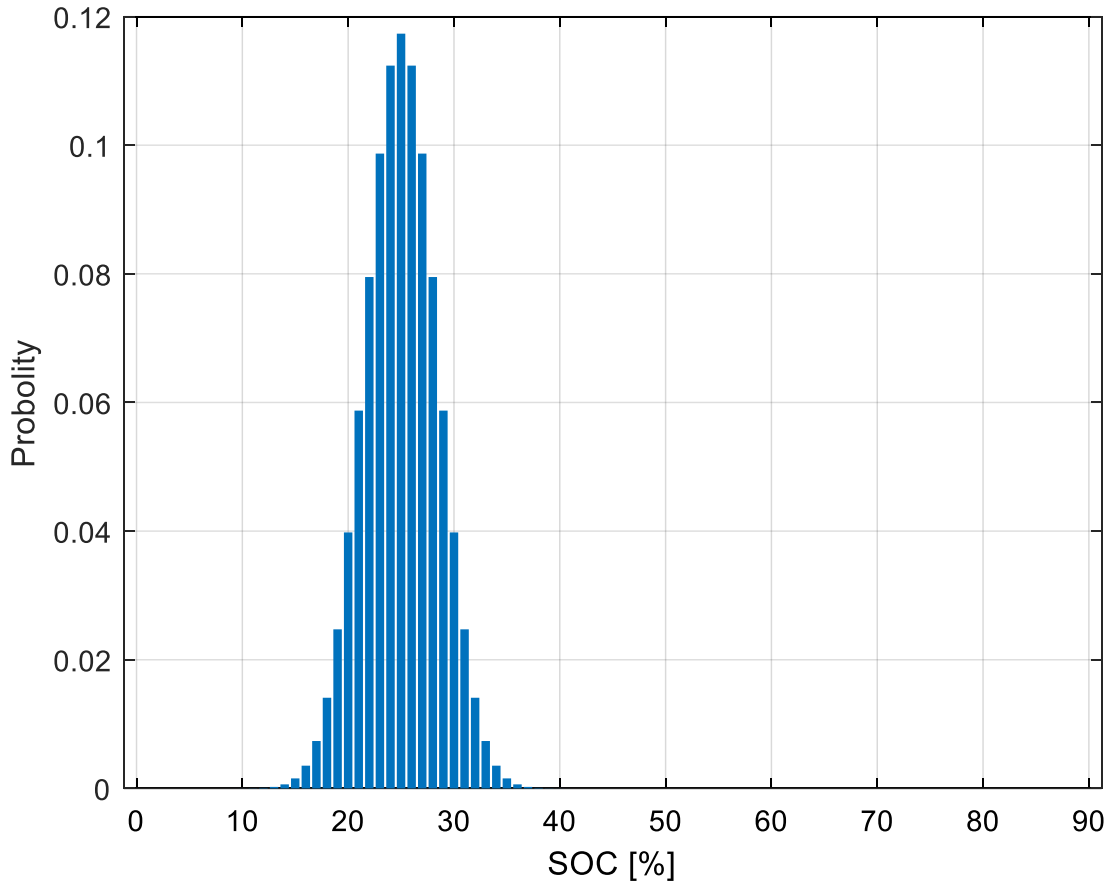

Figure 4.2. The Probability Distribution of Arrival SOC at XFC Stations

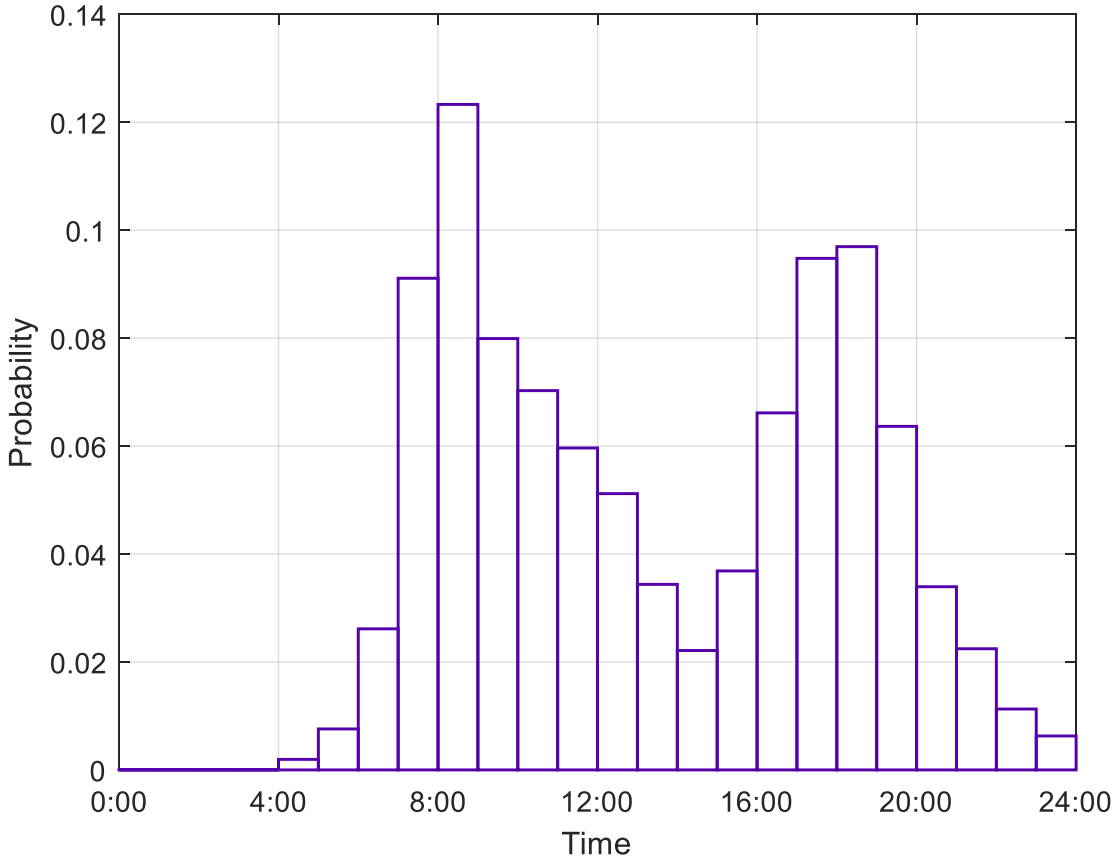

Figure 4.3. The Probability Distribution of Arrival Time at XFC Stations

4.1.2 EV Charging Load Estimation with the Consideration of Charging Curves for Different EV Models

As mentioned previously, the EV charging curves depend on both the charging port power rate and the EV's battery characteristics. For example, an EV with a maximum charge rate of 50 kW can be connected to a 300-kW charger, but it will be charged at 50 kW. Therefore, the battery charging acceptance curve is necessary to be considered while estimating the charging load at XFC stations. The 300-kW charger operated by Fastned is adopted in this paper. The charging curves of various types of EVs are shown in Figure 4.4 [77].

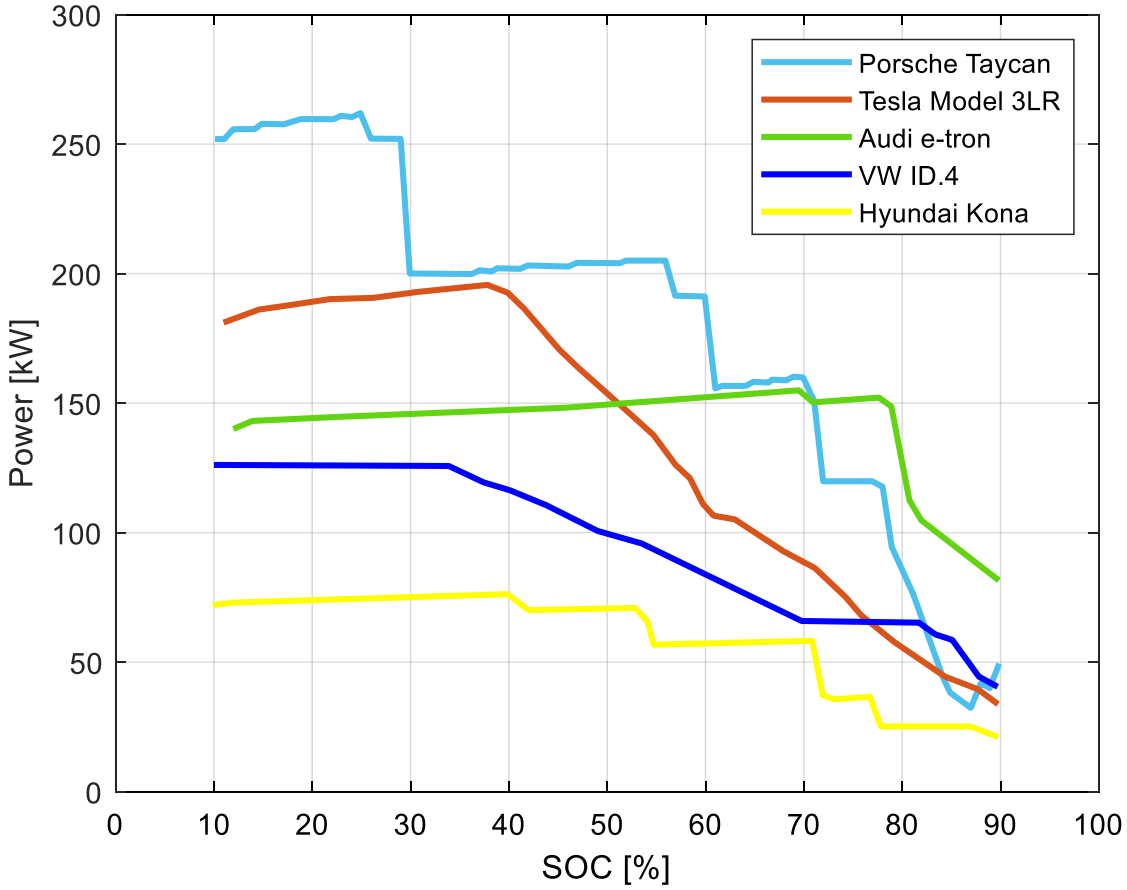

Figure 4.4. EV Charging Curves at 300 kW Chargers [77]

The charging process of n^{th} EV is modeled as a discrete-time linear system as:

$$SOC_{n,ev}(t+\Delta t) = SOC_{n,ev}(t) + \frac{\eta_{n,ev} P_{n,ev}(t) \Delta t}{E_{n,ev}} \tag{4.2}$$

where $\eta_{n,ev}$ is the charging efficiency, $P_{n,ev}$ is the instant charging power, and $E_{n,ev}$ is the battery capacity.

The number of charging ports is also considered as an impact factor of charging load estimation at XFC stations. Based on the data from the Alternative Fuels Data Center [78], many EV charging stations have 2 to 4 ports. Common gas stations in the suburbs have 6 to 12 pumps. Therefore, in this paper, the number of charging ports is

chosen within the range of 2 to 12. Each port has the ability to deliver power up to 300 kW, which can add 200 miles of range within 15 minutes. The maximum waiting time is 15 minutes. Based on the first come, first serve queuing method, the MC simulation can be performed with 1-min resolution over every 24-hour period and generate approximate real-world load profiles and port usage of XFC. The charging load at every simulation time step is calculated based on the number of EVs being charged and the charging curves of these EVs.

4.2 Optimal Configuration of XFC Stations integrated with ESS and PV Panels in Distribution Networks

A schematic illustration of an XFC station with ESS and PV panels in a medium voltage distribution network is shown in Figure 4.5. The XFC station is connected as a distribution node and it receives power through the distribution feeder and transformer. The reverse power flow feeding back to the distribution network is not allowed. Hence, ESS is responsible for storing energy from the PV panels and the distribution network and releasing power to XFC charging loads to meet charging requirements. The operation limitations of the grid also need to be considered while drawing power from the distribution network.

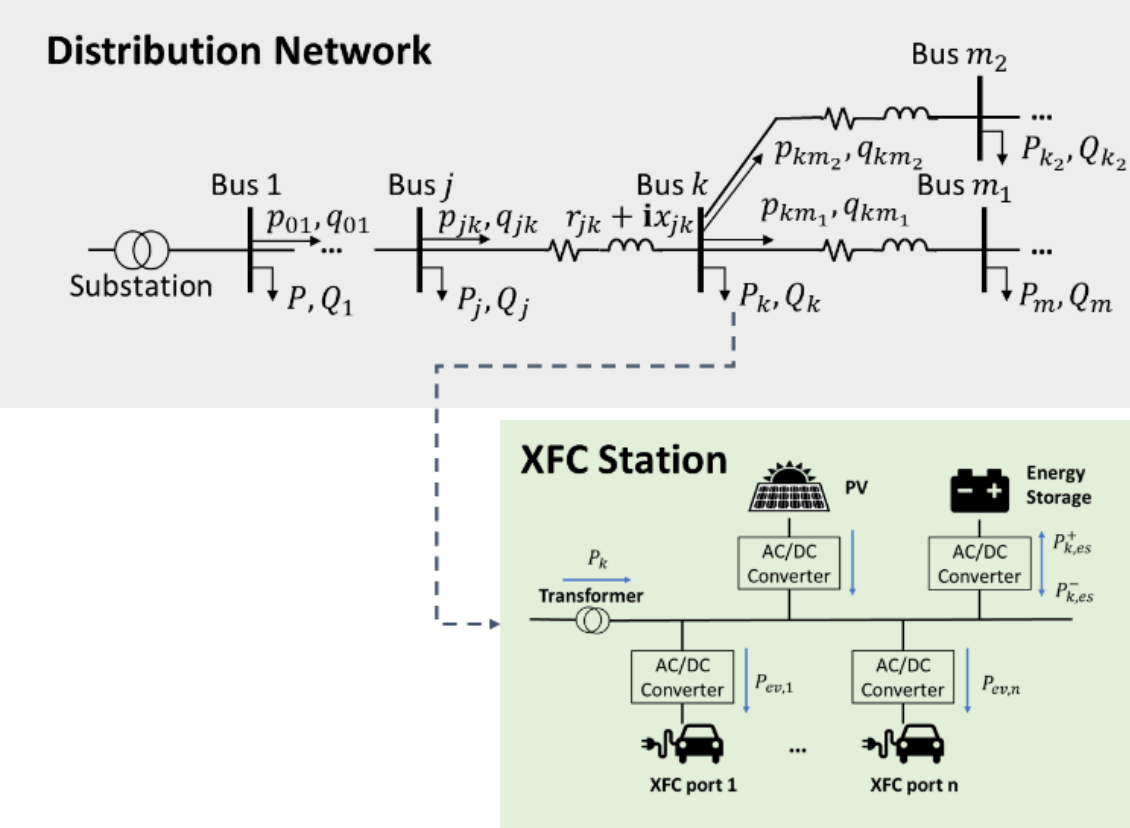

Figure 4.5. Schematic Illustration of an XFC Station with ESS and PV Connected to a Distribution Network

4.2.1 Distribution Network Power Flow

Considering the branch flow model as shown in Figure 4.5, the optimal power flow technique is common to ensure the operation of the distribution network. For each node $k \in \boldsymbol{K}$, let j be its parent node and $m \in \boldsymbol{M}_k$ be its child nodes. The power flow equation can be formulated as:

$$p_{jk}(t) - I_{jk}(t) r_{jk} - \sum_{m \in \boldsymbol{M}_k} p_{km}(t) = P_k(t) \tag{4.3}$$

$$q_{jk}(t) - I_{jk}(t) x_{jk} - \sum_{m \in \boldsymbol{M}_k} q_{km}(t) = Q_k(t) \tag{4.4}$$

$$U_k(t) - U_j(t) - (r_{jk}^2 + x_{jk}^2) I_{jk} + 2(p_{jk}(t) r_{jk} + q_{jk}(t) x_{jk}) = 0 \tag{4.5}$$

$$I_{jk}(t) = \frac{p_{jk}(t)^2 + q_{jk}(t)^2}{U_j(t)} \tag{4.6}$$

where p_{jk} and q_{jk} indicate the active and reactive power that are sent from node j to node k; r_{jk} and x_{jk} denote the resistance and reactance between two nodes; U_{jk} and I_{jk} present the square magnitude of voltage and current; P_k and Q_k are the active and reactive power of node k that draws from the distribution network. To avoid the non-convex optimization, the quadratic equalities in (4.6) are relaxed to a second-order cone expression as below [70]:

$$\left\| \begin{matrix} 2p_{jk}(t) \\ 2q_{jk}(t) \\ I_{jk}(t) - U_k(t) \end{matrix} \right\|_2 \leq I_{jk}(t) + U_k(t) \tag{4.7}$$

The constraints of the power flow optimization are listed below:

$$0 \leq I_{jk}(t) \leq I^{\max} \tag{4.8}$$

$$U^{\min} \leq U_k(t) \leq U^{\max} \tag{4.9}$$

where I^{max} is the maximum of the current magnitude, U^{min} and U^{max} are the minimum and maximum of the voltage magnitude.

4.2.2 PV Model

PV panels are considered as non-dispatchable emission free power generator that depends on the conditions of solar irradiance and ambient temperature. For XFC stations, integrated with PV panels is one of the best choices to improve the quality of charging service and reduce the cost of electricity bills. The instant solar power P_{pv} is modeled as a discrete-time linear system [79].

$$P_{pv}(t) = G(t) A_{pv} P_{pv,rated} \eta_{pv} \left[1 - \beta_T \left(T_C(t) - T_{C,STC}\right)\right] \tag{4.10}$$

where $G(t)$ is the solar radiance; A_{pv} is the area of PV cell; $P_{pv,rated}$ is the nominal power of PV cell, η_{pv} is the power efficiency; β_T is the PV temperature coefficient; $T_c(t)$ is the PV cell temperature; $T_{c,STC}$ is the cell temperature under standard test conditions.

The area of PV panels is determined by the number of PV cells n_{pv} and the area of a single PV cell A_{pv} to be installed. Reference to the roof area of gas stations in the suburbs, the maximum areas of PV panels, A_{pv}^{max}, are assumed to be $80m^2$ for 4-port XFC stations and $160m^2$ for 8-port XFC stations. The constraint of PV panel area can be formulated as:

$$n_{pv}A_{pv} \le A_{pv}^{\max} \tag{4.11}$$

4.2.3 ESS Model

Stational ESS works as an energy buffer to store energy from the grid or PV ahead and release energy when EV charging demand is high. With the optimal charging and discharging control of ESS, the non-dispatchable PV power can be fully utilized, the power demand from the grid can be reduced to further improve the distribution network operation, and the XFC electricity price can be reduced based on the time-variant electricity price.

The charging/discharging process of battery ESS can be formulated as:

$$\begin{aligned} SOC_{k,ess}(t+\Delta t) = SOC_{k,ess}(t) \\ + \phi_{k,ess}^{+}(t)\frac{\eta_{ess}P_{k,ess}^{+}(t)\Delta t}{E_{k,ess}} \\ + \phi_{k,ess}^{-}(t)\frac{P_{k,ess}^{-}(t)\Delta t}{\eta_{ess}E_{k,ess}} \end{aligned} \tag{4.12}$$

$$\phi_{k,ess}^{+}(t)+\phi_{k,ess}^{-}(t)=1 \tag{4.13}$$

where $SOC_{k,ess}$ is the battery state of charge at distribution node k; η_{ess} is the charging/discharging efficiency of battery ESS; $E_{k,ess}$ is the battery capacity at distribution node k; $P_{k,ess}^{+}$ is the battery charging power and $P_{k,ess}^{-}$ is the battery discharging power. $\emptyset^{+}$ and $\emptyset^{-}$ are binary variables to indicate the charging or discharging mode of ESS. (4.13) ensures that the battery cannot be charged or discharged at the same time.

The charging and discharging rate are limited by the rated charging/discharging power $P_{k,ess}^{\text{rated}}$. These can be expressed as (4.14) and (4.15). Meanwhile, the SOC is limited to avoid overcharging and deep discharging as shown in (4.16).

$$0 \le P_{k,ess}^{+}(t) \le P_{k,ess}^{rated} \tag{4.14}$$

$$-P_{k,ess}^{rated} \le P_{k,ess}^{-}(t) \le 0 \tag{4.15}$$

$$10\% \le SOC_{k,ess}(t) \le 90\% \tag{4.16}$$

While operating the battery ESS, it must be fully charged at the beginning of each day to prepare for the daily high XFC charge demand. Let t_0 donates the beginning time slot of a day and $t_0 + \tau$ denotes the end time slot. The constraints of daily ESS operation can be further improved with:

$$SOC_{k,ess}(t_0)=SOC_{k,ess}(t_0+\tau)=90\% \tag{4.17}$$

Finally, the configuration of ESS within XFC stations is aimed to find the size of battery ESS, including the rated power and energy capacity. The constraints can be formulated as:

$$P_{ess}^{\min} \le P_{k,ess}^{rated} \le P_{ess}^{\max} \tag{4.18}$$

$$E_{ess}^{\min} \le E_{k,ess} \le E_{ess}^{\max} \tag{4.19}$$

where $P_{ess}^{\min}$ and $P_{ess}^{\max}$ are minimal and maximal power to determine the range of rated power of battery ESS, and $E_{ess}^{\min}$ and $E_{ess}^{\max}$ are minimal and maximal energy capacity can be invested.

4.2.4 XFC Station Power Flow

As shown in Figure 4.5, the XFC station is connected to the distribution network node k as a microgrid. The XFC station will absorb power from the distribution network to charge either battery ESS or EVs. The feeding power from the XFC station node to the distribution network is not considered. The power flow of the XFC station can be formulated as:

$$\begin{aligned} P_k(t) = \phi_{k,ess}^{+}(t)P_{k,ess}^{+}(t) + \phi_{k,ess}^{-}(t)P_{k,ess}^{-}(t) \\ + \sum_{n_{ev}=1}^{N_{ev}} P_{n,ev}(t) - n_{pv}P_{pv}(t) \end{aligned} \tag{4.20}$$

$$P_k(t) \le P_k^{\max} \tag{4.21}$$

(4.21) indicates that the injected power to the node k is limited to the feeder capacity P_k^{max}.

4.2.5 Optimization Formulation

With a given number of charger ports in an XFC station and the locations of XFC stations in the distribution network, the goal of the optimal configuration is to quantify the power and energy capacity of ESS and the number of PV cells that need to be configured within XFC stations. The optimization objective is to minimize the investment cost of ESS and PV, the electricity purchase cost of XFC stations, and the cost of power

losses in the distribution network. Based on the aforementioned constraints, the optimization problem of XFC stations in the distribution networks is formulated as:

$$\begin{aligned}\min \quad & \sum_{k=1}^{K}\delta_{ess}\left(c_{ess,E}E_{k,ess}+c_{ess,P}P_{k,ess}^{rated}\right)\\ & +\sum_{k=1}^{K}\delta_{pv}c_{pv}n_{k,pv}\\ & +\sum_{t=1}^{T}\sum_{k=1}^{K}\lambda(t)P_k(t)\Delta t\\ & +\sum_{t=1}^{T}\sum_{(j,k)\in L}\lambda(t)r_{jk}I_{jk}(t)\Delta t\end{aligned} \tag{4.22}$$

s.t.:
Distribution network (4.3)-(4.5), (4.7)-(4.9)
PV (4.10),(4.11)
ESS (4.12)-(4.19)
XFC station (4.20),(4.21)

where $c_{ess,E}$ and $c_{ess,P}$ are the costs of energy and power capacity of ESS; c_{pv} is the cost of a single PV cell; n_{pv} is the number of PV cells at distribution network node k; $\lambda(t)$ presents the time-variant electricity price; δ_{ess} and δ_{pv} are the annual discount rate of ESS and PV investment costs. The annual discount rate $\delta_{\cdot}$ is shown in (4.23) [80, 81].

$$\delta_{\cdot}=\frac{i(1+i)^{\gamma_{\cdot}}}{(1+i)^{\gamma_{\cdot}}-1} \tag{4.23}$$

where i is the discount rate of the investment cost and γ is the lifespan of the ESS or PV panels. The lifespan of ESS has assumed 20 years and the lifespan of PV is 30 years. The first term of the objective function is the equivalent annual investment cost of ESS, the second term shows the equivalent annual investment cost of PV, the third term is the electricity cost of XFC stations, and the fourth term indicates the electricity cost of power losses in the distribution network.

The optimal configuration of ESS and PV within XFC stations in the distribution network is formulated as a mixed integer programming with quadratic terms. The variables $\{n_{pv}, P_{k,ess}^{\text{rated}}, E_{k,ess}, P_{k,ess}^{+}, P_{k,ess}^{-}, P_k, Q_k, p_{jk}, q_{jk}, U_k, I_k, \}$ can be solved by

Gurobi or Cplex solver efficiently. The size of PV and ESS, the charging/discharging operation of ESS, and the optimal power flow of the distribution network can be generated simultaneously.

4.3 Case Study

A modified 33-bus system is applied to simulate the presented optimal configuration of XFC stations in the distribution networks. As shown in Figure 4.6, the distribution nodes are classified into residential nodes, commercial nodes, and XFC station nodes with 12.88 kV nominal voltage. The voltage range is plus or minus 5% of the nominal voltage. XFC4 station is located at node 30 which has 4 charging ports and XFC8 station is located at node 8 with 8 charging ports. The feeder capacity of node 8 is chosen as 600 kW and the feeder capacity of node 30 is 300 kW. A total of 220 EVs are used in the MC simulation to estimate the charging load in these two XFC stations.

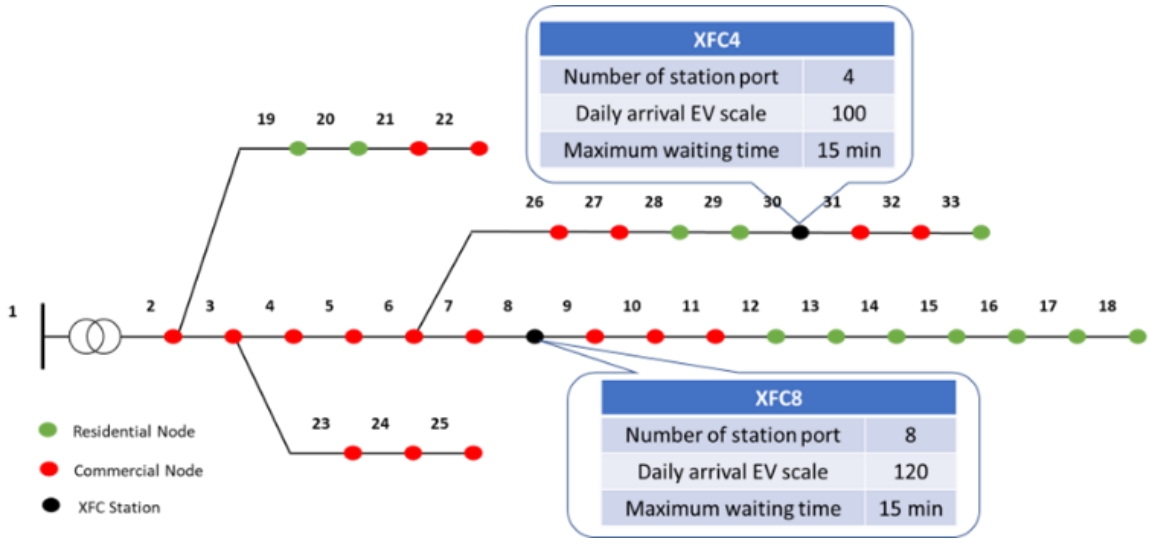

Figure 4.6. 33-bus Distribution System with XFC Stations

4.3.1 Basic Parameters

The battery size of different EV models in the simulation and the corresponding percentages of these models in the total simulated EVs are listed in Table 4.2. It is assumed that 100 EVs are expected to be charged daily at XFC4 and 120 EVs are expected to be charged daily at XFC8. The probability distribution of arrival SOC, arrival time, and charging characteristics are discussed in Section 4.1. The MC simulation is performed with a 1-min resolution over every 24-hour period.

Table 4.2. Battery Size and Percentage of EV Models

EV Model	Battery Size	Percentage
Porsche Taycan	79.3 kWh	5%
Tesla Model 3LR	82 kWh	30%
Audi e-tron	95 kWh	25%
VW ID.4	82 kWh	20%
Hyundai Kona	64 kWh	20%

Assume that the SunPower SPR-E20-327 [82] solar panels are used in the XFC stations. The detailed parameters of this solar panel are listed in Table 4.3. The historical data of ambient temperature and solar irradiance at Aurora, Illinois in 2018 are retrieved from Solcast [83].

Table 4.3. Parameters of Solar Panels

Parameter	Symbol	Value
Area	A_{pv}	$1.559 \times 1.064 m^2$
Nominal power	$P_{pv,rated}$	327W
Power efficiency	η_{pv}	20.7%
Temperature coefficient	β_T	–0.35% / ℃
Cell temperature under standard operation condition	$T_{c,STC}$	25℃
Initial cost	c_{pv}	$600

The parameters of ESS are listed in Table 4.4. The cost of power capacity is converted from the cost of energy capacity by multiplying by the hour duration [84]. For example, a 589 $/kWh, 2-hour battery energy storage system would have a power capacity cost of 1178 $/kW.

Table 4.4. Parameters of ESS

Parameter	Symbol	Value
Cost of energy capacity	$c_{ess,E}$	589 $/kWh
Cost of power capacity	$c_{ess,P}$	$589 \times hour$ $/kW
Maximum energy capacity	$E_{ess}^{\max}$	2 MWh
Minimum energy capacity	$E_{ess}^{\min}$	0
Maximum charging/discharging rate	$P_{ess}^{\max}$	1 MW
Minimum charging/discharging rate	$P_{ess}^{\min}$	0

The variety of building loads, such as supermarkets, offices, restaurants, houses, and apartments, are selected accordingly to simulate the commercial or residential nodes. The whole year hourly load profiles of buildings in Aurora, Illinois are retrieved from the U.S. Department of Energy's Open Energy Data Initiative database [65]. The electricity prices are hourly real-time prices for the distribution network. The dataset is retrieved from the PJM dataset of the North Illinois hub [85]. It represents the full year of real-time electricity prices in 2018. The price curves of a typical winter day and a typical summer day are shown in Figure 4.7.

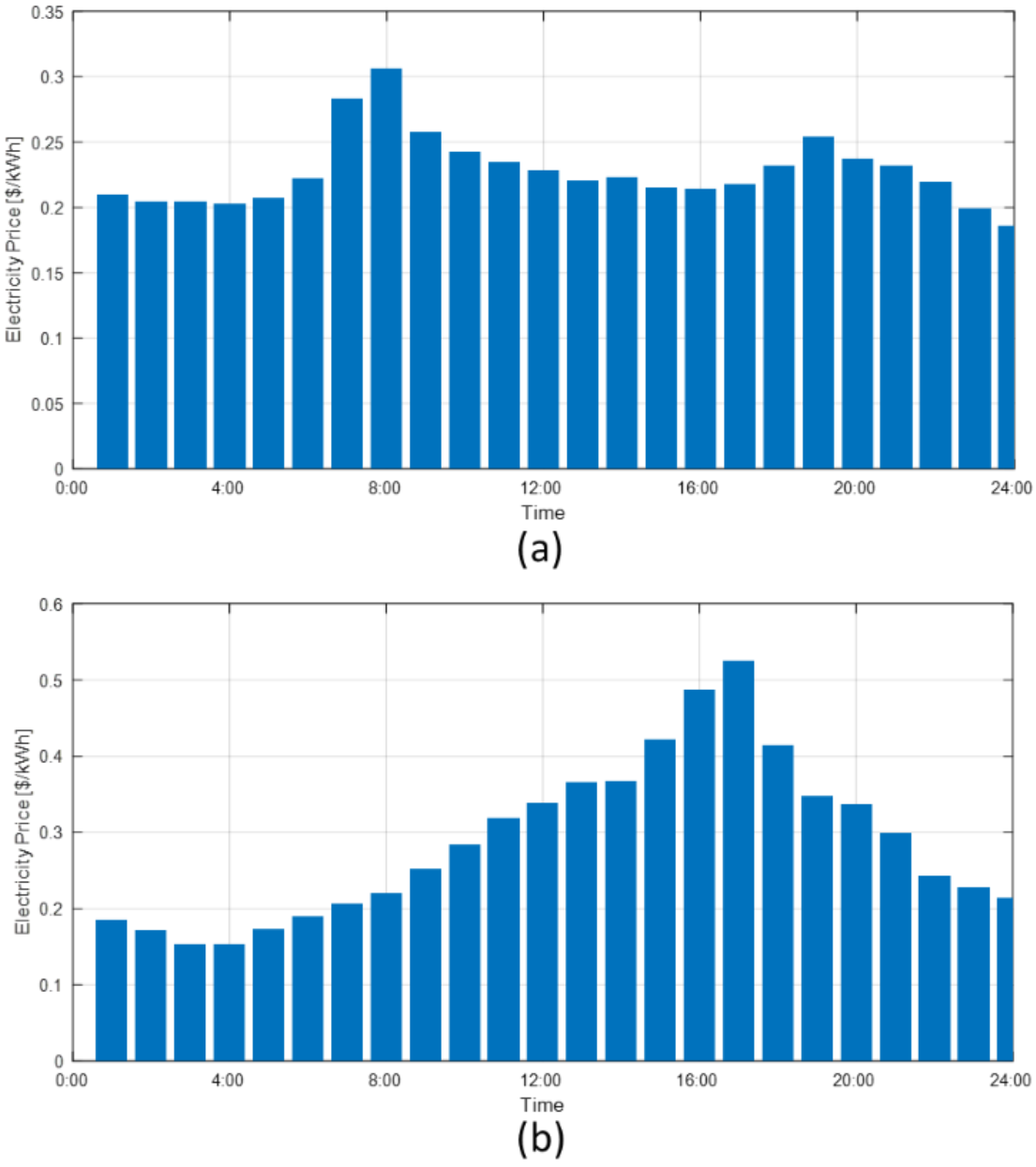

Figure 4.7. Electricity Price Curve on (a) a Winter Day (b) a Summer Day

Different from the MC simulation of EV charging loads with 1-minute resolution, the historical data of solar irradiance, ambient temperature, building loads, and electricity price are hourly based intervals for a whole year. The estimated EV charging load needs to be approximated in 1-hour resolution for analyzing the optimal configuration problem.

Therefore, the average charging power of each hour from the MC simulation is approximated for the optimization. The optimal configuration problem formulated in Section 4.2 is performed with a 1-hour resolution for 365 days.

4.3.2 XFC EV Charging Load Estimation

Figure 4.8 shows a sample of daylong time series of charging load for XFC4. As mentioned previously, XFC4 has 4 charging ports, and each port is a 300-kW charger. The maximum waiting time is 15 minutes. The top plot shows the aggregated charging load of this XFC station. The peak loads occur from 8:00 to 1:00 pm and from 4:00 pm to 8:00 pm. The average charging event duration is around 15 minutes and the peak of daily power demand is about 750 kW. During the charging events, the power demand is always above the feeder capacity that is selected as 300 kW for node 30. If the current feeder is not upgraded or configured with renewable energy resources, XFC events will cause huge damage to the distribution network. The bottom plot shows the station port utilization of XFC4. These XFC station ports are in high utilization with a 100 EVs daily arrival scale.

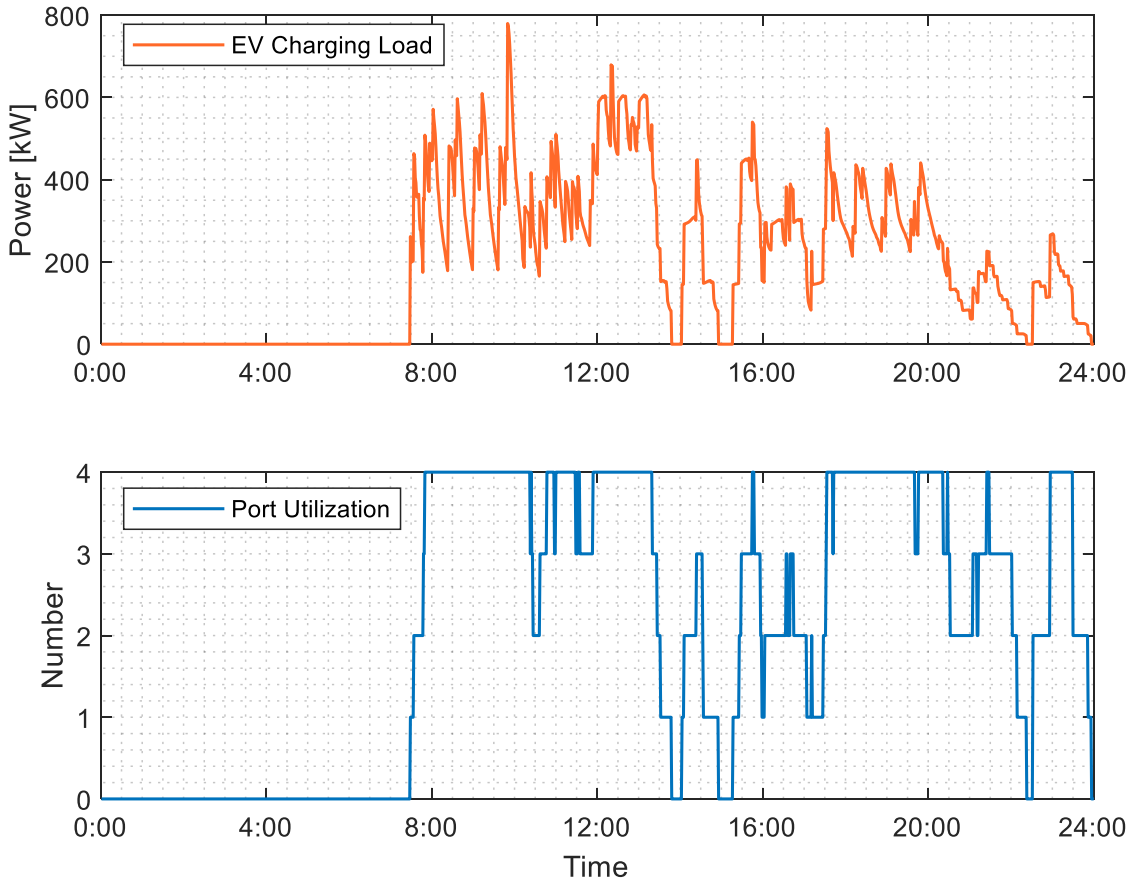

Figure 4.8. EV Charging Load and Port Utilization of XFC4

Figure 4.9 shows a sample of daylong time series of EV charging load for XFC8. As mentioned previously, XFC8 has 8 charging ports, and each port is a 300-kW charger. The maximum waiting time is also 15 minutes. The average charging event duration is around 15 minutes, and the peak of daily power demand is about 1200 kW. It is dangerous if the feeder capacity is 600 kW. The bottom plot in Figure 4.9 shows the station port utilization of XFC8. Slightly different from XFC4, 8 ports are in medium utilization if 120 EVs are expected to be charged daily.

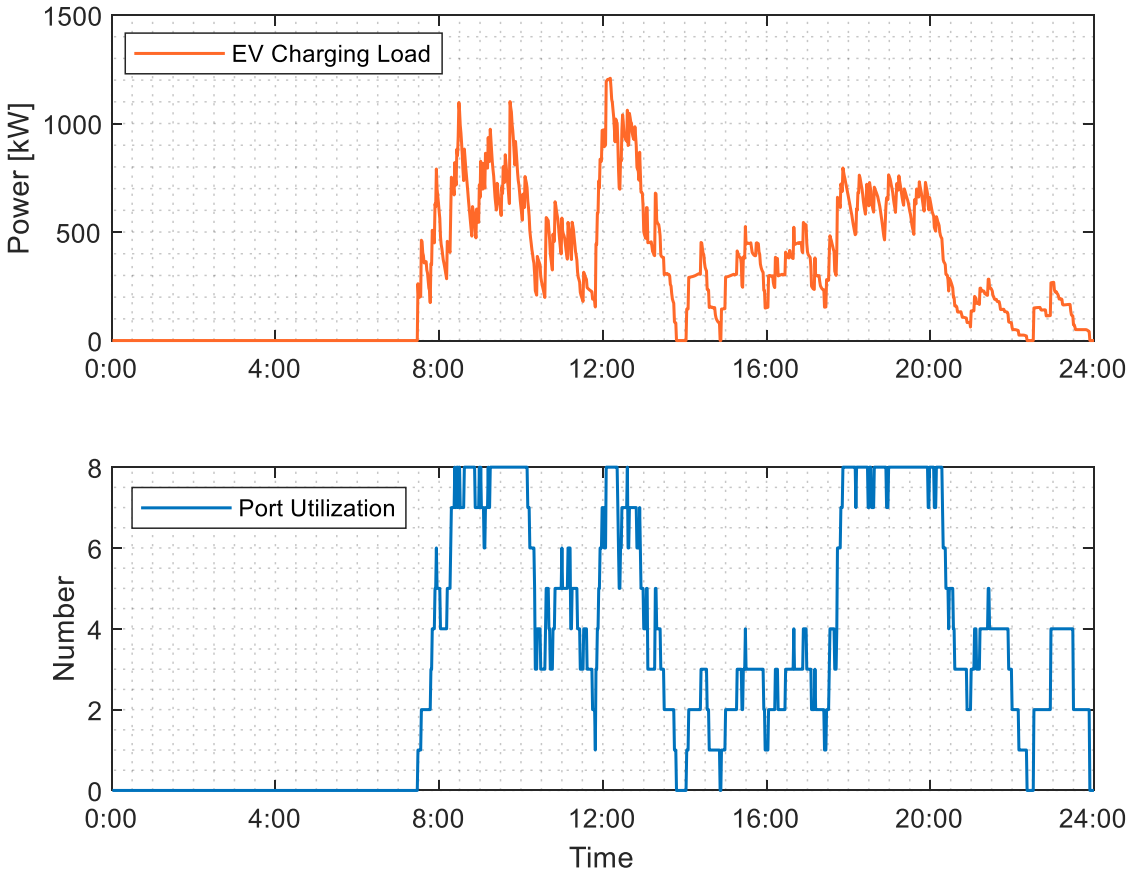

Figure 4.9. EV Charging Load and Port Utilization of XFC8

In summary, the presented MC simulation can generate approximate real-world XFC EV charging load profiles with proper assumptions. Changing input values, the corresponding charging loads and the station port utilization can be obtained. These simulation tools are valuable for understanding the possible effects of XFC on the power grid since little real-world XFC charging data is available now.

4.3.3 The Benefits of Optimal Configuration of XFC Stations Integrated with ESS and PV Panels

The benefits of optimal configuration can be summarized in three aspects: the total annual cost of XFC stations, including the ESS and PV investment cost and the cost

to purchase electricity from the utility, is significantly reduced; the power demand of XFC stations will not exceed the node feeder capacity; and the undervoltage violation will be avoid to address the optimal power flow of the distribution network. Since the optimization is performed with a 1-hour resolution for 365 days, the average charging power of each hour from the MC simulation is approximated.

The optimal configuration results of ESS energy capacity, ESS rated power, and the number of PV cells, and the cost of two XFC stations are summarized in Table 4.5. If the XFC station is not installed with ESS and PV panels, the total annual cost is the electricity purchase cost from the utility. Otherwise, the total annual cost is the sum of the annual investment cost of ESS and PV panels, and the electricity purchase cost from the utility. The results demonstrate that the integration of stational ESS and PV can significantly reduce the total annual cost for both XFC stations. Although the investment cost of ESS and PV is expensive, the PV panels can generate clean energy and the ESS can work as an energy buffer to store electrical energy from the grid during low price periods and output electrical energy to XFC stations during high price periods. As shown in Figure 4.11and Figure 4.13, ESS prefer to recharge themselves at midnight because of the lower electricity price, and then, output the stored energy to support EV charging during the peak electricity price period at daytime. Compare with the XFC stations without ESS and PVs, the electricity purchase cost is reduced significantly. Considering both the investment cost of ESS and PV and the electricity purchase cost, the overall annual cost for XFC4 is reduced by 26.55% and the total annual cost for XFC8 is decreased by 27.01%.

Table 4.5. Benefit of Two XFC Stations

Parameter	XFC4	XFC8
ESS		
Energy Capacity	711.6kWh	1209.3kWh
Power Capacity	257.3kW	469.5kW
Annual Investment Cost	$108,562	$184,487
PV		
Number of PV Cells	70	110
Nominal Power	22.89kW	35.97kW
Annual Investment Cost	$2,732	$4,293
Electricity Purchase Cost		
without ESS and PV	$454,810	$701,227
with ESS and PV	$225,476	$327,317
Cost Saving	50.4%	53.3%
Total Annual Cost		
Cost without ESS and PV	$454,810	$701,227
Cost with ESS and PV	$334,037	$375,553
Cost saving	26.55%	27.01%

Figure 4.10 shows the charging/discharging power and the battery ESS SOC at XFC4 on a winter day. Since XFC4 is in high usage, the ESS outputs power to support XFC events and reaches 10% SOC at 2:00 pm. Then, a short charging period of ESS occurs in the afternoon to prepare for another peak XFC demand. Once the EV charging requirements are satisfied and the electricity price is dropped, the ESS is recharged again.

The SOC is recovered to 90% at the end of the day. The imported power of XFC4 with and without ESS and PVs on a winter day is shown in Figure 4.11. The EV charging demand at XFC4 will exceed the node feeder capacity during the peak period. After integrating with ESS and PV, the maximum power demand of this XFC station is limited below the pre-defined feeder capacity. The optimal configuration can shave the peak load of EV charging. It will reduce the stress on the local transformer and feeder.

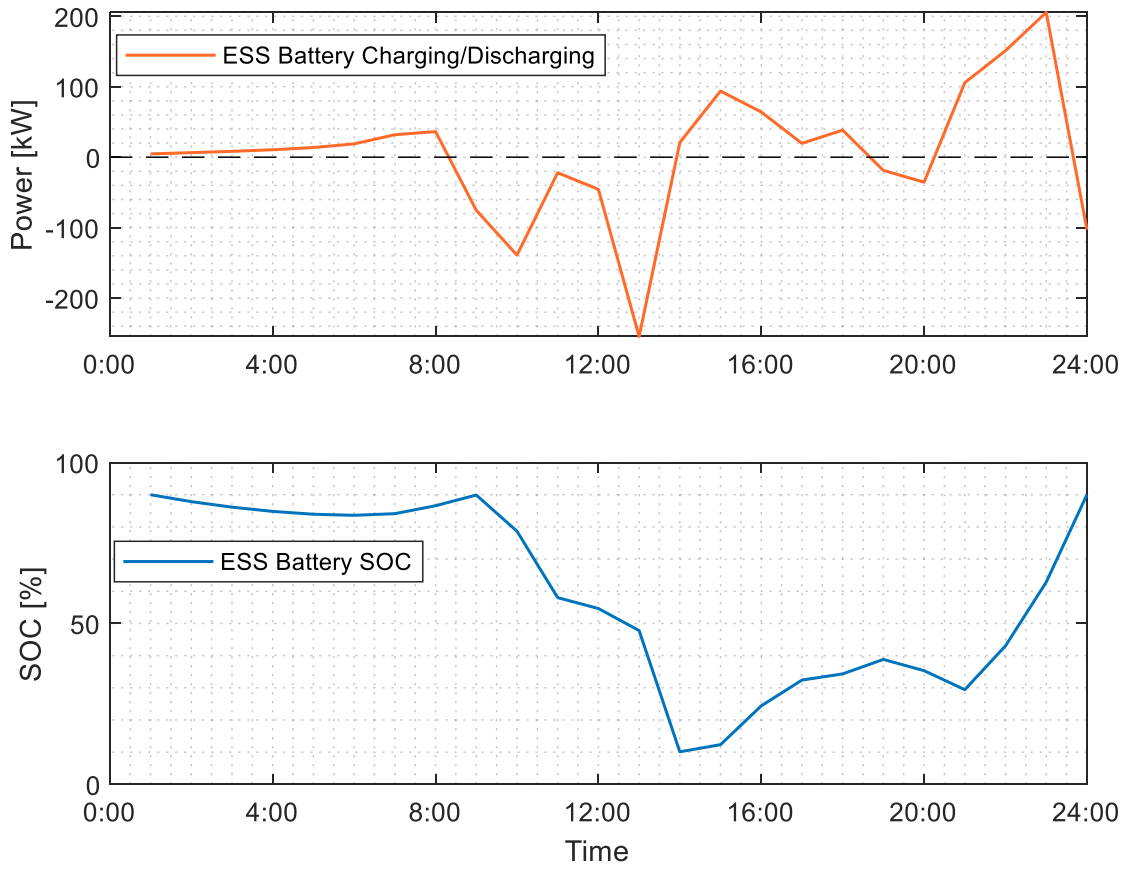

Figure 4.10. ESS Operation at XFC4 on a Winter Day

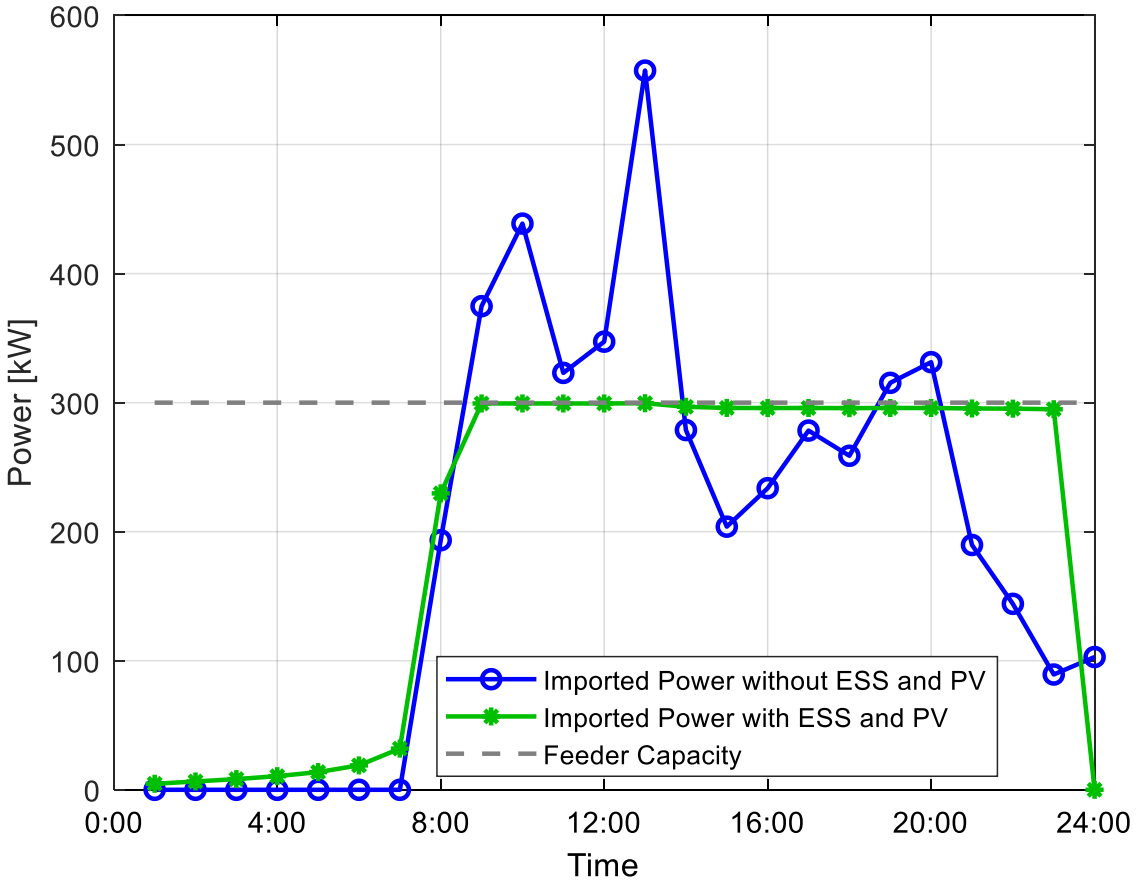

Figure 4.11. Imported Power of XFC4 on a Winter Day

Figure 4.12 shows the charging/discharging power and the battery ESS SOC at XFC8 on a summer day. Since XFC8 is in medium utilization, a short charging period happens at around 11:00 am when the electricity price and EV charging demand are relatively low. Although the EV charging demand at the evening peak is relatively lower than the peaks during the day, the ESS continuously outputs power to supply EV charging because of the higher electricity price. Figure 4.13 shows the imported power of this XFC station integrated with and with ESS and PVs on a summer day. The total power demand is also limited under the pre-defined feeder capacity. Additionally, with an

optimal configuration, ESS can import power from the grid during the low electricity price periods and output power to EV chargers during the high price periods.

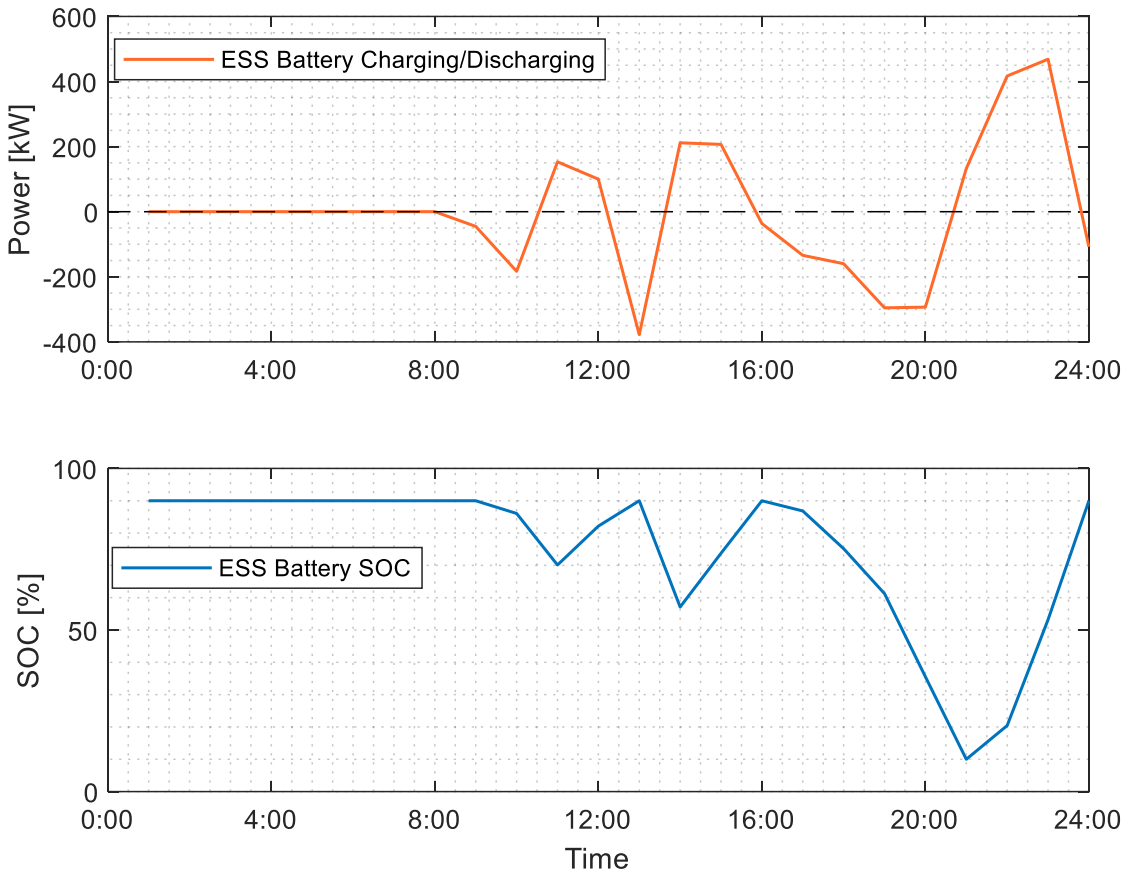

Figure 4.12. ESS Operation at XFC8 on a Summer Day

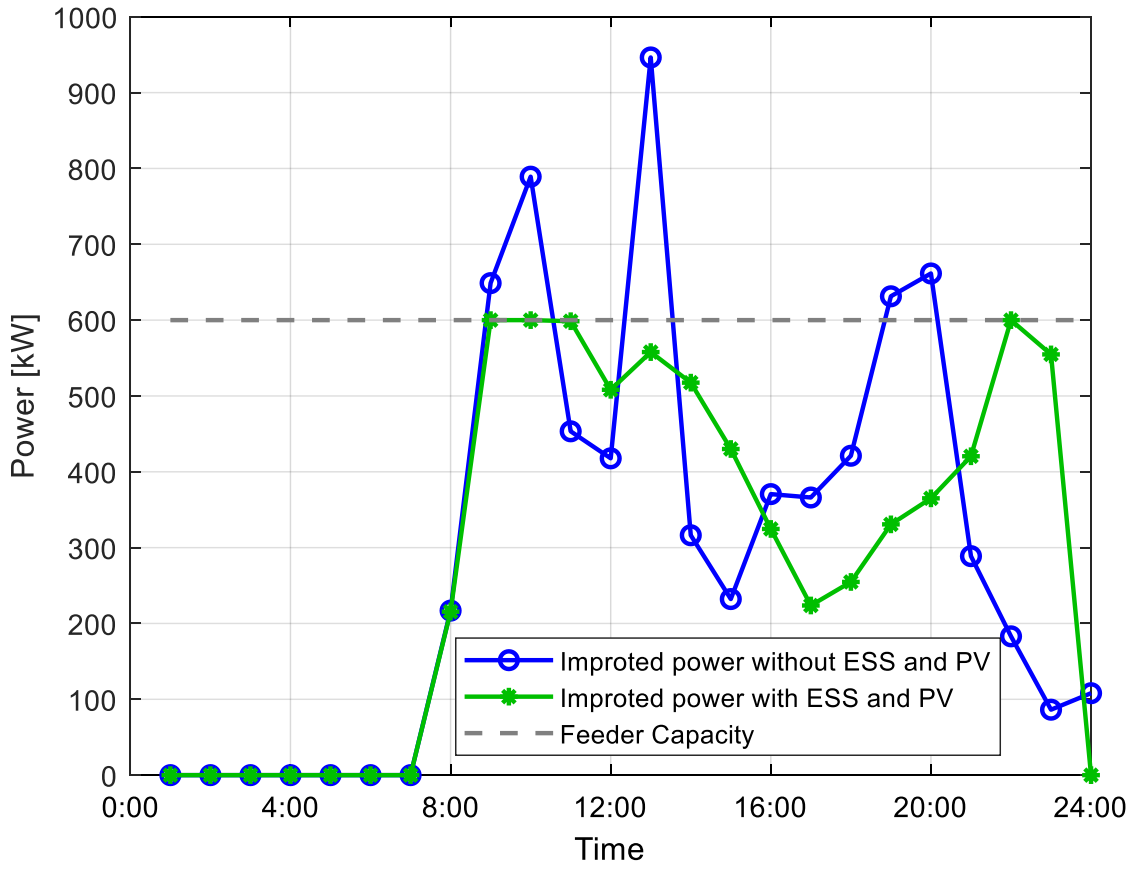

Figure 4.13. Imported Power of XFC8 on a Summer Day

To demonstrate the optimal power flow of the distribution network, Figure 4.14 shows the voltage profiles on a typical winter day and a typical summer day. The voltage distortions are less than 5%. No large voltage distortions are observed because of the coordination of the ESS and PV within the XFC stations. Figure 4.15 shows the voltage profile of node 18 with and without ESS and PV on a summer day. Node 18 is the terminal node of the longest branch, so the voltage violations are more likely to happen. Since the overall peak loads are much higher than the ones in winter, the undervoltage violations are observed at 1:00 pm and evening from 5:00 pm to 8:00 pm if XFC stations are not integrated with ESS and PV panels. However, once the coordination of the ESS

and PV panels within the XFC stations are introduced, the configurations of ESS and PV panels will take the constraints of the optimal power flow into account. The overall voltage distortions are less than 5%. The optimal configuration ensures the stability of the distribution network. These results show that the optimal configuration of XFC stations with ESS and PV in the distribution network can not only reduce the cost but also improve grid performance.

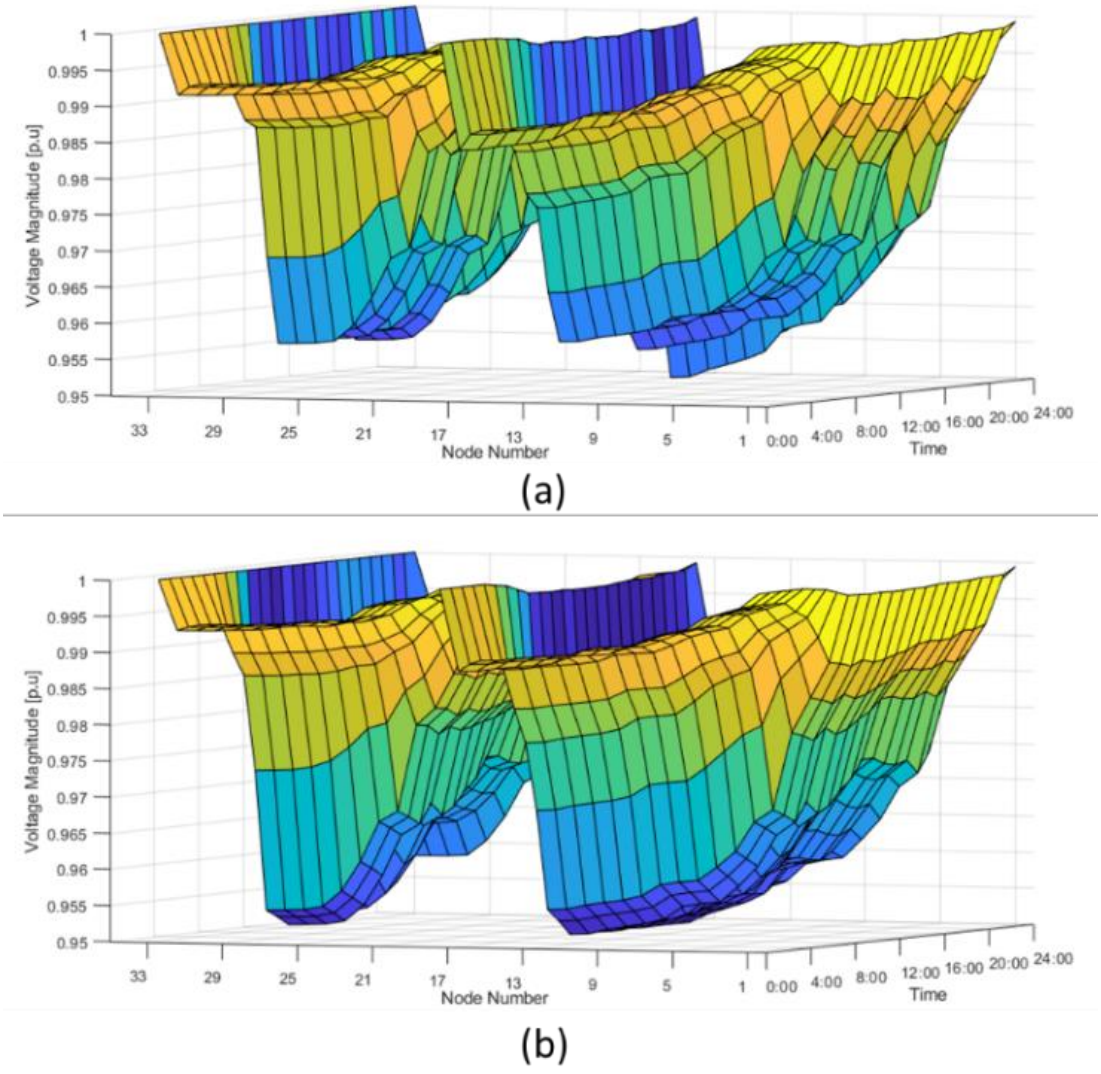

Figure 4.14. Voltage Profiles of the Distribution Network on (a) a Winter Day (b) a Summer Day

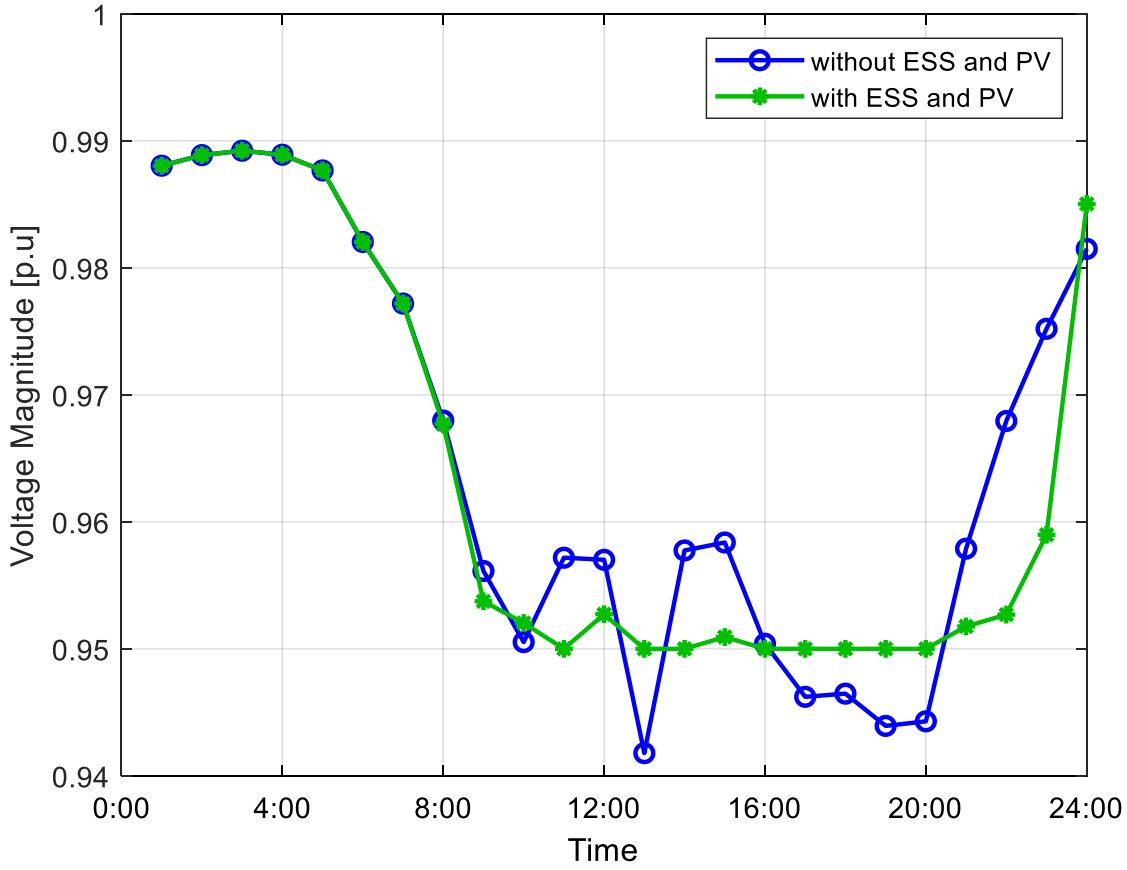

Figure 4.15. Voltage Profiles of Node 18 on a Summer Day

4.4 Chapter Conclusion

In this chapter, a novel Monte Carlo simulation tool has been developed to estimate the EV charging demand at XFC stations based on the distributions obtained from the vehicle travel survey dataset. The estimation algorithm considers various aspects, including EV scale, EV model and the percentage in the total simulated EVs, EV charging curves for different EV models, XFC station port availability, and waiting time. This estimation tool is valuable since little XFC charging dataset is available at the current stage. The paper also presents an optimal configuration method for multiple XFC stations at the distribution network level to determine the optimal ESS energy capacity,

ESS rated power, and the PV size integrated with XFC stations. The objectives of the optimal configuration are to reduce the investment and operation costs of XFC stations while meeting the charging demand and the operational constraints of the distribution network, XFC, ESS, and PV panels.

A case study is performed using public datasets including the daily driving patterns of vehicles from NHTS, the hourly load profiles of buildings from the U.S. Department of Energy's Open Energy Data Initiative database, the hourly real-time electricity prices from PJM, and the hourly ambient temperature and solar irradiance from Solcast. The numerical results indicate that the presented MC simulation can generate approximate real-world XFC charging demand and the optimal configuration can determine the size of ESS and PV for multiple XFC stations in the distribution network. The simulation results show the following benefits of integrating ESS and PV panels with XFC stations. Firstly, the total annual cost savings of 26.55% at XFC4 and 27.01% at XFC8 are observed due to the reduction of electricity purchase from the grid. Secondly, the ESS and PV shave peak load below the capacity of the transformer and the feeder for XFC stations. Thirdly, the ESS and PV avoid voltage violations to improve the performance of the distribution network.

5 A Cloud-Based Simulation and Testing Platform for Large-Scale EV Charging Energy Management and Charging Control [3] [86]

In this chapter, a cloud-based simulation and testing platform is presented. The platform is designed for the development and Hardware-in-the-Loop (HIL) testing of VGI technologies. This Internet of Things platform is developed with the MQTT communication protocol to link multiple subsystems, which include real-time power system simulators (OPAL-RT or RTDS), EV Charge Scheduler (EVCS) applications, and real-word EV charging stations, solar panels, and energy storage systems. The real-time grid simulation and optimal EV charging energy management at the distribution grid level is performed in the OPAL-RT. The OPAL-RT communicates with the node-level EVCS and the real-word EV charging stations to collect real-time charging data and send charging power limit commands. The OPAL-RT can also communicate with transmission-level controllers to provide grid services, such as frequency regulation. The EVCS is developed based on standard communication protocols: OCPP 2.0 for charging station networks and ISO 15118 for the communication between EVs and charging stations. The EVCS manages regional EV charging to limit the effects of clustered EV charging on the distribution grid. The modular open systems design approach of the platform allows the integration of newly developed energy management strategies, EV charging control algorithms, and hardware charging systems for performance evaluation and interoperability testing.

[3] © [2022] SAE. Reprinted, with permission, from [Zhouquan Wu, Bo Chen, A Cloud-Based Simulation and Testing Framework for Large-Scale EV Charging Energy Management and Charging Control, 2022 SAE Technical Paper, 01/2022] See Appendix A for documentation of permission to reuse this material

5.1 An Overview of the Cloud-Based HIL Simulation and Testing Platform

Figure 5.1 gives an overview of the presented cloud-based HIL simulation and testing platform. The platform is designed with following major considerations.

- The platform can incorporate various types of EV charging stations (AC, DC, and XFC) in real-world applications or at the development stage. These hardware charging stations can be spatially distributed. Any charging facilities can be easily connected to the HIL testing platform via a developed communication interface.
- In addition to real-world charging stations, the platform can perform simulate the EV charging process to enable the testing of large-scale EV charging energy management and charging control. The EV charging simulation uses EV models, arrival and departure time, battery state of charge (SOC), charging characteristics, and their geographic locations where the EVs are connected to the grid.
- The platform is able to investigate the impact of EV charging on a distribution grid. A power simulator is designed to perform real-time grid simulation based on real-world/simulated EV charging load and other distribution grid loads.
- The platform can test the performance of distribution level energy management systems and node-level EV charging control systems.
- The platform utilizes standard communication protocols related to EV charging, such as OCPP 2.0 for charging station networks and ISO 15118 for the communication between EVs and charging stations.
- The platform is able to communicate with transmission level control systems, which allows the platform to provide grid services on the transmission level.

- The platform can also study the feasibility and benefit of integrating renewable energy sources such as solar panels and energy storage systems with EV charging stations.
- To facilitate the communication of these spatially distributed subsystems, a cloud-based communication is designed. The MQTT communication protocol is used for the communication between subsystems at different physical locations.

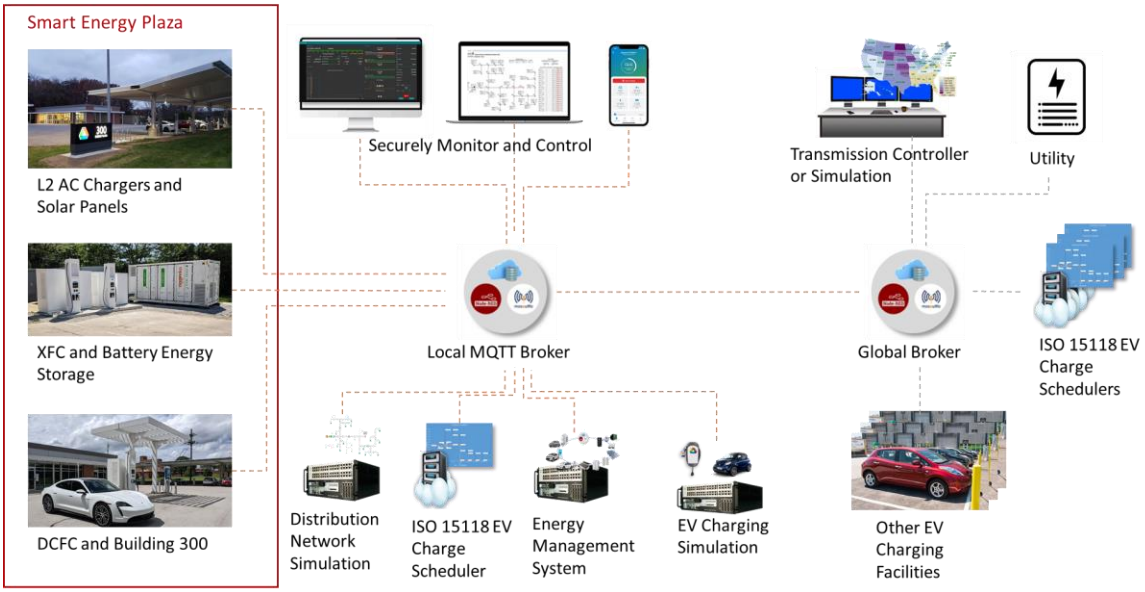

Figure 5.1. System Architecture of the Platform

A local MQTT broker is implemented to bridge the communication among simulators, controllers, and physical facilities in a local region. The physical facilities can include various types of EV charging stations (AC, DC, and XFC), solar panels, and energy storage systems. The controllers consist of distribution level energy management system EMS and EVCS. The simulators are used for distribution network simulation and large-scale EV charging simulation. Meanwhile, several user interfaces are designed to facilitate the monitoring and control of the whole system. Any additional information

besides the local region will be published to a global MQTT broker first, and then, subscribed by the local broker. The information may include the EV charging facilities at different physical locations, charging rates that are controlled by other regional EVCS, and utility signals from a transmission controller or utilities. This system architecture enables the ability to change the configuration of the system easily by adding or replacing system components.

5.2 Implementation of Platform Subsystems

5.2.1 MQTT Communication

All messages within the platform are transported via MQTT communication. MQTT is a lightweight Machine-to-Machine (M2M) communication typically used in constrained networks[87]. MQTT utilizes a pub/sub methodology in which each subsystem of the platform's MQTT client has the ability to publish or subscribe to topics on the MQTT broker. Deployment of the MQTT broker in the cloud provides an efficient message bus on the wide area network that enables communication between the subsystems of the platform. The subsystems of the platform are not necessarily physically connected and can be spatially located at different places. For example, the distribution network simulator can subscribe to the load consumption from both real EV charging stations and virtual EV charging simulation topics. The distribution networks simulator will include these EV loads in the simulation and publish the grid performance data to the MQTT broker. Other subsystems within the platform can subscribe to the simulation performance data topic(s) and act upon that data. Figure 5.2 shows a publish/subscribe structure of the local MQTT network. Each subsystem will publish its topics with related messages to the local broker. Any subsystem can subscribe to the topics of multiple

subsystems for further operation. Within MQTT, all simulation or hardware components can self-define for scenarios. It serves the engineer with automatic, remote execution of various simulation and testing scenarios.

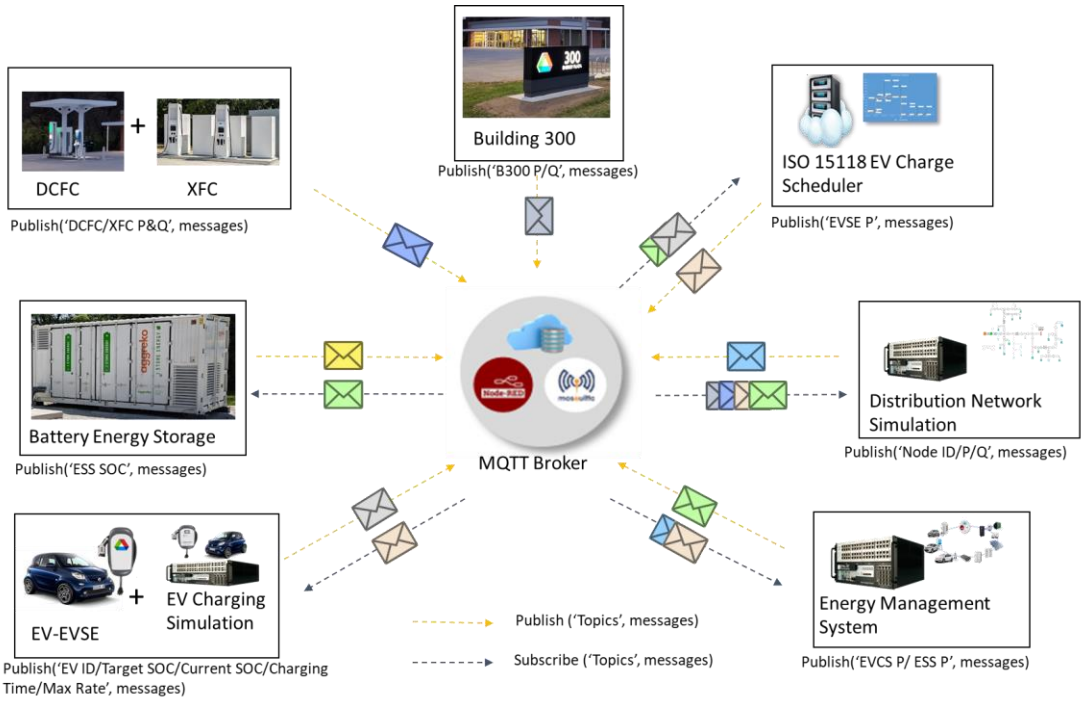

Figure 5.2. Local MQTT Publish/Subscribe Structure

5.2.2 Distribution Network Simulation

For simulation of a distribution network, the OPAL-RT real-time simulator is used to simulate a distribution grid and test the grid influences of a large-scale EV charging process. As shown in Figure 5.3, the distribution network model is developed from a modified IEEE 37 node test feeder [88], which contains commercial and residential areas. Each area has both controllable and uncontrollable loads. The variety of building loads, such as office, restaurant, and house, are modeled as uncontrollable loads. The load profiles of buildings for the DuPage County, Illinois are retrieved from the U.S. Department of Energy's Open Energy Data Initiative database [65]. The controllable

loads are EV charging loads. They are generated by either EV charging simulation or real charging stations and controlled by EVCS via MQTT. The Smart Energy Plaza at Argonne National Laboratory is modeled under one node (775). The ANL Smart Energy Plaza consists of 2 DC fast-charging stations, 2 extreme fast-charging stations, 12 AC level 2 charging stations, solar panels, energy storage systems, and building loads as shown in Figure 5.1. These facilities are equipped with smart meters to obtain energy generation and consumption values. The meter readings are sent to the distribution network simulator via MQTT in real-time.

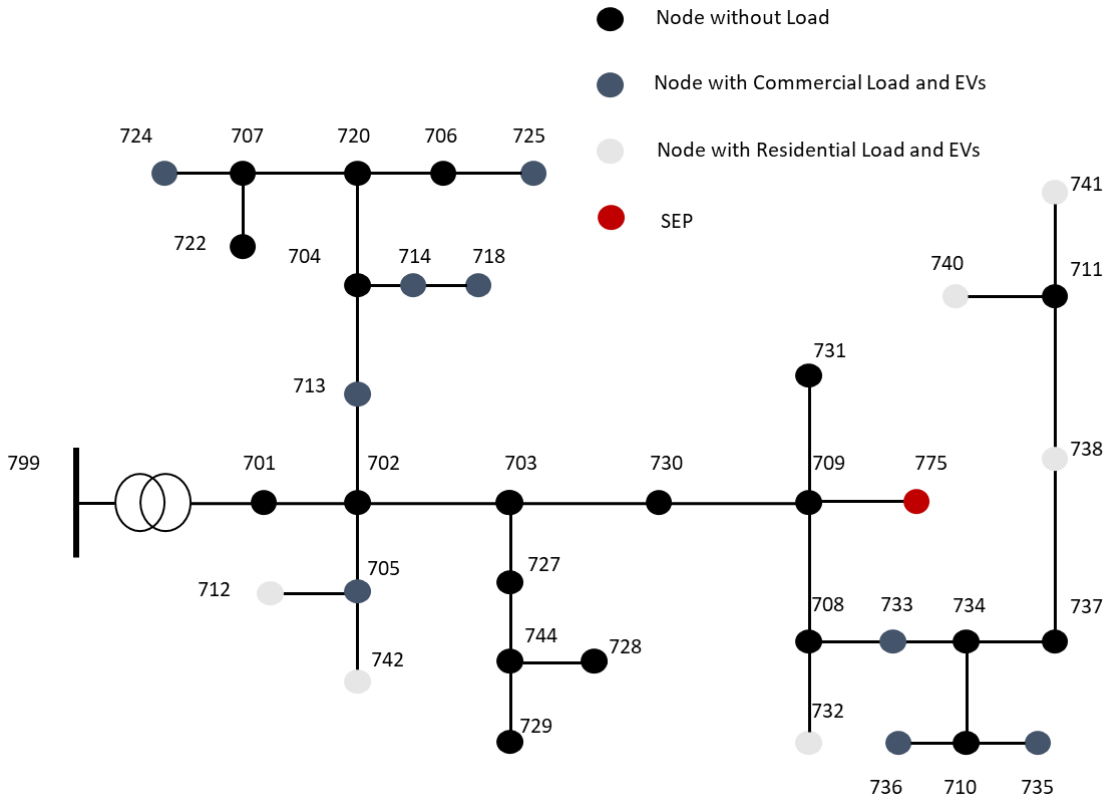

Figure 5.3. Topology of Distribution Network Simulation

The grid model is configured using grid conditions on a timescale of microseconds to provide realistic simulated inputs to either the distribution level EMS or

EVCS. The output signals from the distribution level EMS, EVCS, and the metering readings of real-world facilities are feedback to the power distribution network simulation in real-time.

5.2.3 AC EV Charging Modeling

For AC charging stations, the EV charging process is simulated with a constant-power-constant-voltage charging process.

As shown in Figure 5.4, the EVSE acquires AC power $P_{AC,EV}$ from a grid. The on-board charger converts the AC power to DC with a conversion efficiency of $ef(P_{AC,EV})$, which is a function of AC charging power $P_{AC,EV}$. The on-board charger efficiencies of different EV models are studied in [89].

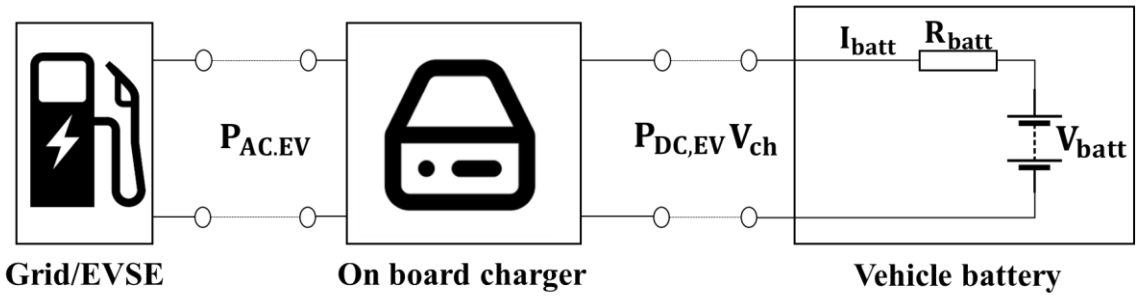

Figure 5.4. EVSE-EV Charging Model

The DC charging power $P_{DC,EV}$ can be updated using equation (5.1)

$$P_{DC,EV} = P_{AC,EV} \cdot ef(P_{AC,EV}) = I_{batt} \cdot V_{ch} \tag{5.1}$$

where I_{batt} is the battery current and V_{ch} is the onboard charger output voltage. The output voltage as a function of SOC can be represented as polynomial equation (5.2) found in [90].

$$V_{ch} = a_1 SOC^n + a_2 SOC^{n-1} + ... + a_n SOC + a_{n+1} \quad (5.2)$$

Where a_1 to a_n are the coefficients. When V_{ch} is smaller than the maximum battery voltage $V_{batt,max}$, EV is charged at a constant power rate.

The battery current can be updated by solving equation (5.3). The EV will be charged at a constant voltage once the charge voltage reaches the maximum battery voltage. The battery current will be updated with equation (5.4).

$$P_{DC,EV} = I_{batt}{}^2 \cdot R_{batt} + I_{batt} \cdot V_{batt}, \text{ if } V_{ch} < V_{batt,\max} \quad (5.3)$$

$$I_{batt} = \frac{V_{batt,\max} - V_{batt}}{R_{batt}}, \text{ if } V_{ch} = V_{batt,\max} \quad (5.4)$$

In this constant-power-constant-voltage charging process, the constant power mode is the major charging period of the entire charging process. In constant power mode, the AC charging power can be controlled by the duty cycle of the control pilot PWM signals. On the contrary, the constant voltage mode only lasts for a brief period and the charging current is uncontrollable in this simulation. The battery SOC can be updated with equation (5.5), where C_{batt} is the EV battery total capacity in ampere-hour unit and Δt is the simulation time interval.

$$SOC_{t_{k+1}} = SOC_{t_k} + \frac{I_{batt} \Delta t}{C_{batt}} \cdot 100 \quad (5.5)$$

5.2.4 DC EV Charging Modeling

For DC fast charging stations, the EV charging process is simulated with a constant-current-constant-voltage charging process.

In the constant-current mode, the station first informs the EV of its available line current, $I_{DCFC,EVSE}$. Then the EV battery management system compares the line current with its own battery current request, $I_{DCFC,EV}$. The battery model shown in Figure 5.4 is also applied in the DC fast charging modeling. The target charging current is identified in (5.6).

$$I_{DCFC} = \min\left(I_{DCFC,EVSE}, I_{DCFC,EV}\right) \tag{5.6}$$

The charger will adjust its charging voltage $V_{DCFC,CH}$ to target the charging current to I_{DCFC}. When the charger voltage reaches the maximum battery open circuit voltage, the DC fast charging enters the constant-voltage mode. The charging current can be resolved as (5.4). Then, the DC charging power can be calculated as:

$$P_{DCFC} = \frac{I_{DCFC} \cdot V_{DCFC,CH}}{ef_{DCFC}} \tag{5.7}$$

where ef_{DCFC} is the charging efficiency of DC fast charging stations.

5.2.5 EV Charging Control

The EV simulation has the function to manage and control the charging rate of EVs within the local node. The controller gathers information from all appliances and provide energy usage guidance for the controllable EV charging stations in real-time. The objective of the control is to distribute the limited power resources to meet all local EVs charging requirement as much as possible. The controller treats each connected EV evenly and minimizes risk of incomplete charging. Different with EVCS, the charging control in EV simulation will be enabled periodically and only control the charging rates for present time based on transient information.

5.2.6 Distribution Level Energy Management System

The distribution level EMS manages EV charging loads within the distribution network to meet charging requirements and get the best grid performance. It is designed to communicate with upper-level transmission controllers and multiple node level EVCS to manage a large-scale EV charging process. With this design, the EMS can provide various grid services with various optimization or control methods. For example, after integrating with a transmission level controller, the EMS can manage the EV charging power of each subarea to provide frequency regulation. As another example, the EMS has the potential to minimize the operating cost if the system is integrated with electric power markets.

5.2.7 EV Charge Scheduler System

The EVCS manages regional EV charging at the grid node level to optimize EV charge scheduling and limit the effects of clustered EV charging on the distribution grid. As shown in Figure 5.5, it uses standardized communication protocols: OCPP 2.0 for charging station networks and ISO 15118 for the communication between EVs and charging stations. EVCS should provide a maximum load profile for the grid node, typically 8 hours with 15-minute intervals. This maximum load profile for instance could be the created to combat historical power peaks at the node. As EVs connect to individual EVSE, a charge schedule is negotiated between the EV and the EVCS via ISO 15118 and OCPP 2.0 through the EVSE. The goal of charge scheduling is to not exceed the constraints of the grid while meeting the EVs energy requirements by their departure time. The EV or EVCS should be able to trigger a charge schedule renegotiation.

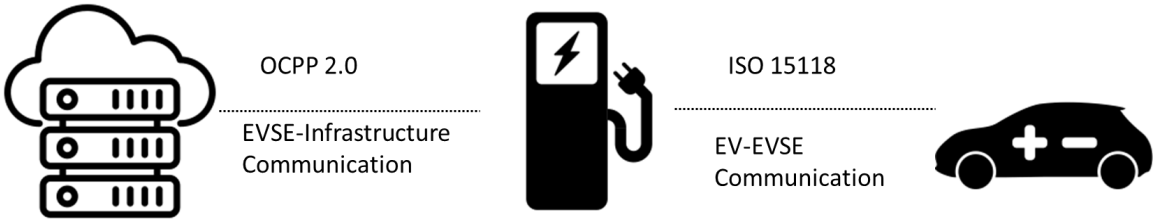

Figure 5.5. Standardized Communication Protocols in EV Charge Scheduler System

A web dashboard of EVCS as shown in Figure 5.6. The dashboard allows the operator to see the available power over a given interval and each EVs negotiated charge schedule. If the total EV charging power for a given interval exceeds the node's available power, the charge scheduler will initiate a renegotiation with the most flexible EVs to achieve its objective function. Furthermore, the system is capable to integrate with multiple functions, such as EV charging reservation and EV charging load forecasting. With EV load forecasting and various control algorithms, the EVCS can schedule and control regional EV charging process precisely and intelligently ensuring that the EV driver's energy requirements are met by their departure time and distribution grid's constraints are not exceeded.

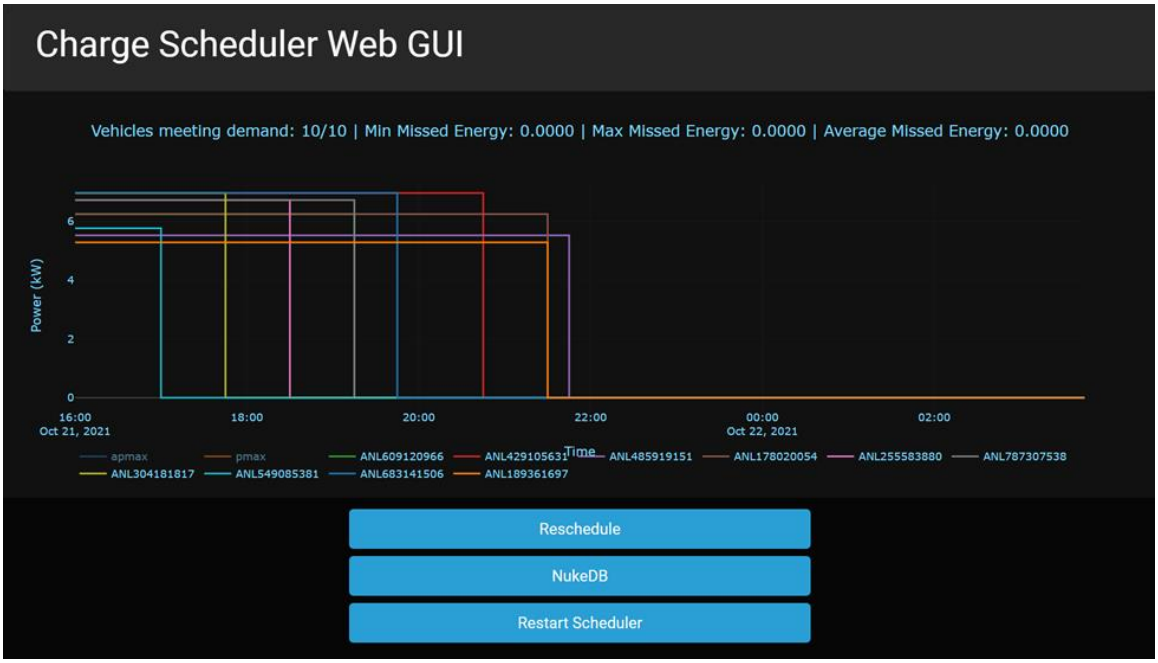

Figure 5.6. An Example of EVCS Dashboard

5.3 Use Case of HIL Platform

5.3.1 HIL Simulation Setup

This section presents a use case of the presented cloud-based HIL simulation and testing platform for frequency regulation. More than 90 buildings, including different types of commercial and residential building loads, are modeled at 15 nodes in the modified IEEE 37 nodes test feeder model. A total of 460 EVs are distributed in the grid. These EVs include 2012 Nissan Leaf, 2015 Nissan Leaf, 2014 BMW i3, and 2012 Chevrolet Volt models. The detailed building loads and EV distribution are listed in Table 5.1.

Table 5.1. List of Building Units and Charging Facilities

Node Number	Building Type	Number of EV Charging Stations	
		AC	DC
Commercial Area			
705	Offices	17	1
713	Super Market	34	
714	Strip Mall & Retail Store	35	1
718	Restaurants & Retail Store & Strip Mall	31	1
724	Warehouses	30	
725	Restaurants & Retail Stores	30	
733	Hotels	35	
735	Restaurants	18	2
736	Offices	30	
775	SEP	12	2
Residential Area			
712	Apartments & Houses	32	
732	Apartments	36	
738	House	29	1
740	Apartments & Houses	18	
741	Apartments	35	
742	Hotel & Apartments	30	
Total		**460**	

Figure 5.7 shows the HIL configuration of the frequency regulation use case. OPAL-RT performs real-time distribution network simulation, EV charging simulation, and distribution level energy management in real-time. The real-world SEP facilities are connected to node 775 as a microgrid of this distribution network. The rest of the EV charging process are generated by EV charging simulation. An EVCS is used to schedule and control the EV charging power for node 705. Other EVs are scheduled and controlled with the same method in OPAL-RT directly. The OPAL-RT receives the real-time SEP smart meter data, frequency, and EV charging load through the MQTT broker. Meanwhile, it performs all simulations and publishes EV charging requirements, grid conditions, and node consumption for the control of EVCS.

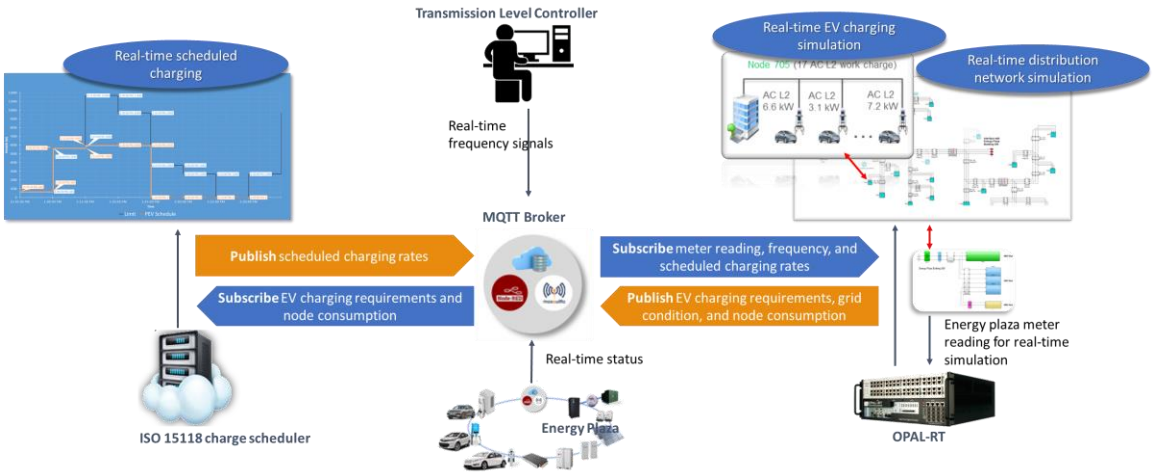

Figure 5.7. Configuration of the Frequency Regulation Use Case

5.3.2 Distribution Level EMS Algorithm

The distribution level EMS plays a role as an upper-level controller to manage EV charge loads with the consideration of grid constraints. In this use case, it manages the energy consumption of each grid node to optimize the distribution grid performance

under the substation limitation. Meanwhile, it will provide load-based frequency regulation to respond to the requests from a transmission level controller.

To respond to the transmission level controller, the distribution level EMS will publish the node consumption and subscribe frequency signal via MQTT. While the frequency deviation is detected, the EMS will shape the load profile of the controllable loads to provide frequency regulation. As shown in Figure 5.8, the load-based frequency controller sets the power modulation ΔP once a deviation of frequency is detected. ΔP follows the droop characteristic. α is the assumed dead-band to avoid the small frequency variations caused by temporary load unbalances. As discussed in [91], this dead-band may vary from 0.02% to 0.09% of the nominal frequency. In this system, the α is selected as 0.05 Hz for a 60 Hz system. In order to reduce frequency deviation, the controller will set a new power limit P^* for the distribution network as the sum of current load power P plus power modulation ΔP.

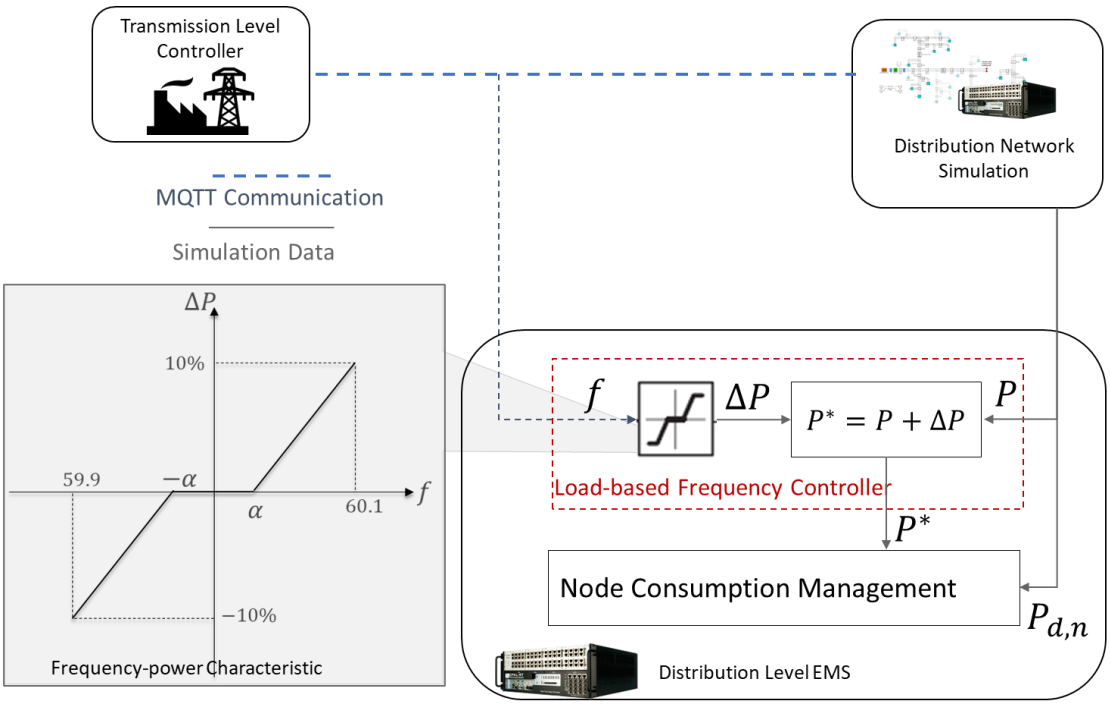

Figure 5.8. Load-based Frequency Control Scheme

The distribution level EMS also manages the power consumption of each node to govern the grid performance. It provides power capacity to each node or EVCS periodically based on the aggregated power demand from each node and power limitation set by either substation or load-based frequency controller. In this use case, the EMS dispatches power to individual nodes and aims to minimize the cost function defined in (5.8), where P_n is the amount of power allocated for node n; $P_{d,n}$ is the node n power demand; pr_n is the average charging priority of node n.

$$\min \quad \sum_{n=1}^{N} pr_n \left(P_n - P_{d,n}\right)^2 \tag{5.8}$$

$$\text{over} \quad P_n, \forall n \in \mathbf{N}$$

$$\text{s.t.} \quad \sum_{n=1}^{N} P_n = P^* \tag{5.9}$$

$$P_n \geq P_{fix,n}, \quad P^* \leq P_{cap} \tag{5.10}$$

Constraint (5.9) indicates that the total power consumption should follow the network power capacity defined by the frequency regulation service. In constraint (5.10), $P_{fix,n}$ are the uncontrollable loads at node n and P_{cap} denotes the substation power limit. Only the controllable loads will be curtailed, and the total amount of power must not exceed substation power limit. The charging priority of each EV is calculated by (5.11). The value of pr_n is the average of charging priorities for all the EVs in the node n.

5.3.3 Control Algorithm of EV Charge Scheduler System

In this use case, the EVCS was applied to control the EV charging processes at node 705. The control algorithm of EVCS limits the EV charging capacity to satisfy a power limit. It can also prioritize each EV's charge rate to optimize its charge schedule to meet the energy requirement by the end of its charging duration as much as possible.

The control algorithm is based on the concept of a charging priority of each charging EV. The charging priority of each charging EV is defined below,

$$pr_i = \frac{1}{\min\left(\frac{\left(SOC_{Tar,i} - SOC_{t,i}\right)\cdot \mathrm{C_{batt}}}{\left(T_{Dep,i} - t\right)\cdot P_{\max,i}}, 1\right)} \tag{5.11}$$

where $SOC_{Tar,i}$ is the target SOC of the ith EV. $T_{Dep,i} - t$ is the remaining time before departure. $SOC_{t,i}$ represents the current SOC. $P_{max,i}$ is the maximum power draw of the ith EV. The EV which has the highest over allocation of energy and the longest departure time would have the highest priority to be rescheduled. Equation (5.11) also ensures that the EV which needs to charge at maximum charging rate will have the least priority to be rescheduled. The priority of each EV is normalized utilizing equations (5.12).

$$pr_{norm,i} = \frac{pr_i}{\sum_{i=1}^{I} pr_i} \tag{5.12}$$

At every control period, the control algorithm determines if the EV load could be decreased to satisfy the node power limit as shown in (5.13).

$$\Delta P_n = P_n - P_{fix,n} - \sum_{i=1}^{I} P_{AC,EV,i} \tag{5.13}$$

This algorithm checks if the total available power is not enough for all the EVs to meet their needs and proportionally reduces decreases the needs of all the EVs. The change in EV load ΔP_n is spread across the charging EVs utilizing equation (5.14).

$$P_{AC,EV,i} = P_{max,i} - pr_{norm,i} \cdot \Delta P_n \tag{5.14}$$

The priority-based charging control scheme is shown in Figure 5.9. The optimal charge schedule is the solution of a version of the bin-packing problem in which there are timeslots as containers with their size being the total available energy during that period. At each control interval, the controller will subscribe the charging requirements of connected EVs and the amount of power for them. Then, it will consider the priority and create individual power plans for each EV based on their energy consumption during each timeslot.

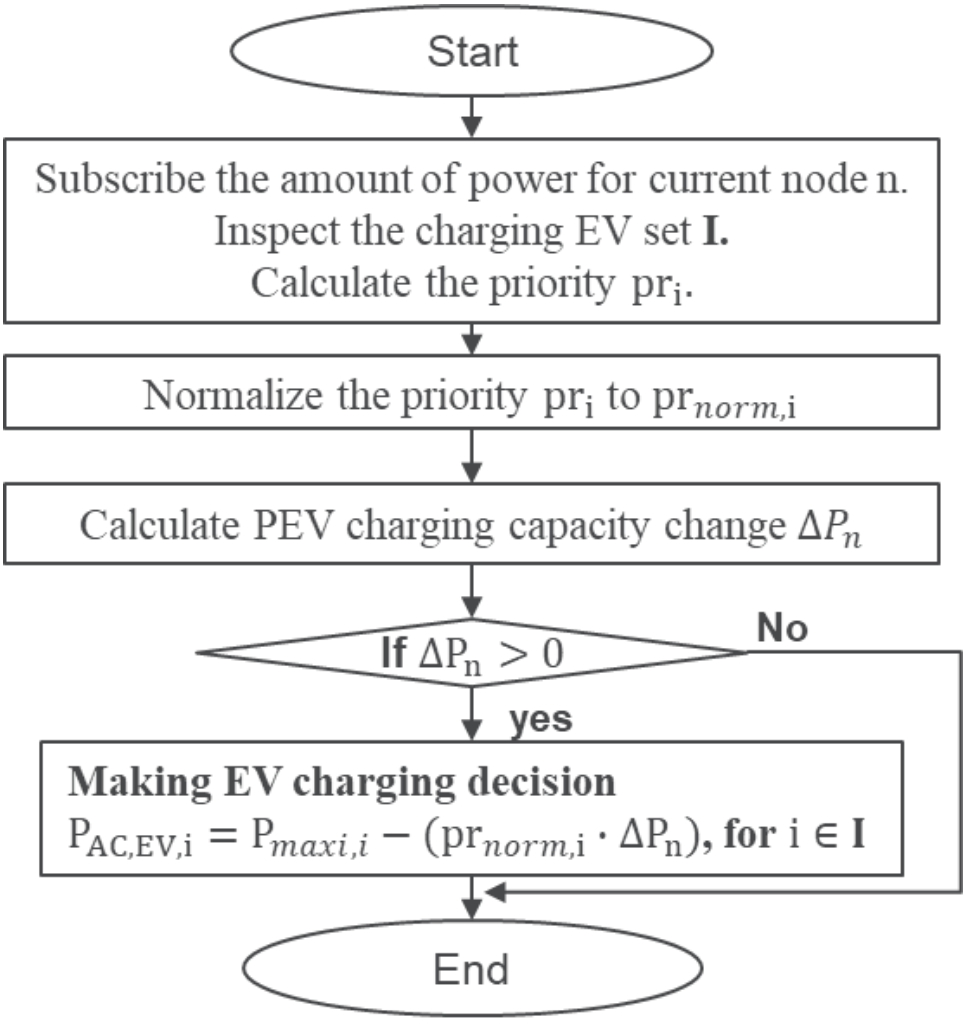

Figure 5.9. Priority-based EV Charging Control Scheme

5.3.4 Simulation and Testing Results

24 hours simulation is performed through multiple subsystems with various timesteps. The distribution network simulation is run in 200 μs to achieve real-time grid analysis; the EV charging characteristic is updated every 5 seconds; the EMS and EVCS are trigged every 1 minute. Figure 5.10 shows the overall load profile of the distribution network. The substation capacity of the distribution network is set to 3 MW. If the EMS and EVCS are disabled, all EVs will be charged with maximum power rate once they are connected. The charging durations are relatively short, but these will cause overloading

during peak time and may cause damages. Once the EMS and EVCS are enabled, the overall load is shifted smoothly and limited under the distribution network capacity.

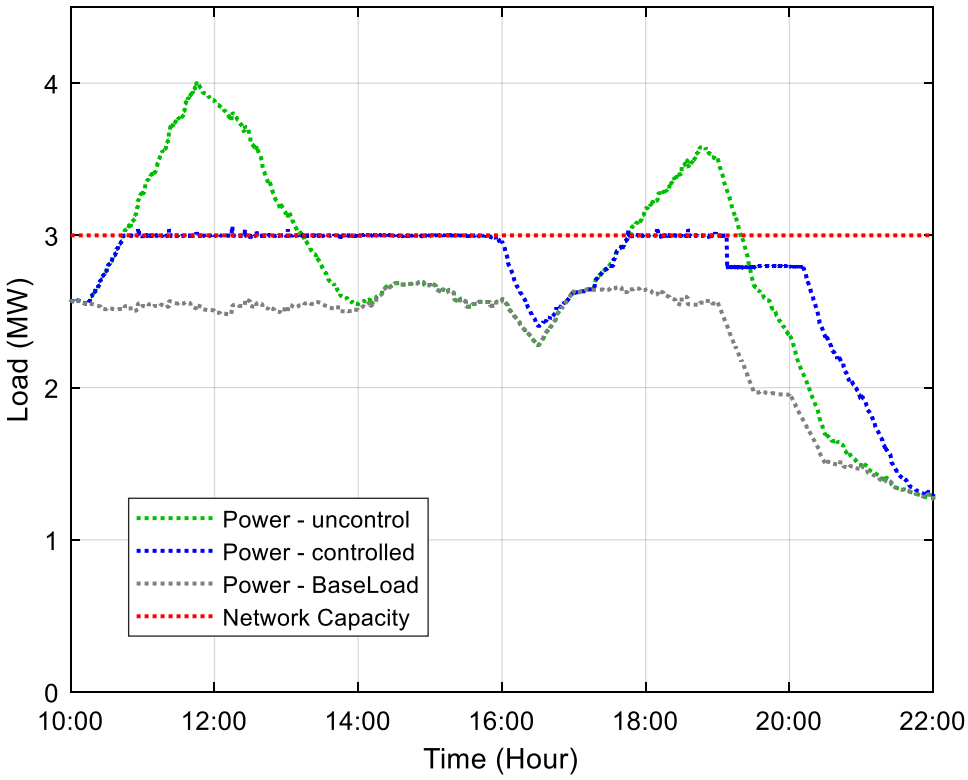

Figure 5.10. Load Profile of the Distribution Network

Figure 5.11 shows the frequency response from a transmission simulation for a certain period. The transmission model is developed from a modified IEEE 39 bus system with 6 generators. The simulation is performed by Idaho National Laboratory and co-simulated through the cloud-based platform. The distribution network simulation by Argonne National Laboratory is connected as one bus on the high voltage transmission line. The results in the uncontrolled scenario show a frequency violation occurs when the distribution network has a heavy EV charging load. The frequency drops below 59.95 Hz as defined in the dead-band due to the heavy EV charging load. In the controlled scenario,

the distribution network capacity is defined at the substation limitation which is 3 MW initially. The EV charging loads are shifted smoothly and the frequency is saturated above the dead-band. At around 19:10, the frequency drops below the defined dead-band in EMS because of the increasing load in the transmission system. Therefore, the load-based frequency control is enabled to further curtail the network capacity from 3 MW to around 2.8 MW. The frequency is covered back the pre-defined dead-band.

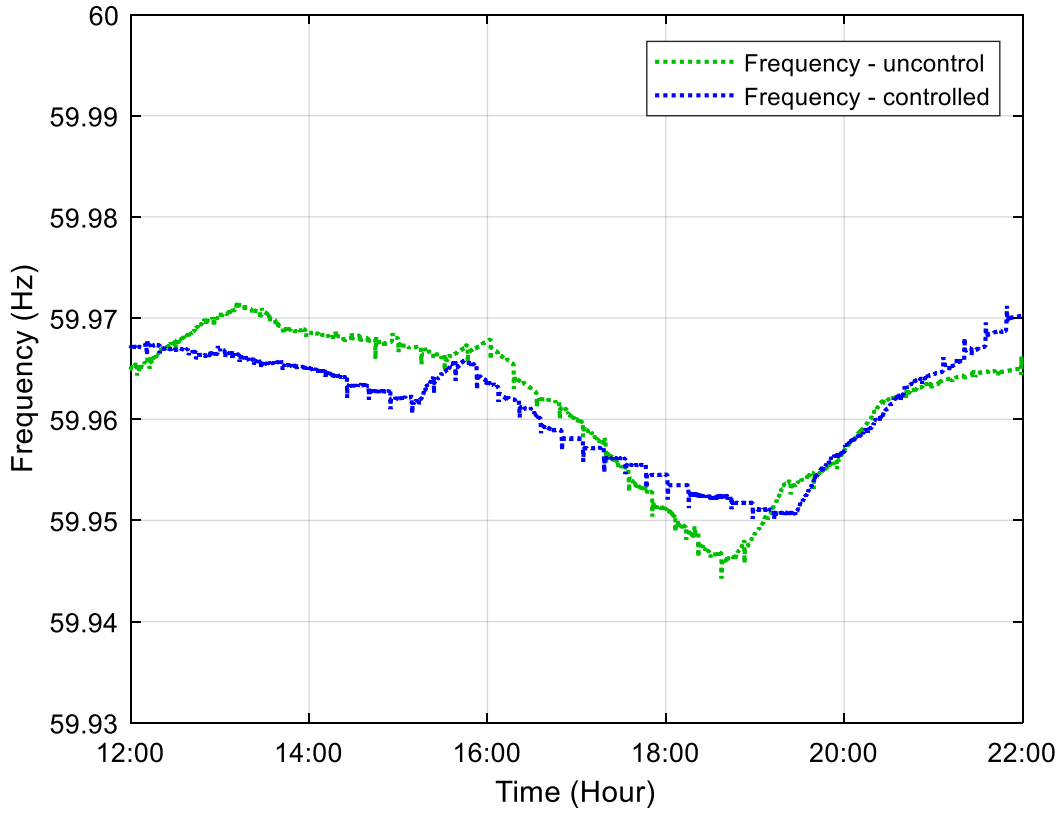

Figure 5.11. Frequency Response from Transmission Simulation

Figure 5.12 shows the EV charging load at Node 705. The charging process of 17 EVs are generated by the EV charging simulation and are controlled by an EVCS. The EVCS adapts to the charging capacity and is enabled at around 11:30. It efficiently

control and re-schedule the charging rates under the charging capacity. Figure 5.13 shows the final SOCs and EV charging SOC requirements. With the proposed control method in EVCS, the final SOC of 17 EVs are close to the target SOC. It can reduce and reschedule the charging rates with minimal impact on EV charging requirements.

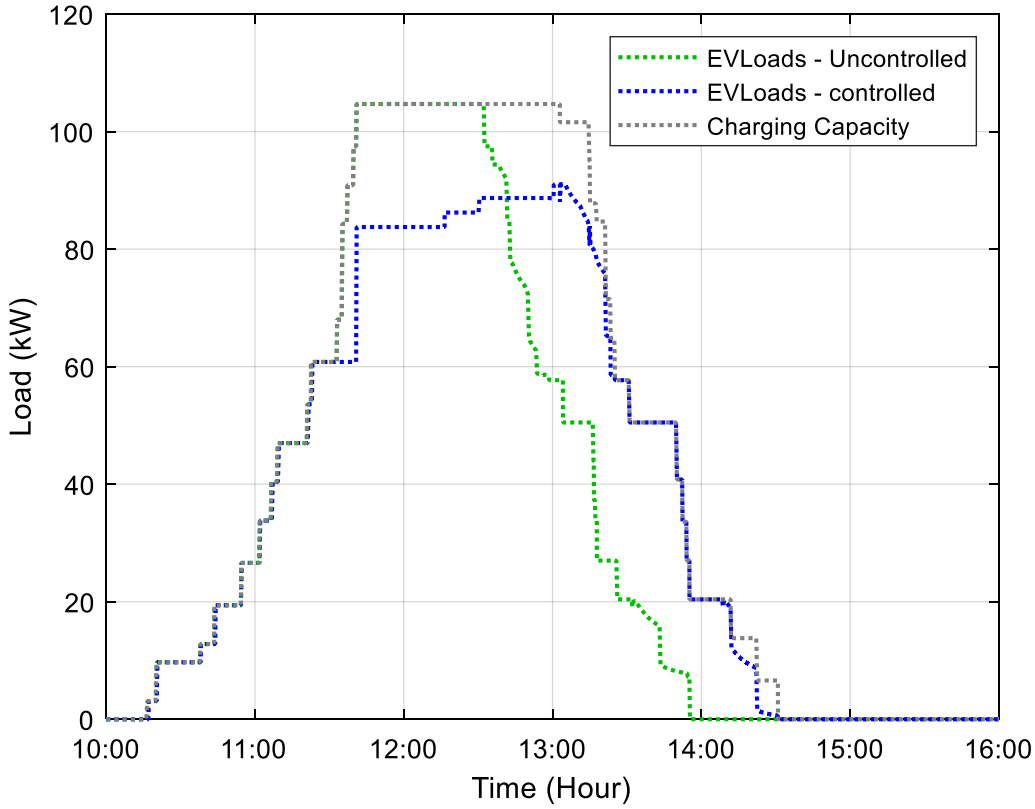

Figure 5.12. EV Charging Load at Node 705

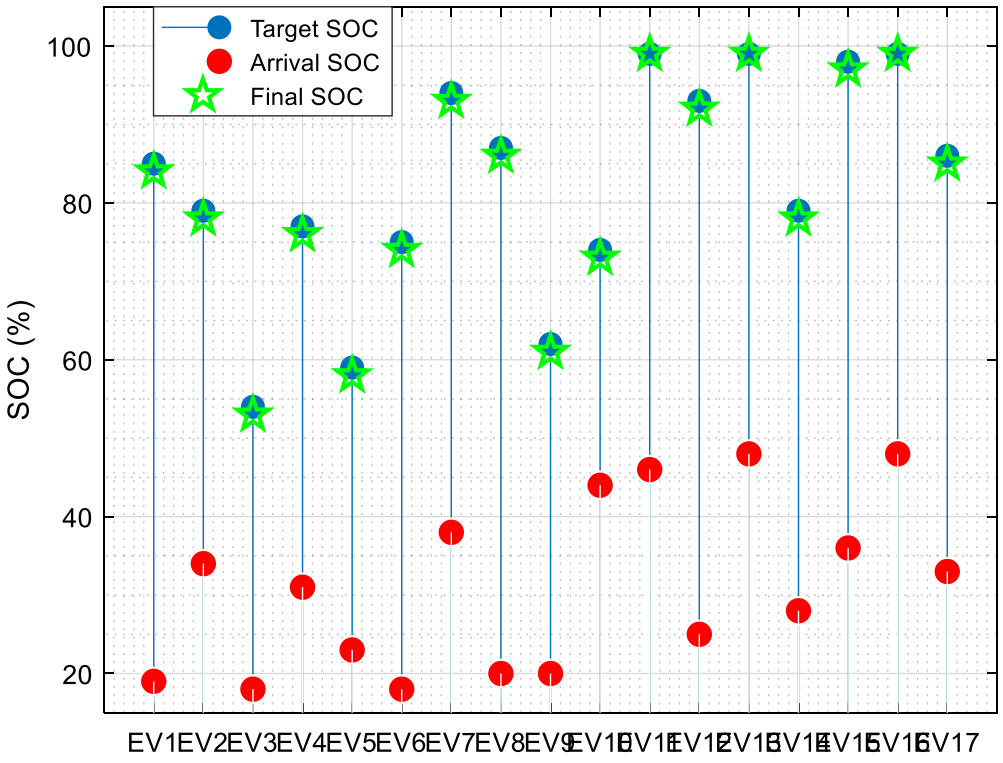

Figure 5.13. Charging Results at Node 705

5.4 Chapter Conclusion

In this chapter, a cloud-based HIL simulation and testing framework is introduced for the development and testing of large-scale EV charging management. MQTT communication provides a cloud-based platform to integrate multi-systems, which include a real-time power system simulator, EVCS, real-world EV charging facilities, and a transmission-level controller. To save the cost for testing EV charging at scale, EV charging is also simulated based on the charging characteristics of real-world charging stations, which can significantly increase the number of charging EVs in a distribution network for the analysis and control of large-scale EV charging. A distribution-level EMS works as a center governor to ensure grid performance and respond to transmission-

level controllers. EVCS is designed for regional EV charging control. It uses OCPP 2.0 and ISO 15118 standard communication protocols. The modular open systems design approach of the platform allows the integration of EV charging control algorithms and hardware charging systems for performance evaluation and interoperability testing. The experimental test results show that the communication links of the platform work properly, the EMS can respond to transmission level grid service requests with minimal impact on local operations. The EVCS can optimize the charging rates for all connected EVs without violating their departure times and energy requirements.

For future work, the testing of XFC stations with stational battery energy storage systems will be explored with this platform. The large-scale EV charging energy management and charging control will be applied with different algorithms to address various benefits for the distribution grid in a more precise and intelligent manner.

6 Conclusion and Future Work

6.1 Conclusions

This dissertation presents a series research of electric vehicle smart charging and energy management for VGI system. A centralized TE-based EV charging control has been developed for VGI system. Optimal charging decisions considering the bidding preferences, charging cost minimization and power limitation are obtained with quadratic programming optimization methods across multiple stages.

To further investigate the modern VGI problem with transactive energy control, the distributed EV charging scheduling has been studied for large-scale EV charging and energy management at various levels, including individual EVs, distribution nodes, and distribution networks. An innovated clearing price mechanism is developed by a negotiation method among the distribution system operator and the EV aggregators. EVAs and EVs can make their charging scheduling autonomously with the clearing price signals. The system reliability, effectiveness, and security were improved significantly.

Then, a novel MC simulation tool has been developed to estimate the EV charging demand at XFC stations based on the distributions obtained from the vehicle travel survey dataset. The estimation algorithm considers various aspects, including EV scale, EV model and the percentage in the total simulated EVs, EV charging curves for different EV models, XFC station port availability, and waiting time. An optimal configuration method for multiple XFC stations at the distribution network level is presented to determine the optimal ESS energy capacity, ESS rated power, and the PV size integrated with XFC stations. The investment and operation costs of XFC stations

are reduced while meeting the charging demand and the operational constraints of the distribution network, XFC, ESS, and PV panels.

Afterwards, a cloud-based simulation and testing platform for the development and Hardware-in-the-Loop (HIL) testing of VGI technologies is presented. The HIL system consists of multiple subsystems: a real-time power system simulator (OPAL-RT), ISO 15118 EV Charge Scheduler System (EVCSS), and a Smart Energy Plaza (SEP) with various types of charging stations, solar panels, and energy storage systems. The modular open systems design approach of the platform allows the integration of EV charging control algorithms and hardware charging systems for performance evaluation and interoperability testing, including the impact of EV charging on the grid, optimal EV charging control at scale, and communication interoperability.

6.2 Future work

This dissertation has explored multiple control methods to effectively integrate the large-scale EVs in the distribution power systems with or without considering the transactive energy control. However, there are still a few details need to be explored in the future. The recommended future work is summarized as below:

- Different types of EV charging characteristics should be explored in charging system's stability analysis. The EV charging curves are highly dependent on the size, lifetime, and electrochemical properties of different types of batteries.
- The combination of different charging levels with transactive energy should be designed for effective smart EV charging control and energy management.

- This dissertation only considers fixed building loads. The market-based co-scheduling of HVAC system and large-scale EV charging control can be further explored for a diversified VGI system.
- More vehicle-to-grid service should be studied, such as voltage regulation and frequency support. The EVs selling the electricity to the distribution power grid with discharging process should be further explored.
- EV charging navigation should be considered in modern VGI systems. This dissertation focuses on energy management when EVs are plugged-in for charging. Proper scheduling EV charging ahead not only reduces grid impact, but also provides opportunities to use EVs for grid services.
- Artificial intelligence can also be applied for VGI control. Once more and more EV charging data are available in the future, artificial intelligence has the advantage of estimating EV charging behavior because fewer initial assumptions are needed.
- The cyber security should be considered in VGI communication systems.

7 Reference List

[1] "COP26 declaration on accelerating the transition to 100% zero emission cars and vans," GOV.UK, 2021.

[2] A. Bui, P. Slowik, and N. Lutsey, "Power play: Evaluating the U.S. position in the global electric vehicle transition," International Council on Clean Transportation. 2021. [Online]. Available: https://theicct.org/publication/power-play-evaluating-the-u-s-position-in-the-global-electric-vehicle-transition/

[3] M. A. Awadallah, B. N. Singh, and B. Venkatesh, "Impact of EV Charger Load on Distribution Network Capacity: A Case Study in Toronto," *Canadian Journal of Electrical and Computer Engineering*, vol. 39, no. 4, pp. 268-273, 2016, doi: 10.1109/CJECE.2016.2545925.

[4] J. Y. Yong, V. K. Ramachandaramurthy, K. M. Tan, and N. Mithulananthan, "A review on the state-of-the-art technologies of electric vehicle, its impacts and prospects," *Renewable and Sustainable Energy Reviews*, vol. 49, pp. 365-385, 2015, doi: 10.1016/j.rser.2015.04.130.

[5] A. Rautiainen *et al.*, "Case studies on impacts of plug-in vehicle charging load on the planning of urban electricity distribution networks," in *2013 Eighth International Conference and Exhibition on Ecological Vehicles and Renewable Energies (EVER)*, pp. 1-7, 2013, doi: 10.1109/EVER.2013.6521542.

[6] L. P. Fernández, T. G. S. Roman, R. Cossent, C. M. Domingo, and P. Frías, "Assessment of the Impact of Plug-in Electric Vehicles on Distribution Networks," *IEEE Transactions on Power Systems*, vol. 26, no. 1, pp. 206-213, 2011, doi: 10.1109/TPWRS.2010.2049133.

[7] H. S. Das, M. M. Rahman, S. Li, and C. W. Tan, "Electric vehicles standards, charging infrastructure, and impact on grid integration: A technological review," *Renewable and Sustainable Energy Reviews*, vol. 120, p. 109618, 2020, doi: 10.1016/j.rser.2019.109618.

[8] "Electric Vehicle Charger Selection Guide," California Energy Commission, 2018.

[9] "Enabling Fast Charging: A Technology Gap Assessment," U.S. Department of Energy, 2017.

[10] T. G. A. Council, "GridWise Transactive Energy Framework Version 1.0," Pacific Northwest National Laboratory, PNNL-22946 Ver1.0, 2015.

[11] M. T. Hussain, D. N. B. Sulaiman, M. S. Hussain, and M. Jabir, "Optimal Management strategies to solve issues of grid having Electric Vehicles (EV): A review," *Journal of Energy Storage*, vol. 33, p. 102114, 2021, doi: 10.1016/j.est.2020.102114.

[12] C. Cao, M. Cheng, and B. Chen, "Optimal Scheduling of PEV Charging/Discharging in Microgrids with Combined Objectives," *Smart Grid and Renewable Energy*, vol. 07, pp. 115-130, 2016, doi: 10.4236/sgre.2016.74008.

[13] N. Jabalameli, X. Su, and A. Ghosh, "Online Centralized Charging Coordination of PEVs With Decentralized Var Discharging for Mitigation of Voltage Unbalance," *IEEE Power and Energy Technology Systems Journal*, vol. 6, no. 3, pp. 152-161, 2019, doi: 10.1109/JPETS.2019.2931396.

[14] M. G. Vayá and G. Andersson, "Centralized and decentralized approaches to smart charging of plug-in Vehicles," in *2012 IEEE Power and Energy Society General Meeting*, 22-26 July 2012 2012, pp. 1-8, doi: 10.1109/PESGM.2012.6344902.

[15] J. Pahasa and I. Ngamroo, "Coordinated PHEV, PV, and ESS for Microgrid Frequency Regulation Using Centralized Model Predictive Control Considering Variation of PHEV Number," *IEEE Access*, vol. 6, pp. 69151-69161, 2018, doi: 10.1109/ACCESS.2018.2879982.

[16] C. Cao and B. Chen, "Generalized Nash equilibrium problem based electric vehicle charging management in distribution networks," *International Journal of Energy Research*, vol. 42, no. 15, pp. 4584-4596, 2018, doi: 10.1002/er.4194.

[17] C. Cao, Z. Wu, and B. Chen, "Electric Vehicle–Grid Integration with Voltage Regulation in Radial Distribution Networks," *Energies*, vol. 13, no. 7, p. 1802, 2020, doi: 10.3390/en13071802.

[18] Y. Zheng, Y. Song, D. J. Hill, and K. Meng, "Online Distributed MPC-Based Optimal Scheduling for EV Charging Stations in Distribution Systems," *IEEE Transactions on Industrial Informatics*, vol. 15, no. 2, pp. 638-649, 2019, doi: 10.1109/TII.2018.2812755.

[19] L. Wang and B. Chen, "Distributed control for large-scale plug-in electric vehicle charging with a consensus algorithm," *International Journal of Electrical Power & Energy Systems*, vol. 109, pp. 369-383, 2019, doi: 10.1016/j.ijepes.2019.02.020.

[20] L. Wang and B. Chen, "Dual-level consensus-based frequency regulation using vehicle-to-grid service," *Electric Power Systems Research*, vol. 167, pp. 261-276, 2019, doi: 10.1016/j.epsr.2018.10.022.

[21] I. Grau Unda, P. Papadopoulos, S. Skarvelis-Kazakos, L. M. Cipcigan, N. Jenkins, and E. Zabala, "Management of electric vehicle battery charging in distribution networks with multi-agent systems," *Electric Power Systems Research*, vol. 110, pp. 172-179, 2014, doi: 10.1016/j.epsr.2014.01.014.

[22] M. G. Vayá and G. Andersson, "Plug-in Electric Vehicle charging approaches: Centralized versus decentralized and strategic versus cooperative," in *2015 IEEE Eindhoven PowerTech*, 2015, pp. 1-6, doi: 10.1109/PTC.2015.7232260.

[23] R. Fachrizal and J. Munkhammar, "Improved Photovoltaic Self-Consumption in Residential Buildings with Distributed and Centralized Smart Charging of Electric Vehicles," *Energies*, vol. 13, no. 5, p. 1153, 2020, doi: 10.3390/en13051153.

[24] A. J. Cheng, B. Tarroja, B. Shaffer, and S. Samuelsen, "Comparing the emissions benefits of centralized vs. decentralized electric vehicle smart charging approaches: A case study of the year 2030 California electric grid," *Journal of Power Sources*, vol. 401, pp. 175-185, 2018, doi: 10.1016/j.jpowsour.2018.08.092.

[25] M. Moeini-Aghtaie, A. Abbaspour, M. Fotuhi-Firuzabad, and P. Dehghanian, "PHEVs centralized/decentralized charging control mechanisms: Requirements and impacts," in *2013 North American Power Symposium (NAPS)*, 2013, pp. 1-6, doi: 10.1109/NAPS.2013.6666904.

[26] J. d. Hoog *et al.*, "Electric vehicle charging and grid constraints: Comparing distributed and centralized approaches," in *2013 IEEE Power & Energy Society General Meeting*, 2013, pp. 1-5, doi: 10.1109/PESMG.2013.6672222.

[27] S. Xu, Z. Yan, D. Feng, and X. Zhao, "Decentralized charging control strategy of the electric vehicle aggregator based on augmented Lagrangian method," *International Journal of Electrical Power & Energy Systems*, vol. 104, pp. 673-679, 2019, doi: 10.1016/j.ijepes.2018.07.024.

[28] H. Tu, H. Feng, S. Srdic, and S. Lukic, "Extreme Fast Charging of Electric Vehicles: A Technology Overview," *IEEE Transactions on Transportation Electrification*, vol. 5, no. 4, pp. 861-878, 2019, doi: 10.1109/TTE.2019.2958709.

[29] G. Sharma, V. K. Sood, M. S. Alam, and S. M. Shariff, "Comparison of common DC and AC bus architectures for EV fast charging stations and impact on power quality," *eTransportation*, vol. 5, p. 100066, 2020, doi: 10.1016/j.etran.2020.100066.

[30] N. Elsayad and O. A. Mohammed, "A cascaded high frequency AC link system for large-scale PV-assisted EV fast charging stations," in *2017 IEEE Transportation Electrification Conference and Expo (ITEC)*, 2017, pp. 90-94, doi: 10.1109/ITEC.2017.7993252.

[31] M. Gjelaj, C. Træholt, S. Hashemi, and P. B. Andersen, "Optimal design of DC fast-charging stations for EVs in low voltage grids," in *2017 IEEE Transportation Electrification Conference and Expo (ITEC)*, 2017, pp. 684-689, doi: 10.1109/ITEC.2017.7993352.

[32] D. Sbordone, I. Bertini, B. Di Pietra, M. C. Falvo, A. Genovese, and L. Martirano, "EV fast charging stations and energy storage technologies: A real implementation in the smart micro grid paradigm," *Electric Power Systems Research*, vol. 120, pp. 96-108, 2015, doi: 10.1016/j.epsr.2014.07.033.

[33] M. O. Badawy and Y. Sozer, "Power Flow Management of a Grid Tied PV-Battery System for Electric Vehicles Charging," *IEEE Transactions on Industry Applications*, vol. 53, no. 2, pp. 1347-1357, 2017, doi: 10.1109/TIA.2016.2633526.

[34] P. García-Triviño, L. M. Fernández-Ramírez, J. P. Torreglosa, and F. Jurado, "Control of electric vehicles fast charging station supplied by PV/energy storage system/grid," in *2016 IEEE International Energy Conference (ENERGYCON)*, 2016, pp. 1-6, doi: 10.1109/ENERGYCON.2016.7514120.

[35] S. Wang, L. Lu, X. Han, M. Ouyang, and X. Feng, "Virtual-battery based droop control and energy storage system size optimization of a DC microgrid for electric vehicle fast charging station," *Applied Energy*, vol. 259, p. 114146, 2020, doi: 10.1016/j.apenergy.2019.114146.

[36] O. Elma, "A dynamic charging strategy with hybrid fast charging station for electric vehicles," *Energy*, vol. 202, p. 117680, 2020, doi: 10.1016/j.energy.2020.117680.

[37] G. Liu, Y. Xue, M. S. Chinthavali, and K. Tomsovic, "Optimal Sizing of PV and Energy Storage in an Electric Vehicle Extreme Fast Charging Station," in *2020 IEEE Power & Energy Society Innovative Smart Grid Technologies Conference (ISGT)*, 2020, pp. 1-5, doi: 10.1109/ISGT45199.2020.9087792.

[38] O. Erdinç, A. Taşcıkaraoğlu, N. G. Paterakis, D. İ, M. C. Sinim, and J. P. S. Catalão, "Comprehensive Optimization Model for Sizing and Siting of DG Units, EV Charging Stations, and Energy Storage Systems," *IEEE Transactions on Smart Grid*, vol. 9, no. 4, pp. 3871-3882, 2018, doi: 10.1109/TSG.2017.2777738.

[39] L. Yang and H. Ribberink, "Investigation of the potential to improve DC fast charging station economics by integrating photovoltaic power generation and/or local battery energy storage system," *Energy*, vol. 167, pp. 246-259, 2019, doi: 10.1016/j.energy.2018.10.147.

[40] M. Muratori *et al.*, "Technology solutions to mitigate electricity cost for electric vehicle DC fast charging," *Applied Energy*, vol. 242, pp. 415-423, 2019, doi: 10.1016/j.apenergy.2019.03.061.

[41] R. J. Bessa, M. A. Matos, F. J. Soares, and J. A. P. Lopes, "Optimized Bidding of a EV Aggregation Agent in the Electricity Market," *IEEE Transactions on Smart Grid*, vol. 3, no. 1, pp. 443-452, 2012, doi: 10.1109/TSG.2011.2159632.

[42] E. Sortomme and M. A. El-Sharkawi, "Optimal Combined Bidding of Vehicle-to-Grid Ancillary Services," *IEEE Transactions on Smart Grid*, vol. 3, no. 1, pp. 70-79, 2012, doi: 10.1109/TSG.2011.2170099.

[43] S. Han, D. Lee, and J. B. Park, "Optimal Bidding and Operation Strategies for EV Aggegators by Regrouping Aggregated EV Batteries," *IEEE Transactions on Smart Grid*, vol. 11, no. 6, pp. 4928-4937, 2020, doi: 10.1109/TSG.2020.2999887.

[44] W. Zhang, K. Zeng, M. Xu, L. Le, J. Fang, and X. Ai, "Multi-time Scale Optimal Bidding Strategy for an EV Aggregator in Energy and Regulation Markets," in *2020 IEEE 18th International Conference on Industrial Informatics (INDIN)*, 2020, vol. 1, pp. 627-632, doi: 10.1109/INDIN45582.2020.9442102.

[45] Z. Jiang, Q. Ai, R. Hao, M. Yousif, and Y. Zhang, "Joint Optimization for Bidding and Pricing of Electric Vehicle Aggregators Considering Reserve Provision and EV Response," in *2019 IEEE Power & Energy Society General Meeting (PESGM)*, 2019, pp. 1-5, doi: 10.1109/PESGM40551.2019.8973464.

[46] L. Hou, C. Wang, and J. Yan, "Bidding for Preferred Timing: An Auction Design for Electric Vehicle Charging Station Scheduling," *IEEE Transactions on Intelligent Transportation Systems*, vol. 21, no. 8, pp. 3332-3343, 2020, doi: 10.1109/TITS.2019.2926336.

[47] S. Zou, Z. Ma, X. Liu, and I. Hiskens, "An Efficient Game for Coordinating Electric Vehicle Charging," *IEEE Transactions on Automatic Control*, vol. 62, no. 5, pp. 2374-2389, 2017, doi: 10.1109/TAC.2016.2614106.

[48] H. Kikusato *et al.*, "Electric Vehicle Charging Management Using Auction Mechanism for Reducing PV Curtailment in Distribution Systems," *IEEE Transactions on Sustainable Energy*, vol. 11, no. 3, pp. 1394-1403, 2020, doi: 10.1109/TSTE.2019.2926998.

[49] X. Duan, Z. Hu, and Y. Song, "Bidding Strategies in Energy and Reserve Markets for an Aggregator of Multiple EV Fast Charging Stations With Battery Storage," *IEEE Transactions on Intelligent Transportation Systems*, vol. 22, no. 1, pp. 471-482, 2021, doi: 10.1109/TITS.2020.3019608.

[50] N. Hashemipour, P. Crespo del Granado, and J. Aghaei, "Dynamic allocation of peer-to-peer clusters in virtual local electricity markets: A marketplace for EV flexibility," *Energy,* vol. 236, p. 121428, 2021, doi: 10.1016/j.energy.2021.121428.

[51] A. T. Eseye, M. Lehtonen, T. Tukia, S. Uimonen, and R. J. Millar, "Optimal Energy Trading for Renewable Energy Integrated Building Microgrids Containing Electric Vehicles and Energy Storage Batteries," *IEEE Access,* vol. 7, pp. 106092-106101, 2019, doi: 10.1109/ACCESS.2019.2932461.

[52] J. Zhang, L. Che, X. Wan, and M. Shahidehpour, "Distributed Hierarchical Coordination of Networked Charging Stations based on Peer-to-peer Trading and EV Charging Flexibility Quantification," *IEEE Transactions on Power Systems,* pp. 1-1, 2021, doi: 10.1109/TPWRS.2021.3123351.

[53] H. Liu, Y. Zhang, S. Zheng, and Y. Li, "Electric Vehicle Power Trading Mechanism Based on Blockchain and Smart Contract in V2G Network," *IEEE Access,* vol. 7, pp. 160546-160558, 2019, doi: 10.1109/ACCESS.2019.2951057.

[54] Y. K. Renani, M. Ehsan, and M. Shahidehpour, "Optimal Transactive Market Operations With Distribution System Operators," *IEEE Transactions on Smart Grid,* vol. 9, no. 6, pp. 6692-6701, 2018, doi: 10.1109/TSG.2017.2718546.

[55] S. M. Sajjadi, P. Mandal, T. B. Tseng, and M. Velez-Reyes, "Transactive energy market in distribution systems: A case study of energy trading between transactive nodes," in *2016 North American Power Symposium (NAPS)*, 2016, pp. 1-6, doi: 10.1109/NAPS.2016.7747895.

[56] Y. Liu, Y. Wang, Y. Li, H. B. Gooi, and H. Xin, "Multi-Agent Based Optimal Scheduling and Trading for Multi-Microgrids Integrated With Urban Transportation Networks," *IEEE Transactions on Power Systems,* vol. 36, no. 3, pp. 2197-2210, 2021, doi: 10.1109/TPWRS.2020.3040310.

[57] G. S. Aujla, N. Kumar, M. Singh, and A. Y. Zomaya, "Energy trading with dynamic pricing for electric vehicles in a smart city environment," *Journal of Parallel and Distributed Computing,* vol. 127, pp. 169-183, 2019/05/01/ 2019, doi: 10.1016/j.jpdc.2018.06.010.

[58] U. u. Rehman, "Optimal Energy Management Algorithm for Smart Cities Using Online Energy Trading Framework," *Electric Power Components and Systems,* vol. 48, no. 14-15, pp. 1660-1672, 2020, doi: 10.1080/15325008.2020.1857474.

[59] J. Li, C. Zhang, Z. Xu, J. Wang, J. Zhao, and Y. J. A. Zhang, "Distributed transactive energy trading framework in distribution networks," *IEEE Transactions on Power Systems,* vol. 33, no. 6, pp. 7215-7227, 2018, doi: 10.1109/TPWRS.2018.2854649.

[60] Z. Wu, C. Cao, and B. Chen, "Transactive Energy Based Approach for Large-Scale Plug-in Electric Vehicle Charging Control," in *2019 IEEE PES Asia-Pacific Power and Energy Engineering Conference (APPEEC)*, 2019, pp. 1-5, doi: 10.1109/APPEEC45492.2019.8994497.

[61] J. Lian, W. Zhang, Y. Sun, L. D. Marinovici, K. Kalsi, and S. E. Widergren, "Transactive System: Part I: Theoretical Underpinnings of Payoff Functions, Control Decisions, Information Privacy, and Solution Concepts," Pacific Northwest National Laboratory, 2018. [Online]. Available:

https://www.pnnl.gov/main/publications/external/technical_reports/PNNL-27235Part1.pdf

[62] J. Lian, Y. Sun, K. Kalsi, S. E. Widergren, D. Wu, and H. Ren, "Transactive System: Part II: Analysis of Two Pilot Transactive Systems using Foundational Theory and Metrics," Pacific Northwest National Laboratory, 2018. [Online]. Available: https://www.pnnl.gov/main/publications/external/technical_reports/PNNL-27235Part2.pdf

[63] H. Hao, C. D. Corbin, K. Kalsi, and R. G. Pratt, "Transactive Control of Commercial Buildings for Demand Response," *IEEE Transactions on Power Systems,* vol. 32, no. 1, pp. 774-783, 2017, doi: 10.1109/TPWRS.2016.2559485.

[64] F. F. W. Mesut E. Baran, "Network Reconfiguration in Distribution Systems for Loss Reduction and Load Balancing," *IEEE Transactions on Power Delivery,* vol. 4, no. 2, pp. 1401-1407, 1989, doi: 10.1109/61.25627.

[65] S. Ong, N. Clark, "Commercial and Residential Hourly Load Profiles for all TMY3 Locations in the United States", NREL, doi:10.25984/1788456.

[66] U.S. Department of Transportation, 2017, " National Household Travel Survey", [Online]. Available: https://nhts.ornl.gov/

[67] ComEd, "Comed's Hpourly Pricing Program", [Online]. Available: https://hourlypricing.comed.com/

[68] Z. Wu and B. Chen, "Distributed Electric Vehicle Charging Scheduling with Transactive Energy Management," *Energies,* vol. 15, no. 1, p. 163, 2022, doi: 10.3390/en15010163.

[69] M. Baran and F. F. Wu, "Optimal sizing of capacitors placed on a radial distribution system," *IEEE Transactions on Power Delivery*, vol. 4, no. 1, pp. 735-743, 1989, doi: 10.1109/61.19266.

[70] M. Farivar and S. H. Low, "Branch Flow Model: Relaxations and Convexification—Part I," *IEEE Transactions on Power Systems,* vol. 28, no. 3, pp. 2554-2564, 2013, doi: 10.1109/TPWRS.2013.2255317.

[71] S. Boyd, N. Parikh, and E. Chu, *Distributed Optimization and Statistical Learning Via the Alternating Direction Method of Multipliers*. Now Publishers, 2011.

[72] C. Cao, L. Wang, and B. Chen, "Mitigation of the Impact of High Plug-in Electric Vehicle Penetration on Residential Distribution Grid Using Smart Charging Strategies," *Energies,* vol. 9, no. 12, p. 1024, 2016, doi: 10.3390/en9121024.

[73] J. Lofberg, "YALMIP : a toolbox for modeling and optimization in MATLAB," in *2004 IEEE International Conference on Robotics and Automation*, 2004, pp. 284-289, doi: 10.1109/CACSD.2004.1393890.

[74] W. Lin *et al.*, "Decentralized optimal scheduling for integrated community energy system via consensus-based alternating direction method of multipliers," *Applied Energy,* vol. 302, p. 117448, 2021, doi: 10.1016/j.apenergy.2021.117448.

[75] W. u. Rehman, R. Bo, H. Mehdipourpicha, and J. W. Kimball, "Sizing battery energy storage and PV system in an extreme fast charging station considering uncertainties and battery degradation," *Applied Energy,* vol. 313, p. 118745, 2022, doi: 10.1016/j.apenergy.2022.118745.

[76] U.S. Department of Transportation, 2017, " National Household Travel Survey", [Online]. Available: https://nhts.ornl.gov/
[77] Fastned. "Can my vehicle charge at Fastned?" [Online]. Available: https://support.fastned.nl/hc/en-gb
[78] U.S. Department of Energy, 2022, "Alternative Fuels Data Center: Alternative Fueling Station Locator", [Online]. Available: https://afdc.energy.gov/stations
[79] M. A. Habib, S. A. M. Said, M. A. El-Hadidy, and I. Al-Zaharna, "Optimization procedure of a hybrid photovoltaic wind energy system," *Energy*, vol. 24, no. 11, pp. 919-929, 1999, doi: doi.org/10.1016/S0360-5442(99)00042-0.
[80] P. Rotella Junior *et al.*, "Economic Analysis of the Investments in Battery Energy Storage Systems: Review and Current Perspectives," *Energies*, vol. 14, no. 9, p. 2503, 2021, doi:10.3390/en14092503.
[81] M. H. Amrollahi and S. M. T. Bathaee, "Techno-economic optimization of hybrid photovoltaic/wind generation together with energy storage system in a stand-alone micro-grid subjected to demand response," *Applied Energy*, vol. 202, pp. 66-77, 2017, doi: doi.org/10.1016/j.apenergy.2017.05.116.
[82] SunPower, "SunPower E-Series Residential Solar Panels | E20-327", 2016, [Online] Available: https://us.sunpower.com/sites/default/files/media-library/data-sheets/ds-e20-series-327-residential-solar-panels.pdf
[83] Solcast, 2018, "Solar resource and weather data in Time Series, typical meteorological year (TMY) and monthly averages", [Online]. Available: https://solcast.com/
[84] W. Cole, A. W. Frazier, and C. Augustine, "Cost Projections for Utility-Scale Battery Storage : 2021 Update," NREL, Golden, CO, USA, 2021, Tech.Rep. NREL/TP-6A20-79236, 2021.
[85] ENGIE. “Historical Electricity Pricing Information”, [Online]. Available: https://www.engieresources.com/historical-pricing-data
[86] Z. Wu, N. N. Manne, J. Harper, B. Chen, and D. Dobrzynski, "A Cloud-Based Simulation and Testing Framework for Large-Scale EV Charging Energy Management and Charging Control," in *2022 WCX SAE World Congress Experience*, Detroit, MI, USA, 2022, doi: 10.4271/2022-01-0169.
[87] "MQTT," [Online]. Available: http://mqtt.org/
[88] “IEEE PES Test Feeder,” IEEE. [Online]. Available: http://ewh.ieee.org/soc/pes/dsacom/testfeeders.html.
[89] "Charging System Testing - Vehicle Charging System Testing," INL, [Online]. Available: https://avt.inl.gov/content/charging-system-testing/vehicle-charging-system-testing.html.
[90] R. Zhang *et al.*, "A Study on the Open Circuit Voltage and State of Charge Characterization of High Capacity Lithium-Ion Battery Under Different Temperature," *Energies*, vol. 11, no. 9, p. 2408, 2018, doi: 10.3390/en11092408.
[91] J. Undrill, "Primary Frequency Response and Control of Power System Frequency," Lawrence Berkeley National Laboratory, LBNL Report #: BNL-2001105, 2018. [Online]. Available: https://escholarship.org/uc/item/46122362

Copyright documentation

A.1 IEEE Copyright documentation for Chapter 2

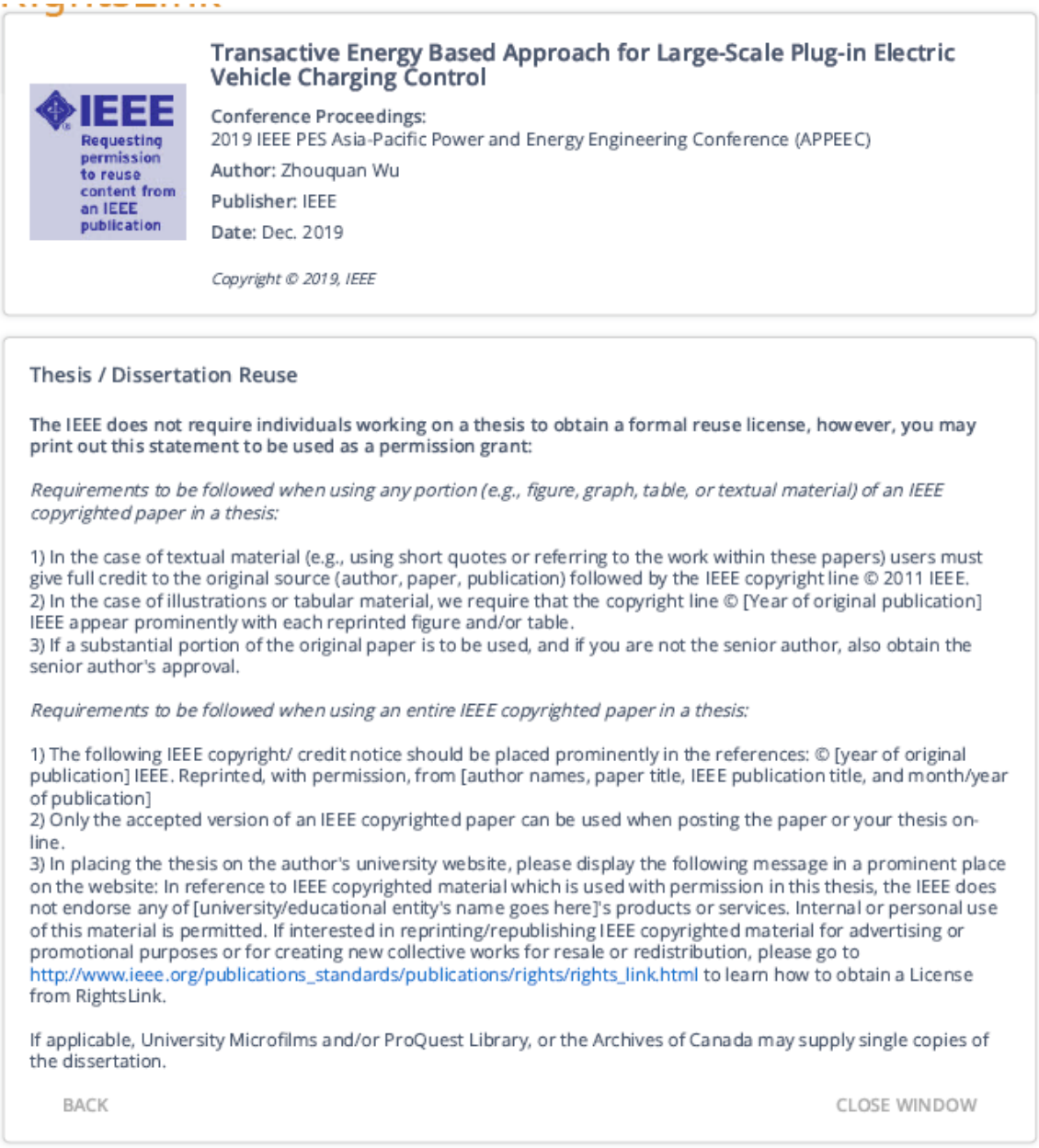

IEEE
Requesting permission to reuse content from an IEEE publication

Transactive Energy Based Approach for Large-Scale Plug-in Electric Vehicle Charging Control

Conference Proceedings:
2019 IEEE PES Asia-Pacific Power and Energy Engineering Conference (APPEEC)

Author: Zhouquan Wu

Publisher: IEEE

Date: Dec. 2019

Thesis / Dissertation Reuse

The IEEE does not require individuals working on a thesis to obtain a formal reuse license, however, you may print out this statement to be used as a permission grant:

Requirements to be followed when using any portion (e.g., figure, graph, table, or textual material) of an IEEE copyrighted paper in a thesis:

1) In the case of textual material (e.g., using short quotes or referring to the work within these papers) users must give full credit to the original source (author, paper, publication) followed by the IEEE copyright line © 2011 IEEE.
2) In the case of illustrations or tabular material, we require that the copyright line © [Year of original publication] IEEE appear prominently with each reprinted figure and/or table.
3) If a substantial portion of the original paper is to be used, and if you are not the senior author, also obtain the senior author's approval.

Requirements to be followed when using an entire IEEE copyrighted paper in a thesis:

1) The following IEEE copyright/ credit notice should be placed prominently in the references: © [year of original publication] IEEE. Reprinted, with permission, from [author names, paper title, IEEE publication title, and month/year of publication]
2) Only the accepted version of an IEEE copyrighted paper can be used when posting the paper or your thesis on-line.
3) In placing the thesis on the author's university website, please display the following message in a prominent place on the website: In reference to IEEE copyrighted material which is used with permission in this thesis, the IEEE does not endorse any of [university/educational entity's name goes here]'s products or services. Internal or personal use of this material is permitted. If interested in reprinting/republishing IEEE copyrighted material for advertising or promotional purposes or for creating new collective works for resale or redistribution, please go to http://www.ieee.org/publications_standards/publications/rights/rights_link.html to learn how to obtain a License from RightsLink.

If applicable, University Microfilms and/or ProQuest Library, or the Archives of Canada may supply single copies of the dissertation.

BACK CLOSE WINDOW

A.2 SAE Copyright documentation for Chapter 5

Hello Zhouquan,

Thank you for reaching out to SAE International with your inquiry. As you are currently unable to obtain a license through copyright.com, we are providing an email permission that you can use until the paper has been properly loaded into the CCC system. Please see below.

This is your interim permission until you can obtain a license through Copyright Clearance Center (copyright.com) once we have uploaded the paper details into the CCC system.

Author: Zhouquan Wu

SAE Publication: A Cloud-Based Simulation and Testing Framework for Large-Scale EV Charging Energy Management and Charging Control". [2022-01-0169]

Author's Thesis: STUDY OF ELECTRIC VEHICLE SMART CHARGING AND ENERGY MANAGEMENT FOR VEHICLE-GRID INTEGRATION SYSTEMS submitted to the
Michigan Technological University

Permission is granted for the author to include the SAE publication above in the
Michigan Technological University thesis as outlined above. Any reproduction must include a full reference to the original published source, as well as the copyright notice for the published paper. Any further use requires
written permission from SAE International.

Please feel free to reach out if you have any questions or concerns.

Regards,

Brandon Joy | Intellectual Property Associate

SAE International
SAE.org | facebook | instagram | linkedin | twitter